AEC
RESEARCH
and
DEVELOPMENT
REPORT

BNWL - 198
108-

CERAMICS RESEARCH AND DEVELOPMENT
QUARTERLY REPORT
JULY - SEPTEMBER 1965

BATTELLE-NORTHWEST

BATTELLE MEMORIAL INSTITUTE / PACIFIC NORTHWEST LABORATORY

LEGAL NOTICE

PACIFIC NORTHWEST LABORATORY
RICHLAND, WASHINGTON
operated by
BATTELLE MEMORIAL INSTITUTE
for the
UNITED STATES ATOMIC ENERGY COMMISSION UNDER CONTRACT AT(45-1)-1830

PRINTED BY/FOR THE U. S. ATOMIC ENERGY COMMISSION

AEC-RLOO RICHLAND, WASH.

BNWL-198

UC-25, Metals, Ceramics,
and Materials

FIRST
UNRESTRICTED

TID-4500

DISTRIBUTION
MADE

EDITION

CERAMICS RESEARCH AND DEVELOPMENT
QUARTERLY REPORT
JULY–SEPTEMBER 1965

PACIFIC NORTHWEST LABORATORY
RICHLAND, WASHINGTON

Printed in USA. Price $4.00. Available from the
Clearinghouse for Federal Scientific and Technical Information
National Bureau of Standards
U. S. Department of Commerce
Springfield, Virginia

INTRODUCTION

The work reported in this and subsequent reports is a continuation of reactor fuels studies previously discussed in reports issued by the Fuels Development and the Plutonium Metallurgy Operations (prior to October 1962) and by Ceramics Research and Development Operation, General Electric Company, Richland, Washington. Recent reports in this series are:

HW-76300	(Unclassified)	October-December 1962
HW-76301	(Unclassified)	January-March 1963
HW-76302	(Unclassified)	April-June 1963
HW-76303	(Unclassified)	July-September 1963
HW-76304	(Unclassified)	October-December 1963
HW-76304A	(Confidential)	October-December 1963
HW-81600	(Unclassified)	January-March 1964
HW-81600A	(Confidential)	January-March 1964
HW-81601	(Unclassified)	April-June 1964
HW-81601A	(Confidential)	April-June 1964
HW-81602	(Unclassified)	July-September 1964
HW-81603	(Unclassified)	October-December 1964
BNWL-91	(Unclassified)	January-March 1965
BNWL-150	(Unclassified)	April-June 1965

SUMMARY OF CONTENTS

PART I - CERAMIC FUEL RESEARCH STUDIES

Differential Thermal Analysis of PuO_{2-x} - C. E. McNeilly

Two reactions were detected during differential thermal analysis (DTA) of PuO_{2-x} compositions. A broad exothermic peak was observed at 250 °C on cooling of all specimens with an O:Pu between 1.92 and 1.60. This may represent the eutectoid reaction which has generally been placed at about 300 °C on Pu-O phase diagrams. The corresponding endothermic reaction on heating has not been observed. However, this is thought to be probably due to low temperature instability of the apparatus.

A second, small exothermic reaction on heating was detected (at about 875 °C) in a specimen having an O:Pu of about 1.6. The corresponding cooling endotherm was also observed. It is proposed that this is indicative of the $\alpha\text{-}Pu_2O_3 \rightleftarrows \alpha'Pu_2O_3$ reaction which had been postulated to occur below 900 °C for O:Pu ratios between 1.5 and 1.62. By comparing the peak height with that for the $\alpha \rightleftarrows \beta$ quartz reaction (86 cal/mole) a crude estimate of about 10 to 20 cal/mole is obtained for the heat of reaction.

Reflection Electron Microscope Studies of the Pu-O System -

T. E. Bauer, T. D. Chikalla, and J. L. Daniel

High temperature reflection electron micrographs (Figures 1.1 through 1.3) were taken during the heating of $PuO_{1.8}$ (prepared by hydrogen reduction of 97% TD PuO_2).

The surface of the polished specimen became rough at about 700 °C, consistent with the phase transformation shown in the phase diagram. On reheating, surface structure changes were again observed at around 700 °C. However, X-ray examination after removal from the microscope indicated the sample had been oxidized, which

may have contributed to the observed behavior. More specimens will be examined, with a provision to eliminate the oxidation.

Subsequent cleanup of the microscope was unexpectedly easy. Plutonium did not spread within the microscope, and the specimen was readily recovered for further examination. No problems were encountered with the transfer box used to service the microscope column with plutonium specimens.

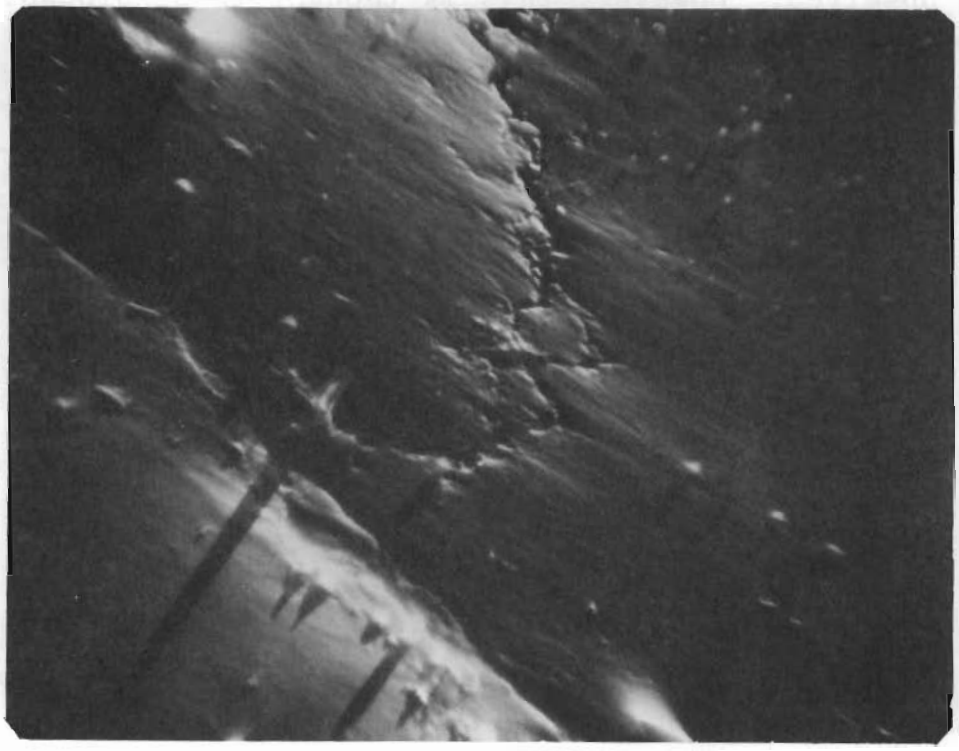

FIGURE 1.1

PuO_{2-x} Sample
Before Heating (1300X)
No. 3413 (18° tilt)

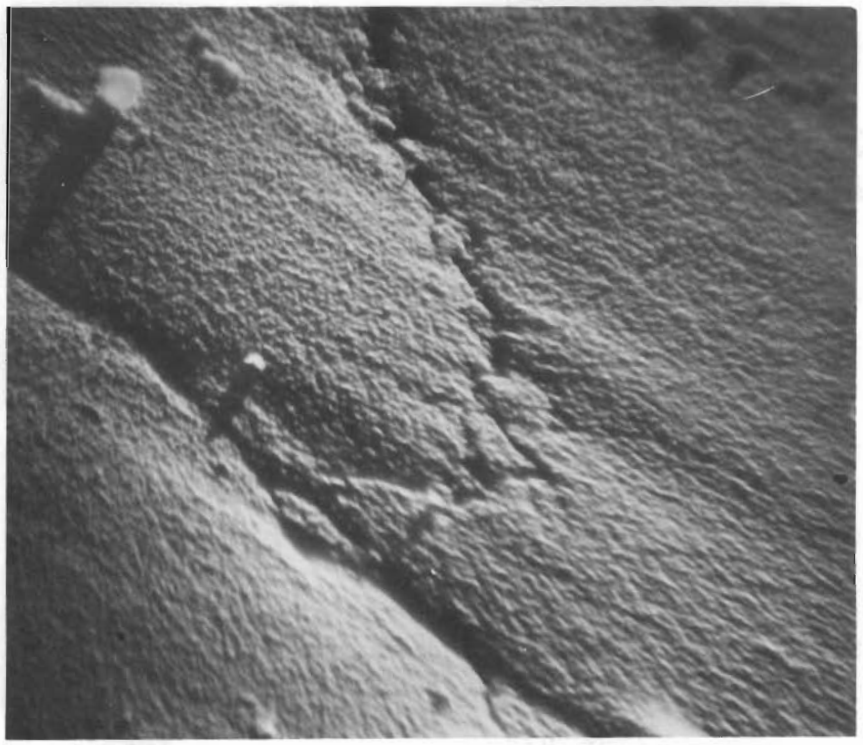

FIGURE 1.2
PuO_{2-x} Sample
at 890 °C (1300X)
No. 3422
(12° tilt)

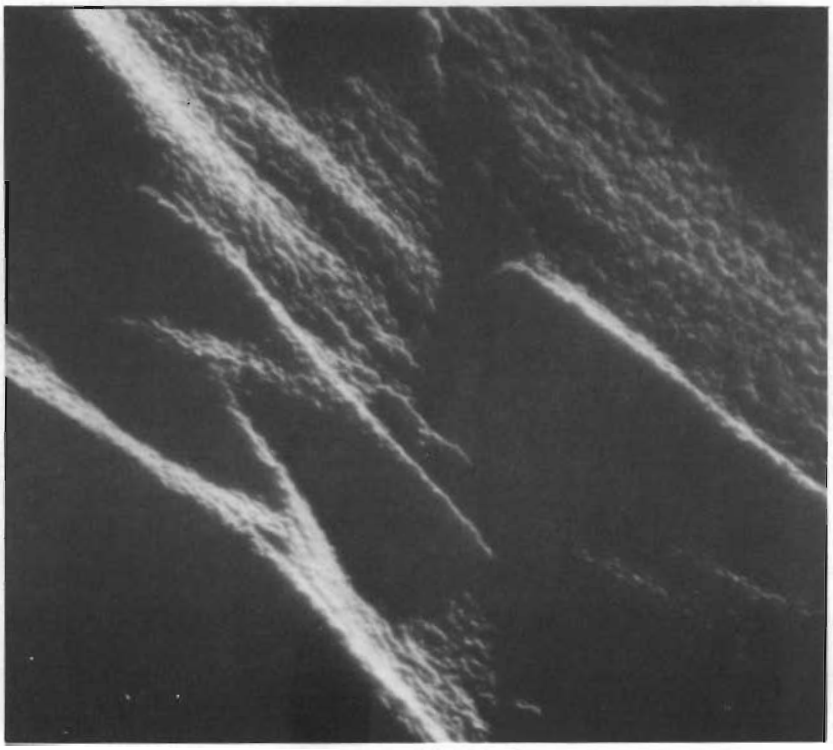

FIGURE 1.3
PuO_{2-x} Sample
After Cooling
(3600X) No. 3430
(15° tilt)

UN-PuN Solid Solution Studies - E. T. Weber

Mixed nitride compositions of UN and PuN are being studied. Lattice parameters of solid solutions in this system were determined, and preliminary experiments were conducted on carbothermic reduction of UO_2-PuO_2 mixtures to yield nitrides.

Mixtures of -200 mesh PuN and UN powder were prepared at 10 mol% composition intervals. The mixtures were blended and pressed into pellets at about 40 TSI. Heat treatment consisted of 4 hr at 1800 °C under 1 atm of nitrogen. Cooling below 1300 °C was performed under helium to preclude formation of the sesquinitride.

X-ray diffraction patterns of each heat treated material revealed a single phase. Lattice parameters determined by Debye Sherrer cameras and the Nelson-Riley extrapolation function are plotted as a function of composition in Figure 1.4. Compositions between 30 and 60 mol% PuN provided slightly better definition of high angle reflections than those of higher or lower PuN content, indicating better homogeneity.

Density changes of pellets during heat treatment were anomalous. A significant volume increase was noted for compositions in the central portion of the system. Changes in weight, volume, and density are shown in Figure 1.5. Densities determined from pellet dimensions ranged between 56 and 80% TD. Future work involving continued heat treatment and ceramographic examination is in progress and should lead to explanation of the observed behavior.

A carbothermic oxide reduction scheme for synthesis of mixed nitrides was attempted, using mixed UO_2, PuO_2, and carbon powders. After blending and consolidating, the mixtures were heated to 1500 °C under 500 to 1000 microns of N_2 with intermittent replacement of N_2

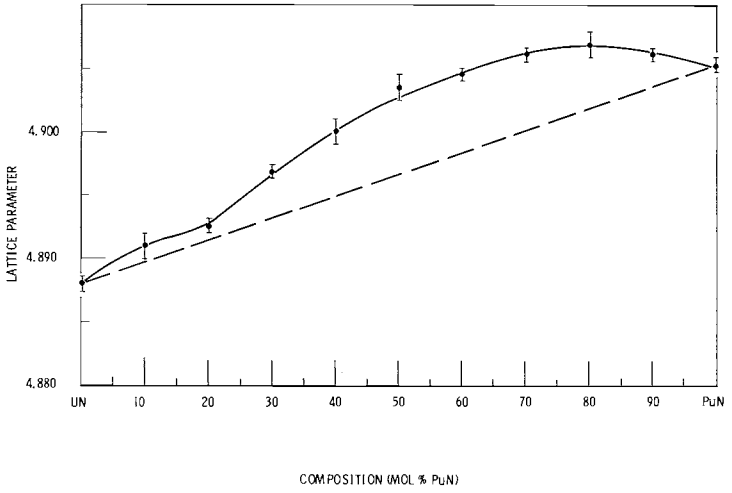

FIGURE 1.4

Lattice Parameters of UN-PuN Solid Solutions

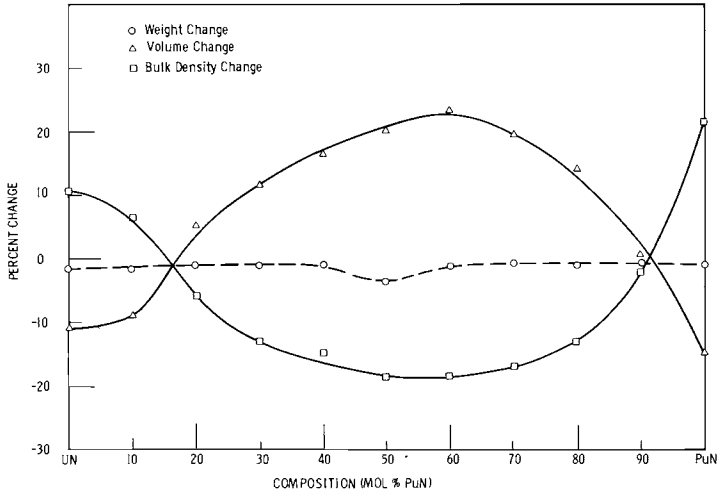

FIGURE 1.5

Changes in Physical Character of Pellets due to Heat Treatment

as the partial pressure of CO increased. The reaction $MO_2 + 2C \longrightarrow M_{(l)} + CO_{(g)}$ appeared to proceed rapidly at 1200°C, as indicated by a rapid increase in pressure. Nitriding was completed under 1 atm of N_2 at 1500 °C. X-ray diffraction patterns indicated that the product was a mixture of a somewhat inhomogeneous UN-PuN phase (possibly a carbonitride) and a UO_2 phase. Carbon content of the product was between 2000 and 6000 ppm. Further analyses of the product are being performed.

Actinide Oxide Phase Studies - T. D. Chikalla

Measurement of oxygen dissociation pressures and study of phase relations in the americium-oxygen system was continued. Seven isotherms at about 50° intervals were investigated between 1150 and 1450 °K. The composition of a substoichiometric oxide in equilibrium with a known oxygen pressure was determined by the weight loss method. Plots of log p_{O_2} versus composition show a gradual change in slope at about $AmO_{1.96}$ for the lower temperatures but become progressively more linear at the higher temperatures. The system is bivariant over the composition interval covered ($1.80 < O/Am < 2.0$), which implies a monophasic region, probably consisting of an anion deficient fluorite structure. However, Debye and Guinier Camera x-ray diffraction patterns made at room temperature showed two phases, a fluorite type and a C rare earth type. These were indexed as AmO_2 and Am_2O_3, respectively. Existence of these two phases at room temperature and the inference of a single phase above 1150 °K from the slope of the isotherms suggests a phase transformation in the system. This is speculative, however, and this probability will be checked with quench tests and by high temperature x-ray diffraction.

Hexagonal Am_2O_3 was retained by quenching the sesquioxide from 1000 °C, while cubic Am_2O_3 is retained by quenching this composition from 400 °C.

The thermodynamic quantities derived from the data are plotted in Figures 1.6 through 1.8. Figure 1.6 is a plot of log p_{O_2} versus 1/T and Figure 1.7 is a plot of $\Delta\overline{G}(O_2)$ versus temperature, both at constant composition. The lines drawn are based upon a least squares fit to the experimental data. The slopes of the curves on these two plots yield, respectively, the relative partial molar heats and entropies of solution of one mole of oxygen in AmO_{2-x}. These quantities, $\Delta\overline{H}(O_2)$ and $\Delta\overline{S}(O_2)$ are plotted as a function of composition in Figure 1.8. The notable feature on these plots is the abrupt change in slope at about $AmO_{1.98}$. The reason for this slope change is unknown; however, it may be associated with domains centered about Am III ions. The data are being fit to several defect models in an effort to explain these results.

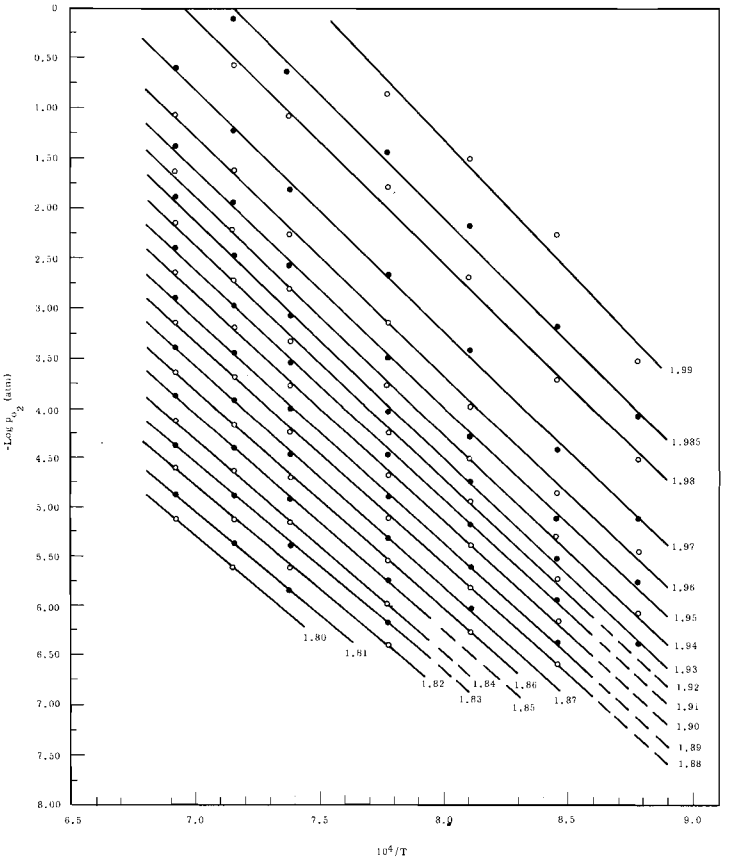

FIGURE 1.6

Log p_{O_2} Versus 1/T at Constant Oxygen/Americium Ratios

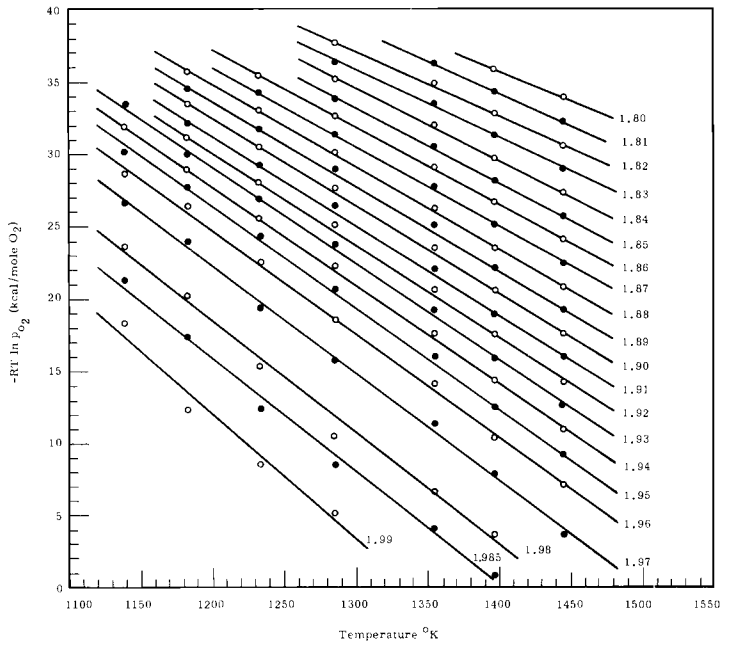

FIGURE 1.7

Relative Partial Molar Free Energy of Solution of Oxygen in AmO_{2-x} Versus Temperature

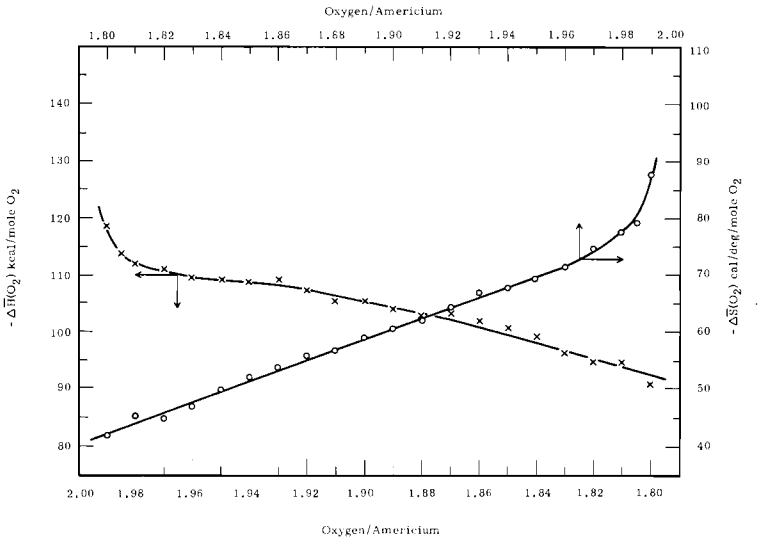

FIGURE 1.8

Relative Partial Molar Heat and Entropy of Solution of Oxygen in AmO_{2-x}

Self-Radiation Damage of Plutonium Compounds -

T. D. Chikalla and R. E. Skavdahl

Measurement of changes in the lattice constants of several plutonium bearing compounds due to self-induced radiation damage have been continued for as long as 4 years. Plots showing the extent of lattice damage versus time were given in the previous Quarterly Report.(1) The data, fitted to curves by the method of least squares, yield the following equations (where t is the time in days):

Pu_2C_3 (carbon rich) $\quad \frac{\Delta a}{a_o} = 1.59 \times 10^{-3} [1-\exp(-1.99 \times 10^{-3} t)]$

Pu_2C_3 (stoichiometric) $\quad \frac{\Delta a}{a_o} = 1.65 \times 10^{-3} [1-\exp(-1.99 \times 10^{-3} t)]$

Pu_2C_3 (carbon poor) $\quad \frac{\Delta a}{a_o} = 1.68 \times 10^{-3} [1-\exp(-1.99 \times 10^{-3} t)]$

PuC $\quad \frac{\Delta a}{a_o} = 4.65 \times 10^{-3} [1-\exp(-1.45 \times 10^{-3} t)]$

PuO_2-10 mol% UO_2 $\quad \frac{\Delta a}{a_o} = 1.84 \times 10^{-3} [1-\exp(-2.00 \times 10^{-3} t)]$

---

(1) Ceramics Research and Development Quarterly Report, April-June 1965, BNWL-150.

Thermal Expansion of Plutonium Fuels - C. A. Hinman and R. P. Nelson

Initial thermal expansion studies of pneumatically impacted PuO_2 indicate that irreversible dimensional changes occur in addition to reversible expansion. In Figure 1.9 is shown the first continuous heating cycle to 1435 °C (2.5°/min) for a PuO_2 specimen (initial O:Pu = 1.998) compacted to 96.9% TD. Heating to about 950 °C produced a contraction which is thought to have resulted from sintering of the fine grained specimen. Continued heating results in an equally sharp expansion starting at 1200 °C caused by the relief of internal stress imparted by the impaction process. The net dimensional change at cycle end was an 0.742% increase in length.

A type 304 SS–20 vol% PuO_2 impaction-formed cermet specimen was tested through three step-type thermal expansion cycles to 1290 °C (Figure 1.10). In the first cycle annealing of thermal stress caused a 0.53% net increase in length, while subsequent cycles produced no observable net dimensional change.

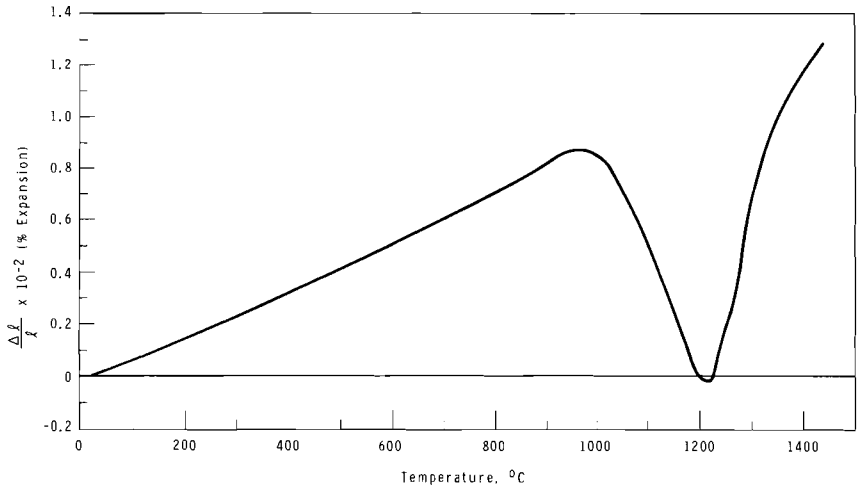

FIGURE 1.9

First Thermal Expansion Cycle Heating Curve for a Pneumatically Impacted PuO_2 Specimen, Showing an Effect of the Fabrication Process

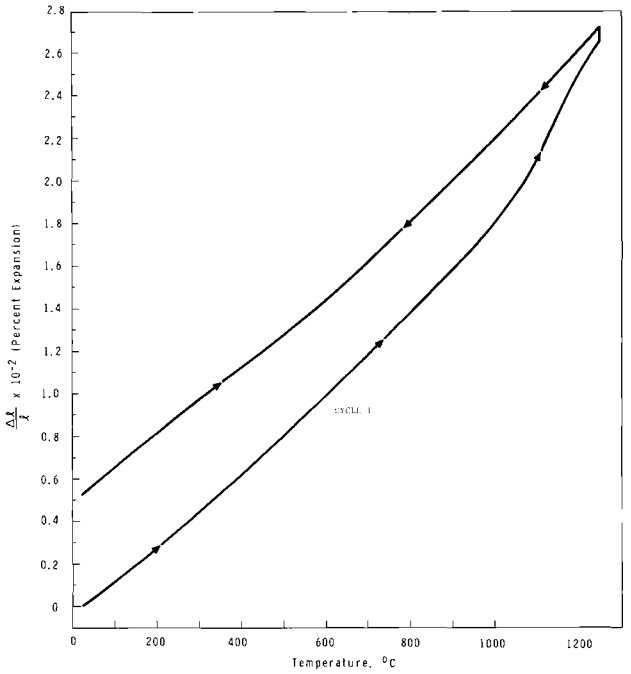

FIGURE 1.10(a)

First Thermal Expansion Cycle for a Pneumatically Impacted 304 SS–20 vol% PuO_2 Cermet.

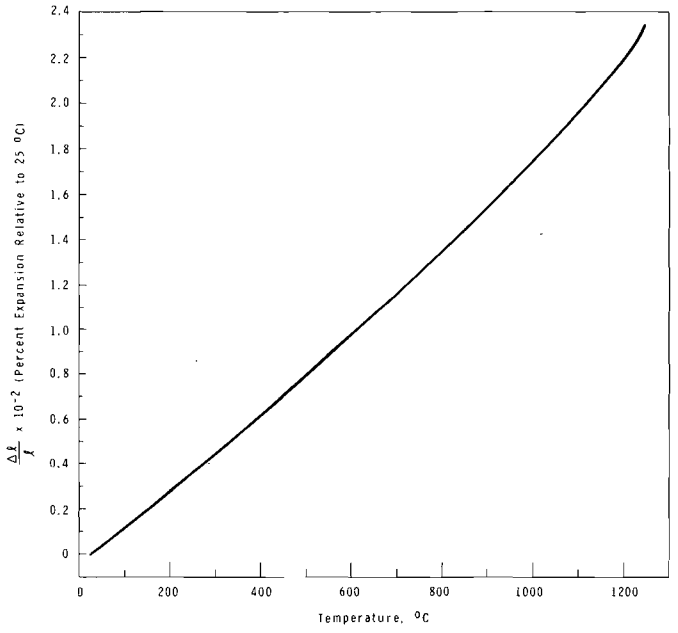

FIGURE 1.10(b)

Thermal Expansion Curve for an Annealed 304 SS–20 vol% PuO_2 Cermet. (These Results Represent the Average of Two Thermal Cycles.)

These results indicate that fuel materials formed by pneumatic impaction must be annealed to eliminate dimensional instability. Time-temperature relationships for complete annealing have not yet been established. Similar instabilities were observed for a tungsten–20 vol% UO_2 cermet formed by impaction at 1200 °C.

The second thermal expansion cycle on the impacted PuO_2 specimen showed no discontinuities on heating (Figure 1.11). However, on cooling, two discontinuities were observed that are associated with phase changes occurring in the solid state (Figure 1.12). The first appeared as an increase of the expansion coefficient beginning at about 600 to 700 °C, the second appeared as a peak at 300 °C.

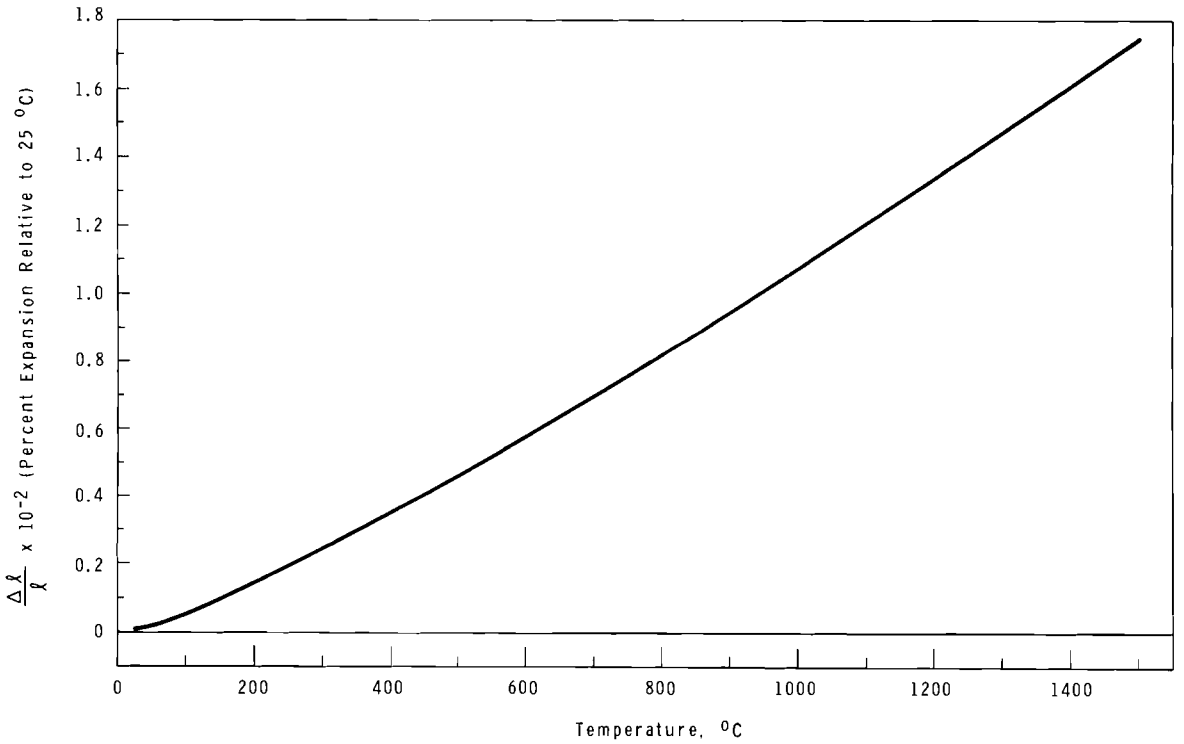

FIGURE 1.11

Thermal Expansion Curve for an Annealed Pneumatically Impacted PuO_2 Specimen

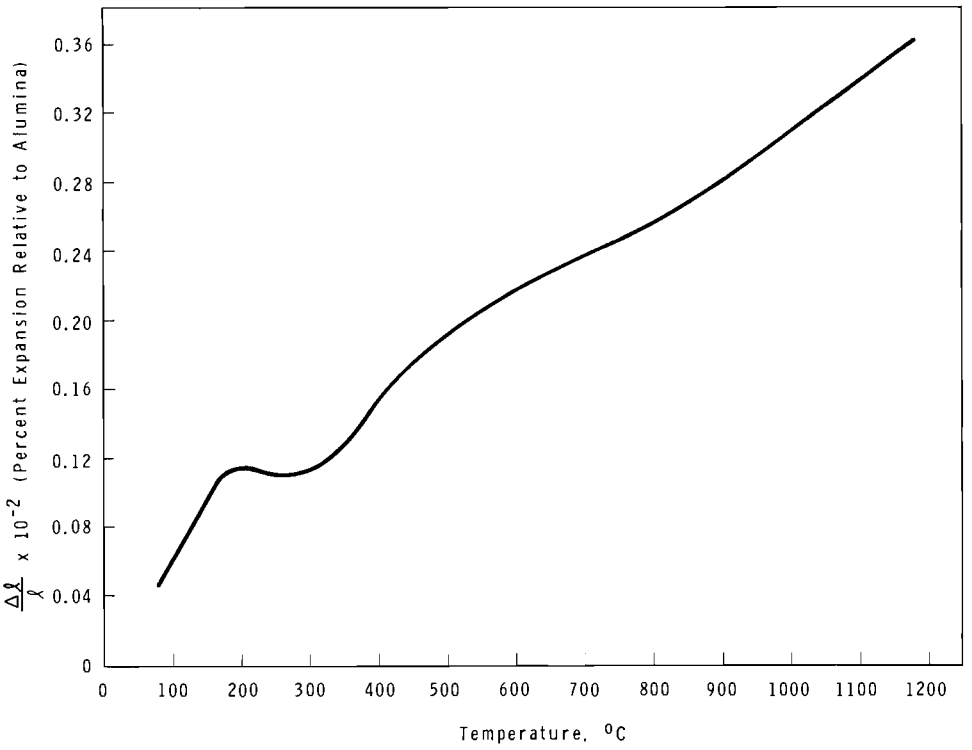

FIGURE 1.12

Cooling Curve for $PuO_{1.996}$. (The Thermal Expansion of the Alumina Sample Holder has not been Eliminated in the Data Shown.)

These discontinuities indicate that the specimen was reduced slightly in the vacuum during the high temperature part of the cycle. A weight measurement after the cycle determined that the O:Pu ratio had decreased from 1.995 to 1.983. The initial change in slope at 600 to 700 °C corresponds to the immiscibility loop over the phase field PuO_{2-x} and PuO'_{2-x} and the peak at 300 °C corresponds to the isothermal separation of α-Pu_2O_3.

With the use of a redesigned tungsten sample holder to improve the resolution, additional thermal expansion measurements will be made on specimens having O:U ratios between 2.00 and 1.70.

Thermionic Emission Work Function Measurements - C. E. McNeilly

An apparatus was completed for determining thermionic work function of plutonium bearing compounds by the retarding potential technique. Work function measurements were continued on the polycrystalline tantalum emitter used in the present apparatus, as a check on the accuracy of the equipment. A Fortran IV computer program was written to calculate the work function and emission constant based on the retarding potential difference technique being used. There is still some problem with the program for obtaining the emission constant. However, the work function values seem to agree quite well with the accepted published value. Two different high-purity, polycrystalline tantalum emitters yielded average values of 4.282 and 4.082 eV compared with 4.356 eV reported for high purity single crystal tantalum. There is also some evidence that the value of 4.082 was determined against a contaminated collector.

The apparatus is being prepared to make a third and final check on the tantalum work function after which it will be installed in the hood for measurements on plutonium compounds.

Thermal Diffusivity of UO_2 - J. L. Bates

The thermal diffusivity of several single crystals and polycrystalline UO_2 specimens were measured between 100 and 1100 °C. The equipment and methods used to measure the thermal diffusivity and to calculate the thermal conductivity have been previously described.[1] Characteristics of the UO_2 specimens are given in Table 1.1.

---

(1) Ceramics Research and Development Quarterly Report, April-June 1965, BNWL-150.

TABLE 1.1

CHARACTERISTICS OF UO_2 THERMAL DIFFUSIVITY SPECIMENS

Single Crystal UO_2	Thickness, cm	O:U Ratio	Density, g/cm^3
B-15	0.076	2.0023[1]	10.97[3]
B-29	0.051	2.005[1]	10.92[3]
	0.076		10.95[4]
	0.102		
B-33	0.076	2.0006[1]	10.90[3]
		2.001[2]	10.93[4]
			10.94[5]
Polycrystalline UO_2			
70	0.076	2.005[1]	10.45
1000	0.132	2.002[1]	10.22[3]

1. Determined by controlled potential coulometry
2. Determined by gravimetric oxidation to U_3O_8
3. Determined in H_2O
4. Determined in CCl_4
5. Determined in Hg

The thermal conductivity* data for the single crystal and polycrystalline UO_2 are shown in Figures 1.13 through 1.15.

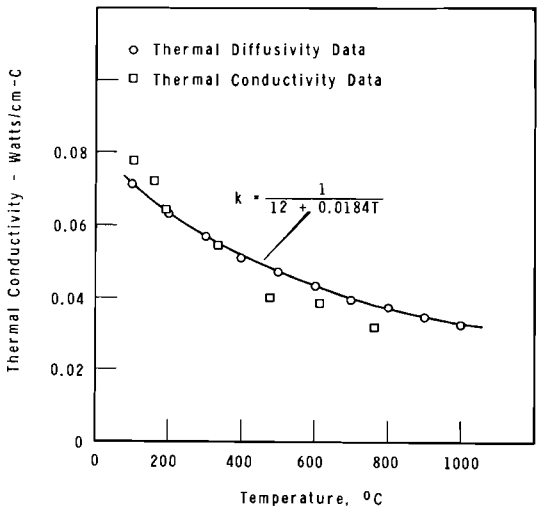

FIGURE 1.13

Thermal Conductivity of Polycrystalline UO_2 Reference Specimen 70 Comparing Thermal Diffusivity and Steady State Thermal Conductivity Data. [Data Are Given for UO_2 Density of 10.45 g/cm^3 (95% TD)]

* Thermal conductivity values (k) were calculated by using specific heat data reported by Kelley, et al, [Kelley,K. K. Bull. U.S. Bureau of Mines, p. 476, 1949; A. B. McIntosh and T. J. Heal. "Materials for Nuclear Engineering," Interscience Publishers, New Jersey, 1960. pp. 143,164.

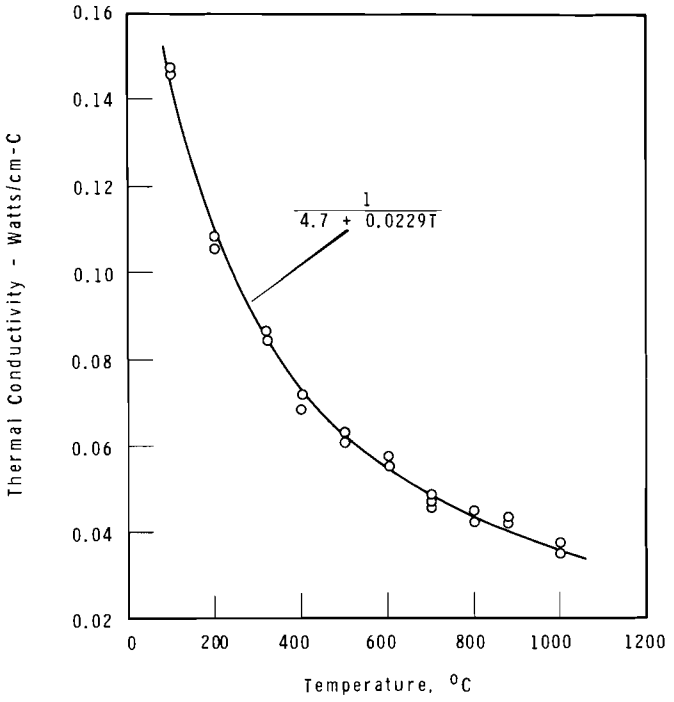

FIGURE 1.14

Thermal Conductivity of UO_2 Single Crystal (B-33). [Data Are Given for UO_2 Density of 10.93 g/cm^3 (99.5% TD)]

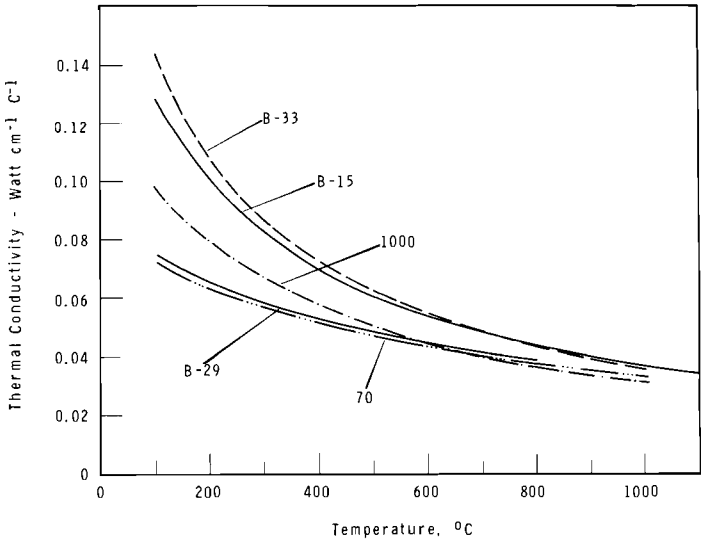

FIGURE 1.15

Thermal Conductivity of UO_2 Calculated from Thermal Diffusivity Data Showing Variations Between Polycrystalline and Single Crystal UO_2 Specimens. (Data are Uncorrected for Density. See Table 1.1 for Specimen Densities.)

Thermal conductivity values obtained from the thermal diffusivity data were compared with thermal conductivity data measured by an absolute, steady state method.[1] The polycrystalline UO_2 (Specimen 70) was a small disc cut from a larger UO_2 specimen previously used for the steady state thermal conductivity measurements.[1] The results agree fairly well. The steady state thermal conductivity values are slightly higher than those calculated from the thermal diffusivity data below 200 °C. The curves cross between 200 and 300 °C. These differences may reflect uncertainty in heat capacity values used to calculate the thermal conductivity, or possibly an inhomogeneity in the original large UO_2 specimen from which the small wafer was cut.

The single crystal specimen, B-33, exhibited an unexpectedly high thermal conductivity at less than 600 °C (Figure 1.14). The single crystal conductivity at 100 °C was about twice that of the polycrystalline UO_2 specimen (No. 70).

A comparison of the thermal conductivities calculated from thermal diffusivity data* for several UO_2 single crystal and polycrystalline UO_2 specimens is shown in Figure 1.15. A wide difference is observed in the thermal conductivities below 1000 °C. At the higher temperatures, the differences are relatively small.

The large variations in the low temperature thermal conductivity values are difficult to explain. Some explanations for such large differences typically involve grain size and stoichiometry. Single crystal UO_2 exhibits a higher thermal conductivity, and hypostoichiometric UO_2 exhibits an enhanced thermal conductivity.

---

(1) J. L. Daniel, J. Matolich, and H. W. Deem. Thermal Conductivity of UO_2, HW-69945, 1962.

* The thermal conductivities of specimens 1000, B-15, and B-29 were reported previously in Reference (1) page 1.14.

Neither of these explanations appears to apply to the current specimens. The thermal conductivity of one UO_2 single crystal(B-29) is as low as that of the polycrystalline specimen (70) showing the lowest conductivity. This would indicate that grain size, per se, is not the cause of the differences or that the effect is overridden by another. However, large grains may be a necessary requirement for an increased thermal conductivity, since only single crystal UO_2 exhibits it. Hypostoichiometry does not appear to be the cause of the low temperature increase. The O:U ratio of all of the specimens, both single crystal and polycrystalline UO_2, was between 2.005 and 2.0006.

Analyses are being made to determine if other characteristics (e.g., impurity content, gas content, crystal orientation) of the single crystal UO_2 caused the large variations. Preliminary investigation shows that crystal B-29 contained 0.6 g/cm^3 of gas while B-33, the high thermal conductivity specimen, contained 0.05 g/cm^3 of gas. The concentration of other impurities in the two crystals was about the same.

Method of fabrication may also be important. Crystals B-33 and B-15 (high thermal conductivity specimens) were grown by solidification from an arc-fused melt, whereas crystal B-29 (low conductivity specimen) was grown by a vapor deposition process.

Thermal Diffusivity of Phosphate Glass - J. L. Bates

The thermal diffusivity of a special phosphate glass [1] was measured between 25 and 600 °C. The glass was dark grey in color, partially translucent, and contained a second phase. The heat

---

(1) The phosphate glass was prepared by W. B. DeMier of Chemical Engineering Section, Battelle-Northwest.

capacity of the glass was approximately 0.25 cal/g-C´. Measurements were made on three specimen thicknesses (0.041 cm, 0.061 cm, and 0.079 cm). No systematic variation with specimen thickness was observed. Thin specimens were required because of the low thermal diffusivity. The results are shown in Figure 1.16.

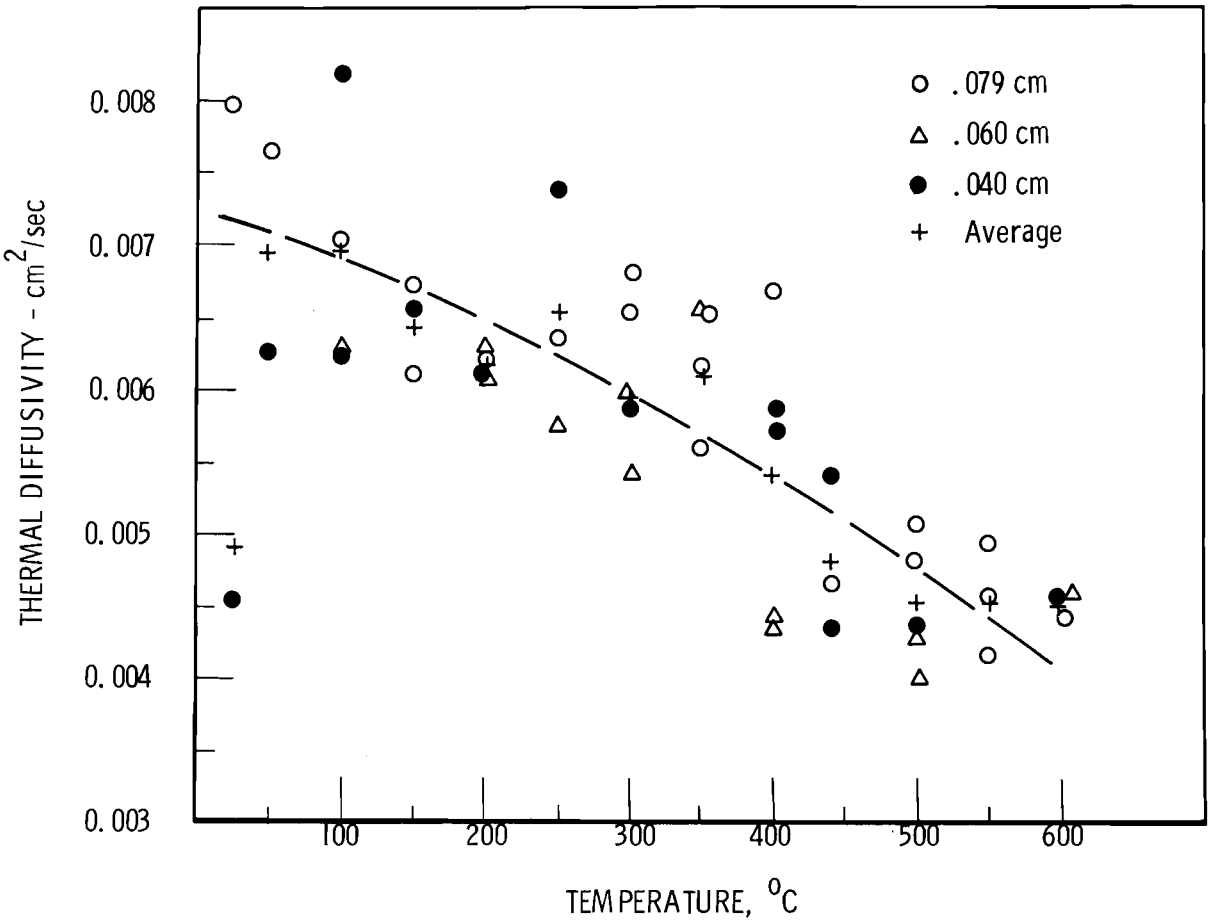

FIGURE 1.16
Thermal Diffusivity of Phosphate Glass
Showing Data for Three Sample Thicknesses

A wide scatter was observed in the data. Variation appeared independent of specimen thickness. Changes occurring during

heating suggested a change in composition or structure at the higher temperatures. In addition, some scatter is attributed to inhomogeneity of the specimens.

There was encouraging evidence of the capability of the laser pulse diffusivity system to measure very low thermal diffusivities with partially translucent materials.

High Frequency Induction Heating of Oxides - J. A. Christensen

The feasibility of direct coupling of UO_2 in a 10^7 cycles/sec field was previously demonstrated by McPartland.(1) This method of heating is ideal for reactive materials because the specimen is the only heated portion of the system and it need contact no foreign object at high temperature. The technique is severely limited for materials of low thermal conductivity, however, because the steep thermal gradients established in the specimen preclude isothermal heating. These gradients arise at high temperatures because the specimen is the only hot object in the system. Thus the net radiant flux from its surface is maximized. A modification of the system which may eliminate this problem is to introduce an inert susceptor, heated directly by the induction field, which will transmit radiant energy to the specimen. Tubular ThO_2, ZrO_2, or BeO susceptors seem the most logical for work with UO_2 or UO_2-PuO_2 because they are sufficiently refractory to achieve the required temperatures and are stable in all oxygen pressures. A furnace so equipped will be valuable for studying phase equilibrium in the metal-oxygen systems of interest, as in nuclear fuels.

---

(1) Ceramics Research & Development Operation Quarterly Report, April-June 1964, HW-81601, General Electric Company, Richland, Washington.

A major problem in inductively heating oxide susceptors is the need to preheat the oxide before coupling is possible. Attempts to couple to a 1/2 in. ID, 1/16 in. wall ZrO_2 tube proved futile at room temperature even in a 10^7 cycles/sec field. In an attempt to circumvent the need for preheating, a second tube was coated with graphite (from a soft pencil). This tube coupled readily to the field and was successfully heated to an outer surface temperature of 1800 °C at which the tube began to slump. Postheating examination showed that the inner surface of the tube had melted, indicating a minimum ΔT across the wall of 900 °C.

High Density PuO_2 Research Specimens - H. J. Anderson

Two specimens were prepared from pneumatically impacted PuO_2 and UO_2–15 wt% PuO_2 material, approximately 98% TD, for basic studies including measurement of thermal diffusivity and thermal conductivity. The UO_2–PuO_2 specimen is about 6 mm diam and 1.5 mm thick. The PuO_2 specimen, prepared for thermal expansion measurements, is about 10 mm diam and 20 mm long.

Materials and Information Exchange - H. J. Anderson

Single crystal specimens of UO_2 and ThO_2 were prepared, characterized, and sent to Watson Research Center (IBM Corporation) to be used in basic studies. A single crystal of UO_2 about 13 mm diam by 40 mm long was prepared and sent to AECL, Chalk River. A cylindrical polycrystalline UO_2 specimen (16 mm diam by 66 mm long) was prepared and sent to Mound Laboratory for thermal conductivity studies.

Approximately 1 kg of 15 wt% PuO_2-UO_2 (93% enriched) was pneumatically impacted to 95% TD in response to a request from AERE-Dounreay. The oxides were ball-milled 67 hr before impaction to assure uniform PuO_2 distribution throughout the UO_2. PuO_2

distribution was found to be uniform both by autoradiography and chemical analyses. Additional characterizing of physical and chemical properties was completed.

PART II - MATERIALS AND JOINING DEVELOPMENT

Spheroidization of UO_2 - R. E. Lyon, R. E. Bardsley, and L. R. Bunnell

The following equipment was used to produce UO_2 agglomerates up to 96% TD:

- Planetary mixer
- Twinshell blender
- Drier
- Hydrogen sintering furnace

The fabrication process is shown in Figure 2.1. A 0.1% addition of TiO_2 is mixed with micronized UO_2 to act as a sintering aid.

Carbowax binder is added as the powders are being mixed. After mixing and while still damp, the powders are tumbled in a twinshell blender to form agglomerates. When agglomerates of the desired size are formed, the fuel is then dried and sintered. Size fractions may be separated either before or after sintering. Particles +65 mesh are predominant; however, -65 +100 mesh particles can be produced.

Particles of lower densities might also be made by leaving out the TiO_2 or not micronizing the UO_2. Table 2.1 shows the densities achieved by the various techniques.

TABLE 2.1

SPHEROIDIZATION TECHNIQUES

	%TD
Ceramic Grade UO_2	72
Ceramic Grade UO_2 + 1% TiO_2	90
Micronized UO_2 + 0.1% TiO_2	96

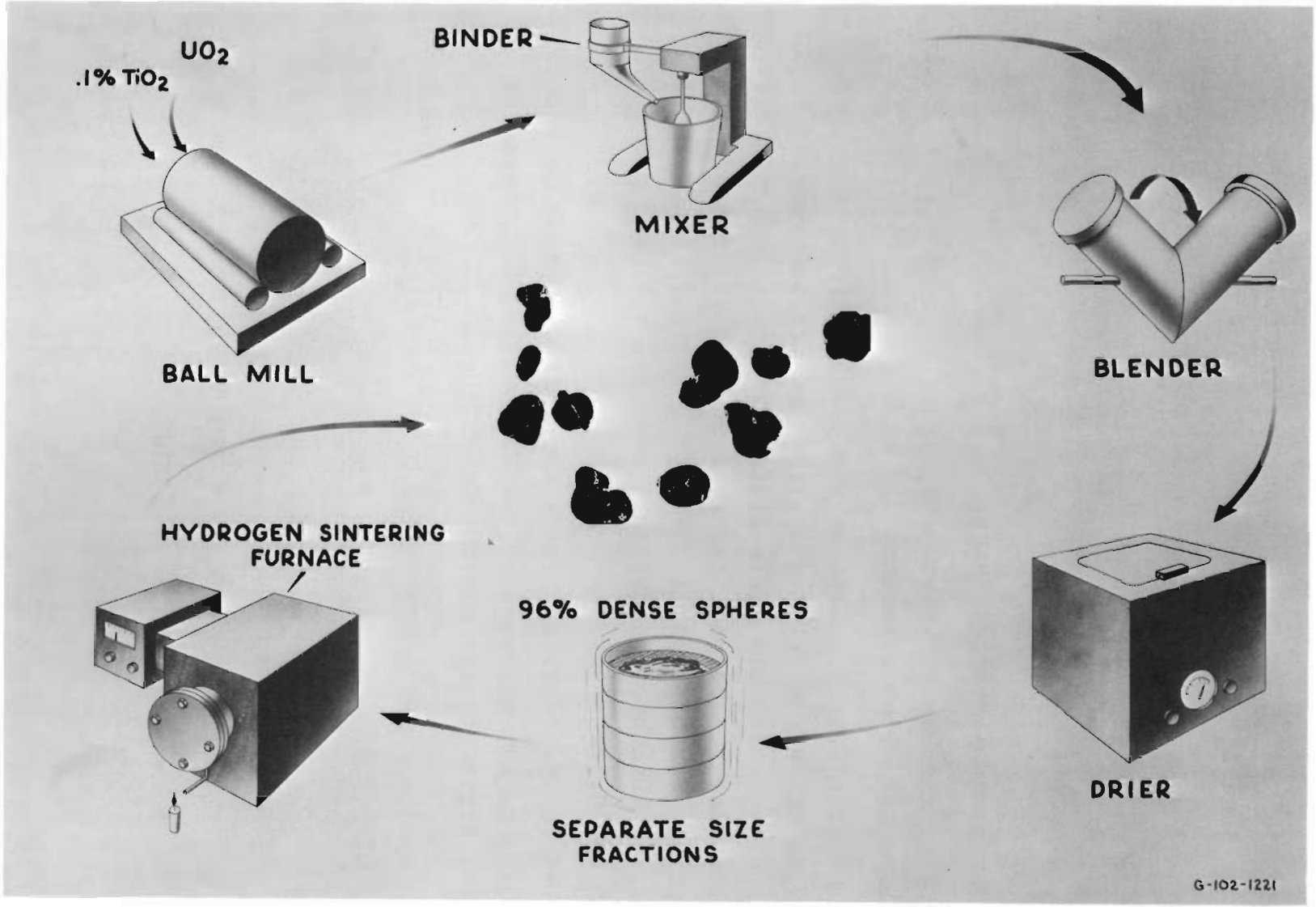

FIGURE 2.1

Spheroidization of UO_2

Pneumatic Impaction of BeO and BeO-Containing Fuels -

J. R. Hague

High energy-rate forming studies of BeO and BeO-UO_2 have demonstrated that brittle ceramics can be pneumatically impacted to high density without gross laminar cracking. This achievement, in conjunction with the inherent grain size control of the process, may ultimately lead to the fabrication of brittle materials having improved physical, nuclear, and mechanical properties.

Pneumatic impaction studies have previously shown that although some plastic deformation in ceramics was obtained, brittle behavior is more common. In highly densified ceramics, microcracks are often present; presumably, this cracking is caused by excessive tensile stresses generated by shock wave reflections after initial densification, thermal stress, or springback of the material(s) after impaction. This study was directed toward (1) application of higher temperatures to promote plastic flow, and (2) achievement of tensile stress relief and thermal stress reduction by "cushioning" the compacts with an encapsulating ceramic oxide powder.

Japanese NGK-type, CF-Grade BeO was used for pneumatic impaction studies. This submicron sized material [1] is reported to have excellent sinterability at comparatively lower temperatures (1400 to 1500 °C) than most other grades of BeO; however, the fluffy powder tends to agglomerate easily, resulting in inhomogeneous densification during sintering.[2]

---

(1) Supplied by General Atomic, Div. of General Dynamics Corp., LaJolla, Calif.

(2) R. A. Myer. Unpublished Data. General Atomic, Div. of General Dynamics Corp., LaJolla, California

To achieve adequate green density, pellets of BeO and BeO–25 vol% UO_2 were initially cold pressed without the aid of a binder. Table 2.2 summarizes the pressing data. For the BeO-UO_2 compositions, cold pressing was preceded by mechanically mixing the BeO with 95% dense, spherical UO_2 particles (-100+140 mesh). The ultrafine BeO particles readily agglomerated during blending, and also appeared to coat the UO_2 spheres.

The pellets were subsequently inserted in small graphite cans, and the assemblies centrally located in larger molybdenum impaction containers (5.080 cm OD by 0.160 cm wall thickness by 10.160 cm long). Wall thicknesses of the graphite cans were 0.318 cm for the BeO assemblies and 0.160 to 0.635 cm for the BeO-UO_2 assemblies. The resultant voids between the graphite and molybdenum containers were then vibrationally filled with powdered MgO or Al_2O_3, and the cans were sealed, evacuated, and impacted under conditions shown in Table 2.3.

Visual examination of the impacted BeO specimens revealed no apparent laminar cracking. The pellets had fairly uniform surface characteristics and dimensions. The BeO compacts were subsequently fractured by impact and, again, revealed no internal laminations. The BeO-UO_2 specimens were similarly intact, with the exception of a checkering effect on their surfaces.

Mercury porosimetric densities of the BeO pellets (Table 2.3) revealed no significant variation under pressures resulting in mercury penetration of pores ranging from 100 to 0.06 micron in diameter. H_2O and CCl_4 displacement densities of these specimens were all ~99% TD, indicating that the lower density samples (83 and 85% TD) contained considerable interconnected (open) porosity, the pore size being generally greater than 0.02 micron in diameter

TABLE 2.2

COLD-PRESSING DATA FOR BeO AND BeO–25 vol% UO_2

Material	Pellet No.	Pellet wt, g	Pellet diam, cm	Pellet Length, cm	Pressure, kg/cm^2	Pellet Density, %TD(1)
BeO	1	6.4	1.588	1.969	2275	55
BeO	2	6.3	1.600	1.969	2240	53
BeO	3	8.0	1.588	2.413	2275	54
BeO	5	6.1	1.613	1.854	2205	54
BeO–25 vol% UO_2	3	11.9	1.600	1.803	4480	66
BeO–25 vol% UO_2	4	11.8	1.600	1.816	4480	65
BeO–25 vol% UO_2	5	10.9	1.600	1.727	4480	63

(1) BeO: 3.01 g/cm^3; BeO–25 vol% UO_2: 4.99 g/cm^3

TABLE 2.3

PNEUMATIC IMPACTION DATA FOR BeO and BeO–25 vol% UO_2

Material	Pellet(1) No.	Ceramic(2) Oxide Filler	Preheat(3) Temperature, °C	Impact Pressure kg/cm^2	Pellet(4) Density, %TD
BeO	1	Al_2O_3	1510	14,280	83
BeO	2	Al_2O_3	1600	15,400	85
BeO	3	MgO	1700	18,480	99
BeO	5	MgO	1500	17,500	96
BeO–25 vol% UO_2	3	MgO	1800	19,530	>95
BeO–25 vol% UO_2	4	MgO	1675	15,960	>95
BeO–25 vol% UO_2	5	MgO	1700	19,180	>95

(1) All BeO pellets and BeO-UO_2 pellet No. 3 were inserted in graphite containers having a wall thickness of 0.318 cm. The corresponding graphite wall thicknesses were 0.635 and 0.160 cm for BeO-UO_2 pellet Numbers 4 and 5, respectively.

(2) Metco alumina spray powder, <40 microns particle size, calcined MgO, ~75 to 100 microns particle size

(3) ~15 min normal duration

(4) BeO: 3.01 g/cm^3; BeO–25 vol% UO_2: 4.99 g/cm^3. Densities of the BeO specimens determined by mercury porosimetry; densities of the BeO–25 vol% UO_2 specimens determined by weight and dimensional measurements.

(limits of pore size penetration by H_2O or CCl_4). The absence of extensive open porosity in the denser BeO specimens indicates more complete particle bonding, presumably achieved through the development of higher impact pressures. The effects of preheat temperature, impaction pressure, oxide filler material, and green pellet characteristics are currently being investigated.

Within the limits of accuracy of the UO_2 distribution (25±10 vol%), the bulk density of the BeO-UO_2 specimens were all greater than 95% of theoretical, with no appreciable difference in density noted for variations in impaction conditions.

Photomacrographs of the 85 and 99% dense BeO pellets are shown in Figures 2.2 and 2.3, respectively. The striking contrast is evidence of more extensive particle bonding in the denser specimen. The less dense sample had a chalky appearance, and resolution of microstructural characteristics by polishing and etching (1 min immersion in 200 °F concentrated HF) could not be obtained. However, good resolution was obtained with the denser BeO sample, as evidenced by the higher degree of transparency (Figure 2.3) and microstructural details exhibited in the higher magnification photomicrographs in Figure 2.4. The average grain size of this specimen, as approximated from the photomicrographs, was about 10 microns. Much larger particles, apparent in the photomacrographs of both BeO specimens, were determined to be agglomerates of small (less than 2 microns) BeO particles; a typical agglomerate is shown in Figure 2.5.

Since BeO reportedly reacts with graphite at temperatures as low as 1500 °C, an x-ray diffraction pattern was obtained on BeO pellet No. 2 (impacted at 1600 °C). In support of metallographic evidence, no Be_2C or other phases were detected by x-ray diffraction, within the limits of accuracy of the technique. Likewise, no reaction appeared to have occurred between the graphite and UO_2 in the BeO-UO_2 specimens.

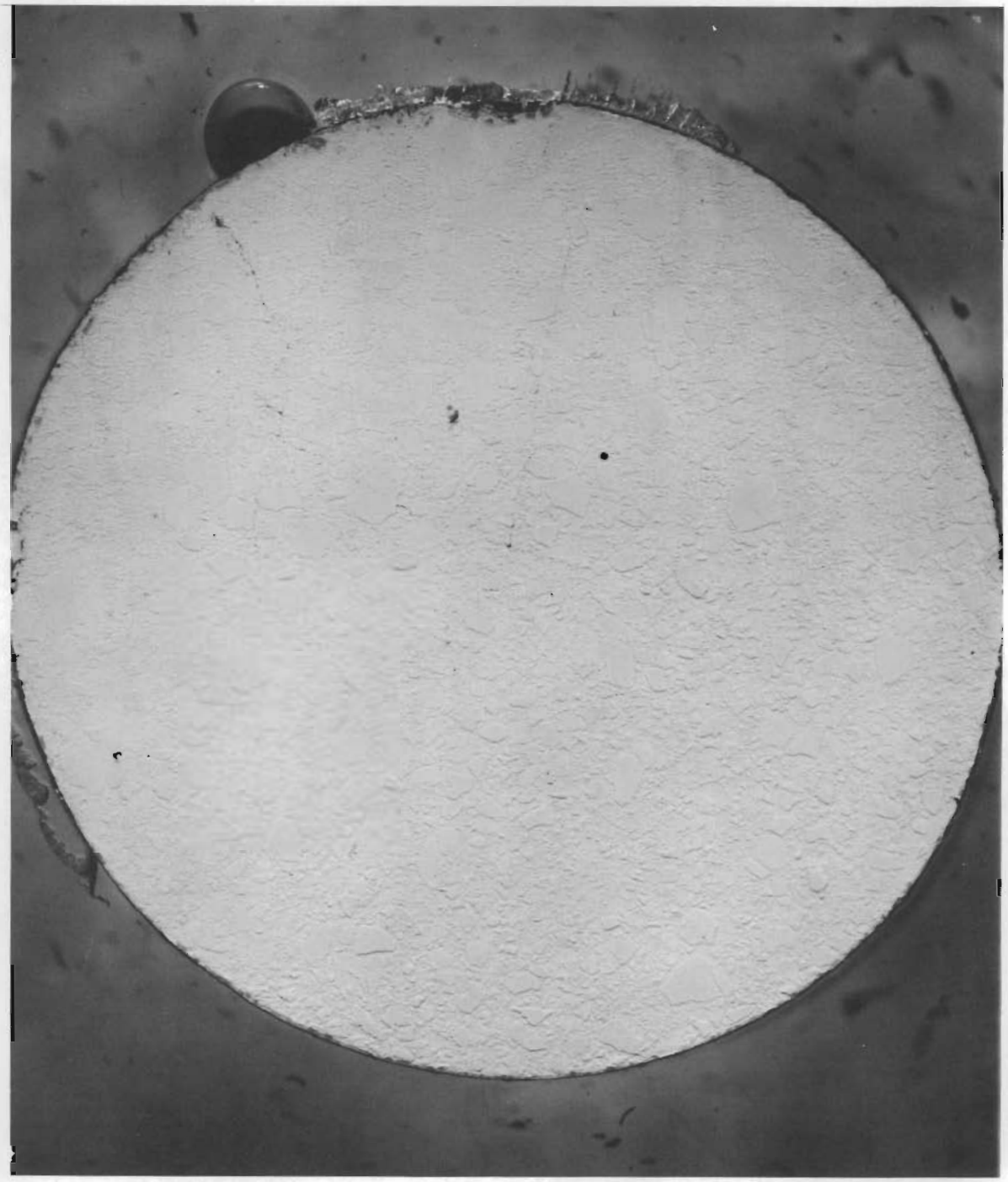

FIGURE 2.2

Photomacrograph of a Cross Section of BeO Pellet No. 2 (85% TD) Pneumatically Impacted at 1600 °C and 15,400 kg/cm^2 (~13-1/2X). No. 565-6334

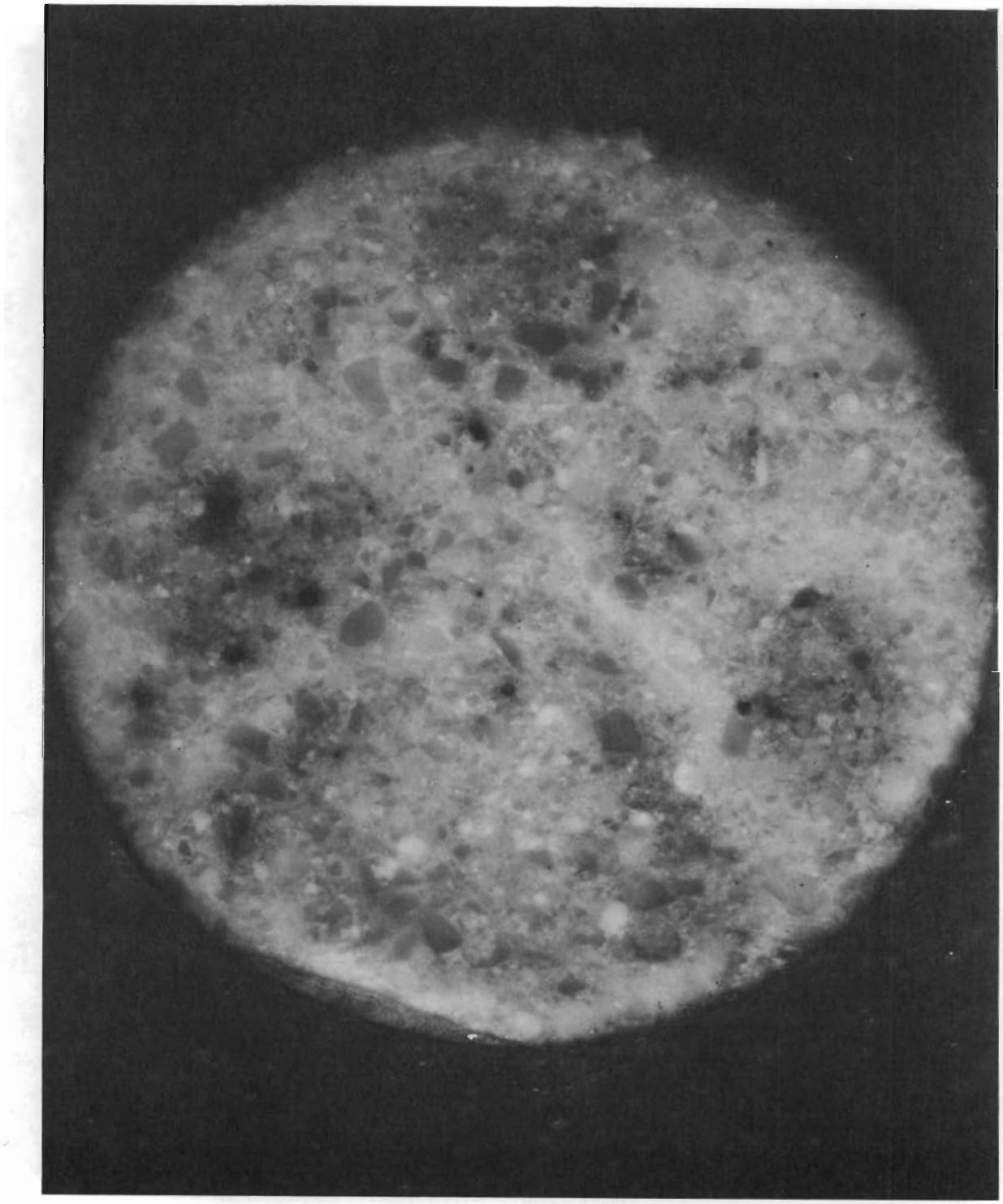

FIGURE 2.3

Photomacrograph of a Cross Section of BeO Pellet No. 3 (99% TD) Pneumatically Impacted at 1700 °C and 18,480 kg/cm^2 (~13-1/2X) No. 565-6445

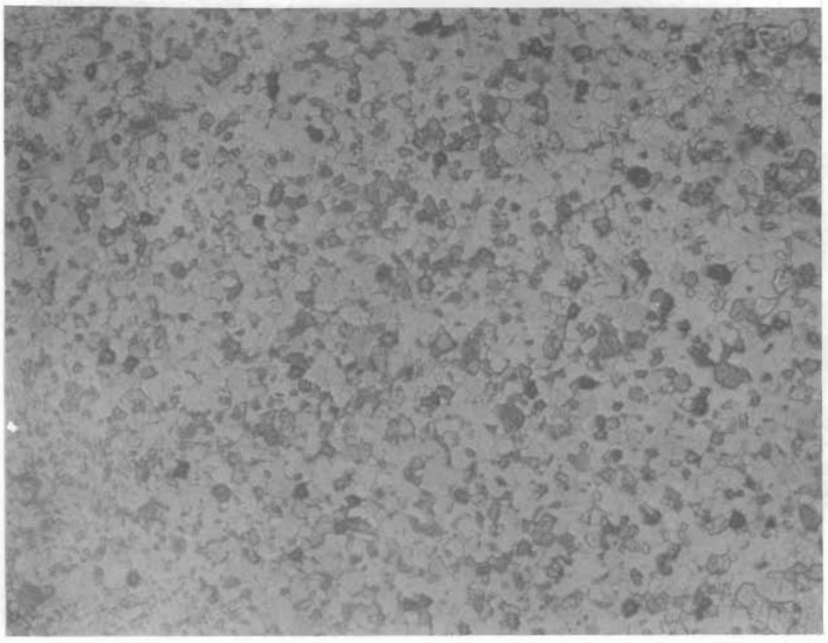

250X

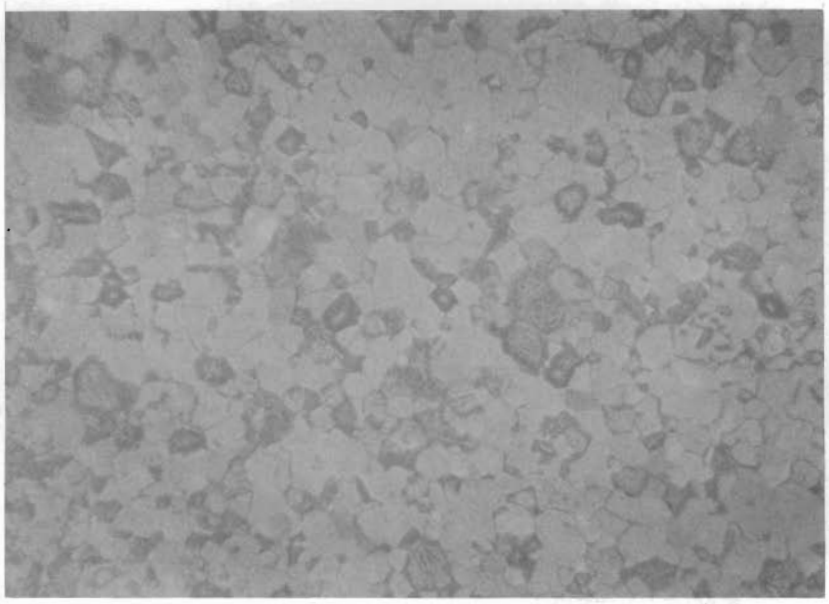

500X

FIGURE 2.4

Photomicrographs of BeO Pellet No. 3 (99% TD), Pneumatically Impacted at 1700 °C and 18,480 kg/cm^2

(Specimen polished and etched by immersing in 200 °F, concentrated HF for 1 min.)

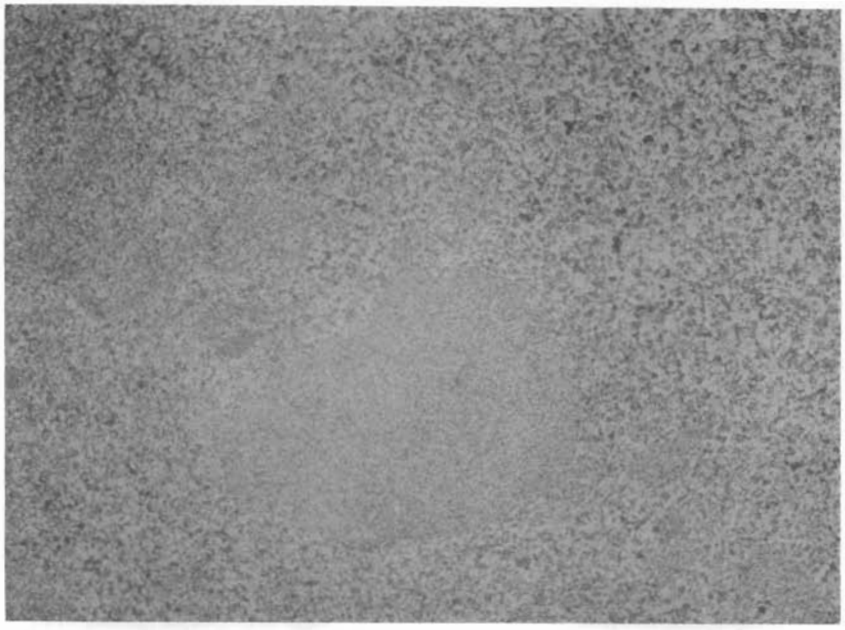

100X

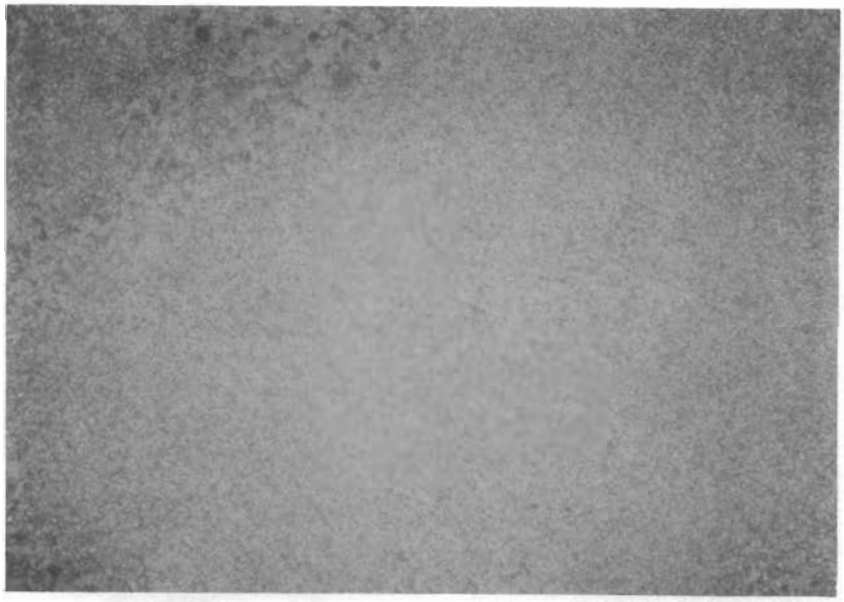

250X

FIGURE 2.5

Photomicrographs of BeO Pellet No. 3 (99% TD), Pneumatically Impacted at 1700 °C and 264,000 psi

(Note agglomeration of small (<2μ) BeO Particles.)

Pellets of BeO-coated, sintered UO_2 spheres (supplied by General Atomic) were fabricated for additional pneumatic impaction studies. During the next quarter, these specimens will be impacted at 1600 to 1800 °C, and directly compared to similarly fabricated BeO-UO_2 mechanical mixtures.

Pneumatic Impaction of Tungsten Powders - P. L. Farnsworth

Pneumatic impaction studies were performed on tungsten powders (-5 micron and -100 micron) to determine the optimum conditions for producing strong, crack-free bodies. These studies are designed to furnish information on bonding mechanisms in materials during pneumatic impaction and to provide preliminary evaluation of pneumatically impacted tungsten as a potential matrix material for dispersed UO_2 fuel elements. Research efforts so far have shown:

- Dense, crack-free bodies can be produced from tungsten powder by means of the pneumatic impaction process.
- Strengths up to 128,000 psi have been achieved.
- Effects of impaction temperature on density and strength are not yet clear; they probably have been masked by unexpected impaction pressure variations.
- Grain growth occurred in specimens air-cooled from impaction temperatures above 1600 °C.
- There is a need for preimpaction powder purification and postimpaction heat treatment experiments to improve strength and ductility.

The major particulars of the program are as follows:

A. Sample Preparation

The preliminary pneumatic impaction studies were performed on nominally -5 micron conventional tungsten powder and -100 micron spherical polycrystalline tungsten particles. About

1 lb of the -5μ powder was vibrated into each of three molybdenum impaction cans, and about 2 lb of the -100μ spherical particles were vibrated into each of three other molybdenum cans.

Preimpaction powder densities were about 25 and 44% TD, respectively. Powder purification was attempted by treating the loaded cans for 5 hr in flowing hydrogen at 1000 °C. Impaction conditions for the six cans, after welding, are summarized in Table 2.4.

The impacted billets (clad with the molybdenum cans) were air-cooled. The outer can was then removed by machining plus acid dissolution. Samples were prepared by cutting and grinding for strength testing, density, microhardness testing, and metallography.

TABLE 2.4

PNEUMATIC IMPACTION CONDITIONS FOR TUNGSTEN

Can No.	Powder Size, μ	Green Density, %	Impaction Temperature, °C	Impaction Pressure, psi
1	-100	44	1400	252,000
2	-100	44	1600	208,000
3	-100	44	1800	209,000
4	-5	25	1400	241,000
5	-5	25	1600	192,000
6	-5	25	1800	146,000

B. Material Evaluation

1. Cracking

The impacted billets were cut in halves, polished, and examined visually for cracks. Figure 2.6 shows the sectioned billets. Samples 2, 3, and 6 were not cracked, indicating that

the greater plasticity of the tungsten at the higher temperatures inhibits crack formation and propagation. Note the extreme deformation and collapse that have taken place in the -5 μ samples because of their low preimpaction density. This may have contributed to the greater cracking tendency observed in these samples.

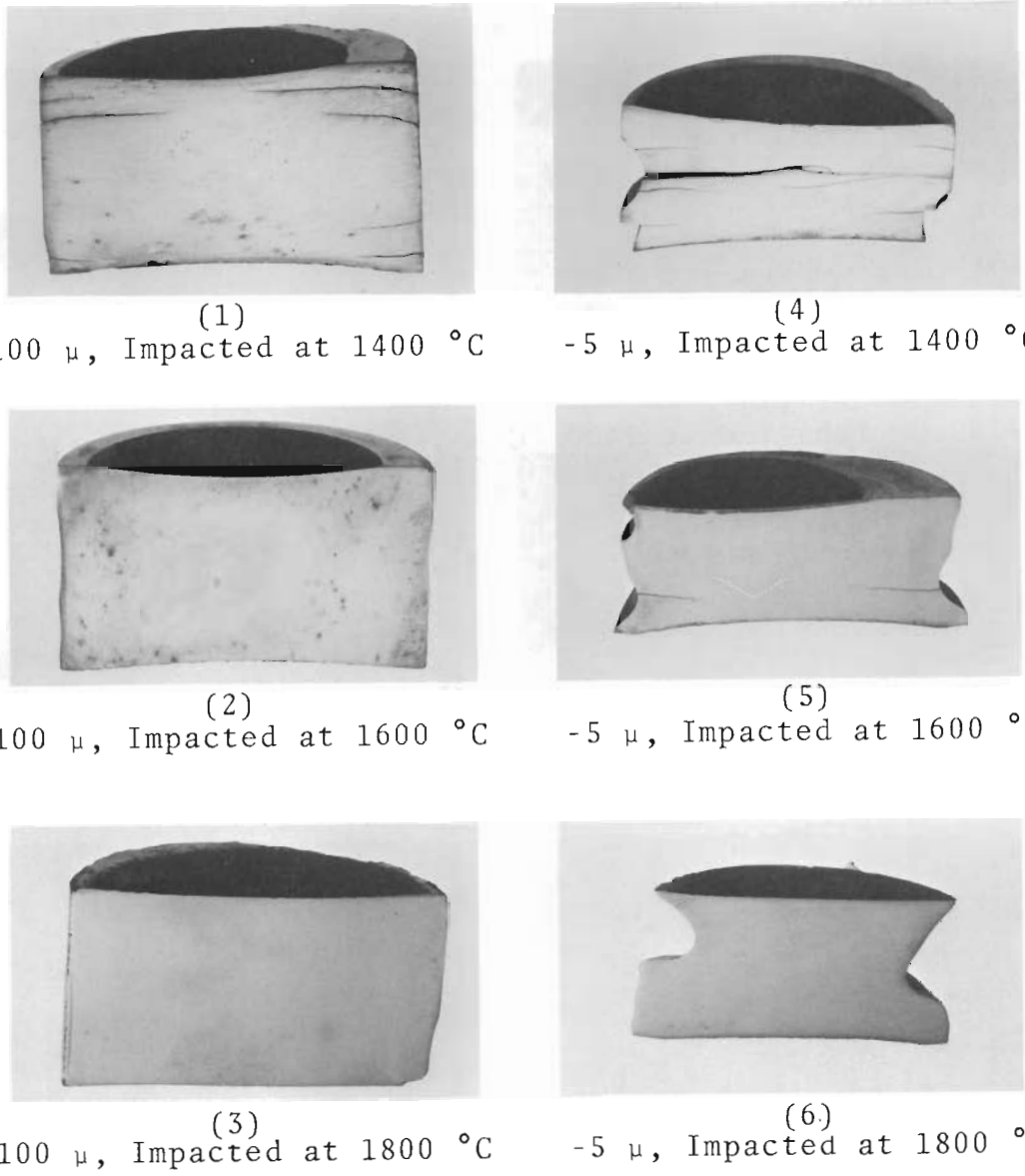

(1) -100 μ, Impacted at 1400 °C

(4) -5 μ, Impacted at 1400 °C

(2) -100 μ, Impacted at 1600 °C

(5) -5 μ, Impacted at 1600 °C

(3) -100 μ, Impacted at 1800 °C

(6) -5 μ, Impacted at 1800 °C

FIGURE 2.6

Pneumatically Impacted Tungsten Billets

2. Metallographic Examination

Microstructures of the as-impacted samples are shown in Figure 2.7. Significant grain growth has occurred in Samples 2 and 3, and some grain growth has occurred in Sample 6. In general, grain growth is undesirable. Faster cooling rates after impaction may inhibit this grain growth.

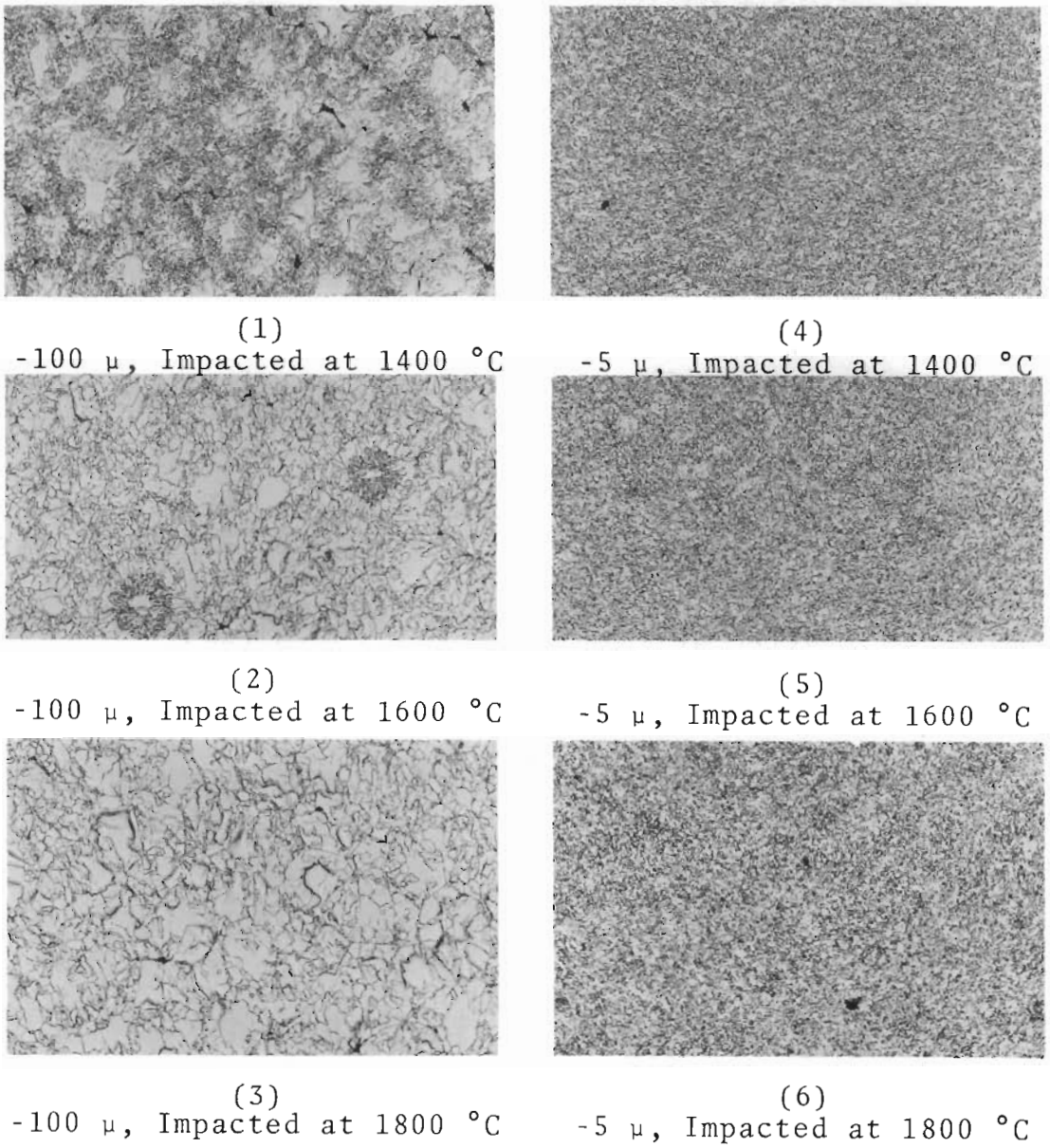

FIGURE 2.7
Microstructures of Pneumatically Impacted Tungsten Powders (100X)

3. Density

Densities were determined on machined shapes which were measured and weighed (Table 2.5). The rather surprising effect that lower densities accompany higher impaction temperatures for the -5 tungsten may not be real. A combination of low green density and low impaction pressure may be the true cause of this effect.

TABLE 2.5

PROPERTIES OF PNEUMATICALLY IMPACTED TUNGSTEN POWDERS

Can No.	Powder Size,μ	Impaction Temperature,°C	Impaction Pressure, psi	Density, %TD	Knoop Microhardness No.*	Modulus of Rupture, psi
1	-100	1400	252,000	99.5 ± 0.5	570	92,500
2	-100	1600	208,000	99.5 ± 0.5	510	87,600
3	-100	1800	209,000	99.5 ± 0.5	459	96,000
4	-5	1400	241,000	97.0 ± 0.5	529	127,000
5	-5	1600	192,000	96.0 ± 0.5	487	115,000
6	-5	1800	146,000	94.5 ± 0.5	407	128,000
Plate	--	--	--	98.0 ± 0.5	570	398,000

* Average of 8 numbers

4. Microhardness

Knoop microhardness measurements were made on all six samples (Table 2.5). The hardness of commercial rolled tungsten plate is included for comparison. These results apparently reflect annealing, recrystallization, and grain growth effects at higher impaction temperatures.

5. Strength

With the use of an Instron testing machine, preliminary room temperature modulus of rupture values were obtained on specimens of the impacted tungsten billets in four-point bending. All specimens were polished through 3/0 silicon carbide polishing paper before testing (Table 2.5). Temperature effects are not obvious; they may be masked by pressure variations. In any event, the achieved strengths do not approach the strength of commercial rolled tungsten plate, indicating that the particles

are not well bonded together, and that powder purification treatments and/or postimpaction heat treatments are required to fully develop the strengths of the impacted tungsten bodies.

Pneumatic Impaction Studies - E. A. Snajdr

Nickel and aluminum powders were consolidated by pneumatic impaction (Table 2.6). Physical properties are to be studied as a function of the process variables.

TABLE 2.6

PNEUMATIC IMPACTION CONDITIONS

Powder Material	Density, g/cc Before Impaction	Impaction Temperature, °C	Impaction Pressure, psi
Nickel	54.3	1250	285,000 (198,000*)
Nickel	55.7	1200	273,000
Nickel	54.3	1200	284,000
Nickel	54.8	1000	279,000
Nickel	59.5	750	282,000
Nickel	54.6	500	183,000
Aluminum	66.3	550	407,000
Aluminum	62.0	550	334,000
Aluminum	62.0	450	337,000
Aluminum	60.3	350	323,000

* Pressure reading from a cathode ray oscilloscope. All other values from an oscillograph.

In addition to the compaction of powders, a method was investigated for reliably determining the pressures applied during the pneumatic impaction process. Present methods use an oscillograph. A cathode ray oscilloscope was used for one impaction

because it was thought to have a response superior to the oscillograph. The instrument was calibrated at static pressures four times less than the dynamic pressure pulses of the pneumatic impaction process. These values were then extrapolated to the pressure range of interest (200,000 to 400,000 psi). On this basis, the duration of a pressure pulse of the pneumatic impaction process is 3 msec. The rise time to peak pressure is 1.5 msec.

Elastic Properties of Materials - J. R. Hague

Electronic equipment was installed for rapidly and accurately measuring the dynamic moduli of elasticity and damping factor (internal friction) of materials. In contrast to static techniques, the dynamic method is nondestructive, simpler and extremely more sensitive, thus allowing macro- and microstructural characteristics of materials to be more closely examined.

Briefly, the dynamic apparatus works on the principle of a simple beam excited in resonance. A test rod is supported at its nodal points by adjustable cross wires or foam rubber. Mechanical vibrations are transmitted to the specimen from a piezoelectric transducer by means of a fine coupling wire. In turn, a similar system receives the mechanical vibration from the specimen, and transmits the converted electrical signal to an electronic frequency counter, where frequencies of 600 to 25,000 cycles/sec are periodically read out to an accuracy of 0.01 to 0.001%.

In operation, the sample is vibrated in flexural, longitudinal, or torsional resonance by means of a variable frequency oscillator. These resonant frequencies are identified by observing the vibrational amplitude and oscilloscope Lissajous figures. The elastic moduli can then be calculated according to

equations derived by Pickett[1], given the resonant frequency, mode of vibration, dimensions, density, and Poisson's Ratio of the specimen. Likewise, the internal friction (measure of a body's ability to absorb mechanical energy when subjected to a periodic vibration) can be simultaneously obtained by observing the decay in vibration amplitude during free oscillation, after the energy fed to the specimen has been interrupted.

A mild steel test cylinder (0.374 in. diam by 4.000 in. long) was used to check out the equipment. Flexural, longitudinal and torsional resonant frequencies were determined and the elastic moduli were calculated. Results are shown in Table 2.7. The experimental data were in excellent agreement with values reported in the literature.[2] Furthermore, good agreement was also obtained with moduli calculated from the fundamental, fractional fundamental, and harmonic frequencies of the specimen. These frequencies were identified by observing the associated Lissajous figures on the oscilloscope. The fundamental resonant frequencies and harmonics appear as a circle or ellipse (one lobe), whereas the fractional fundamental frequencies are inversely related to the observed number of lobes (e.g., two lobes for half the fundamental frequency, etc.,), the latter relation holding only for flexural vibration. The harmonic frequencies are, in turn, related to the fundamental resonant frequencies of the sample by a shape factor [1] for flexural vibration, and direct integer multiples for torsional or longitudinal vibration. The slightly higher moduli obtained from the harmonic flexural frequencies are probably due to a small inaccuracy in selecting the appropriate shape factor.

---

(1) Gerald Pickett. Proc. ASTM, vol. 45, pp. 846-865, 1945.

(2) Handbook values list E = 28 - 30 x 10^6 psi, G = 11 - 12 x 10^6 psi, μ = 0.25 - 0.30

TABLE 2.7

EXPERIMENTAL ELASTIC PROPERTY DATA FOR MILD STEEL[1]

Vibration	Overtone	Experimental Frequency, cycles/sec	Resonant Frequency, cycles/sec	Modulus of Elasticity, 10^{-6} psi	Modulus of Rigidity, 10^{-6} psi	Poisson's Ratio, μ
Flexural	1/3 Fundamental	1374	4122	30.2		0.26[3]
Flexural	1/2 Fundamental	2061	4122	30.2		0.26[3]
Flexural	Fundamental	4121	4121	30.2		0.26[3]
Flexural	1st Harmonic	10949	4155	30.7		0.28[3]
Flexural	2nd Harmonic	20446	4151	30.6		0.28[3]
Torsional	Fundamental	15987	15987[2]		12.0	0.25[4]
Longitudinal	Fundamental	25282	25282[2]	30.1		0.25[3]

(1) Weight: 56.51 g; dimensions: 0.374 in. diam by 4.000 in. long

(2) From Pickett, $f_2/f_1 = 2.635$, $f_3/f_1 = 4.925$

(3) Poisson's Ratio calculated according to equation: $\mu = 1/2\ (E/G)-1$, where E = value calculated and G = 12 x 10^6 psi.

(4) As for (2), except E = 30 x 10^6 psi

Preliminary tests were also made on three tungsten specimens with the following fabrication history:

1. 100μ spherical tungsten powder, pneumatically impacted at 1600 °C and 208,000 psi (97.4% TD, 0.126 in. by 0.127 in. by 1.000 in. long prism).

2. 5 μ spherical tungsten powder, pneumatically impacted at 1400 °C and 241,000 psi (95.3% TD, 0.124 by 0.125 in. long prism).

3. Commercially supplied tungsten rolled plate (96.4% TD, 0.049 by 0.123 by 1.000 in. long prism).

Results are shown in Table 2.8. Size limitations prohibited the determination of elastic moduli from longitudinal or torsional frequencies (>25,000 cycles/sec).

The two pneumatically impacted specimens each exhibited two distinct, flexural resonance points, resulting in two elastic moduli values about 2 and 9% apart, for the 5 μ and 100 μ tungsten specimens, respectively. This discrepancy is believed to be due to

TABLE 2.8

EXPERIMENTAL ELASTIC PROPERTY DATA FOR TUNGSTEN (FLEXURAL VIBRATION)

Specimen Number	Density, % TD	Overtone	Experimental Frequency, cycles/sec	Resonant Frequency, cycles/sec	Elasticity, 10^{-6} psi(4)
1 (1) (100 μ)	97.4	1/4 Fundamental	5585	22340	58.4
	97.4	1/3 Fundamental	7448	22344	58.4
	97.4	1/2 Fundamental	11170	22340	58.4
	97.4	Fundamental	22340	22340	58.4
	97.4	1/3 Fundamental	7124	21372	53.4
	97.4	Fundamental	21380	21380	53.5
2 (2) (5 μ)	95.3	1/3 Fundamental	7120	21360	54.3
	95.3	Fundamental	21340	21340	54.3
	95.3	1/3 Fundamental	7064	21192	53.5
	95.3	Fundamental	21190	21190	53.5
3 (3) (Commercial)	96.4	1/3 Fundamental	2990	8970	55.9
		1/2 Fundamental	4505	9010	56.3
		Fundamental	9000	9000	56.2

(1) 100 μ spherical tungsten powder, impacted at 1600 °C and 208,000 psi (weight: 4.925 g; dimensions: base, 0.127 in; height, 0.126 in.; length, 1.000 in.)

(2) 5 μ spherical tungsten powder, impacted at 1400 °C and 241,000 psi (weight: 4.812 g; dimensions: base, 0.124; height, 0.125 in.; length, 1.000 in.)

(3) Commercial tungsten rolled plate (weight: 1.822 g; dimensions: base, 0.049 in.; height, 0.123 in.; length, 1.000 in.)

(4) E calculated by assuming Poisson's ratio of 0.33 for tungsten

variations in the edge dimensions, since one edge of each sample appeared slightly tapered (0.001 in.). If the two moduli values of each sample are averaged, good agreement is shown with the commercial tungsten specimen, considering the density variations involved. Excellent agreement was also obtained with moduli calculated from the fundamental and fractional fundamental resonant frequencies of all three tungsten samples. This correlation will become increasingly important when testing materials and shapes having fundamental flexural resonances greater than the limits of the equipment.

PART III - BASIC DEVELOPMENT OF PLUTONIUM FUELS

Detection of Oils in Fuel Supplies - H. J. Anderson and D. S. Skeie*

Organic materials, such as oil, must be excluded from nuclear fuels because they can supply hydrogen, during irradiation, that may lead to hydriding of the fuel element Zircaloy cladding. There is also the possibility that excessive carbon from oil impurity in the fuel may enter into side reactions with moisture impurity or with excess oxygen from the fuel to release hydrogen or carbon oxide gases. Since in-reactor test studies of UO_2-PuO_2 fuel elements can be abruptly terminated by cladding failures caused by hydriding or internal gas pressures,[1] an accurate analysis is required of organic impurities in fuel materials before fabrication.

Methods were developed for continuous extraction of UO_2-PuO_2 fuel materials and for infrared analysis of the carbon tetrachloride (CCl_4) extracts.

Analysis of CCl_4 extractions of oil contaminated powders removed from a faulty disc pulverizer and storage containers showed a pickup of organic (oil) materials during the fuel processing. The infrared analysis of the CCl_4 extracts indicated an organic (C-H) material was present from 5 to 300 ppm in the crushed powders. One test of carbon content by combustion techniques indicated about 3000 ppm versus 200 ppm carbon in input fuel materials. The combustion technique for carbon content is not routinely used as an indicator of organic content in fuels because silicone oils often are used in fuel processing equipment.

---

(1) Ceramics Research and Development Operation, Quarterly Report, October - December, 1963. Hanford Laboratories, General Electric Company, HW-76304.

* Chemist, Physical Analysis

The continuous extraction and infrared technique does, however, include detection of silicone oils by measurement of the ($Si-CH_3$) deformation band.

If normal precautions are taken during the extraction of the UO_2-PuO_2 fuel inside the glovebox, radioactive contamination is low enough to permit the mounting of infrared samples in an open hood. The samples are then analyzed in a routine laboratory room with little extra care. After about one year of operation, no serious contamination of the infrared spectrophotometer has taken place.

Approximately 50 g of powder fuel are extracted with 150 ml CCl_4 in a conventional 60 ml Soxhlet extraction apparatus, using a mantle heated 300 ml boiling flask. Extraction requires a minimum of 4 hr. After extraction is complete the extract is reduced to about 5 ml by evaporation of the CCl_4 solvent and analyzed by infrared absorption.

Infrared analyses of concentrated carbon tetrachloride extracts of PuO_2-UO_2 fuel mixtures were completed on an infrared spectrophotometer equipped with a NaCl prism. The following instrument settings are recommended for the Perkin-Elmer Model 21:

Resolution	927
Response	1:1
Gain	2.5 (normal for our instrument)
Speed	Pulley 2, setting 4
Suppression	0
Scale	1 x
Source I	0.3A
Sample Thickness	0.5 mm
Region Scanned	2 to 10 μ

The instrument is used in the dual beam recording mode with the reference beam compensated by CCl_4. Standards of SAE-30 (hydrocarbon) and Dow 702 (silicone) oil were prepared and calibration curves were completed. The C-H stretching band (3.33 μ) and Si-CH_3 deformation band (8.87 μ) were selected as the analytical bands. Absorption measurements are corrected for background by an averaging technique. Some nonlinearity of the silicone oil calibration curve was noted at 0.4 vol% but the hydrocarbon curve is linear throughout the useful analytical (0 to 0.4%) range. The oil concentration of the extracts is determined from the appropriate calibration curve and the contamination of the fuel calculated.

Plutonia Microspheres - J. B. Burnham

A crush strength analyzer was designed to evaluate plutonium ceramic particles for use in cermets. The apparatus used the same pneumatic-hydraulic loading system as that used at Mound Laboratory. Load measurement is made directly with a load cell rather than with the beam deflection method used by other investigators. The design load range is from 0 to 2.5 kg maximum, depending on the particles being tested. Any load in this range may be selected for full scale recorder deflection. Precision will be ±1/2% of the full scale reading. This equipment is designed to test 40 to 60 particles per hr when operated in a hood, with about a 20% increase outside the hood.

Compaction Studies of Spheroidized UO_2 - L. R. Bunnell

A 50 lb force vibrator and accessory equipment (Figure 3.1) were used to evaluate the compaction characteristics of the UO_2 spheres produced by an agglomerative method reported on page 2.1 of this report. In all, 18 different three-component mixes were evaluated (Table 3.1).

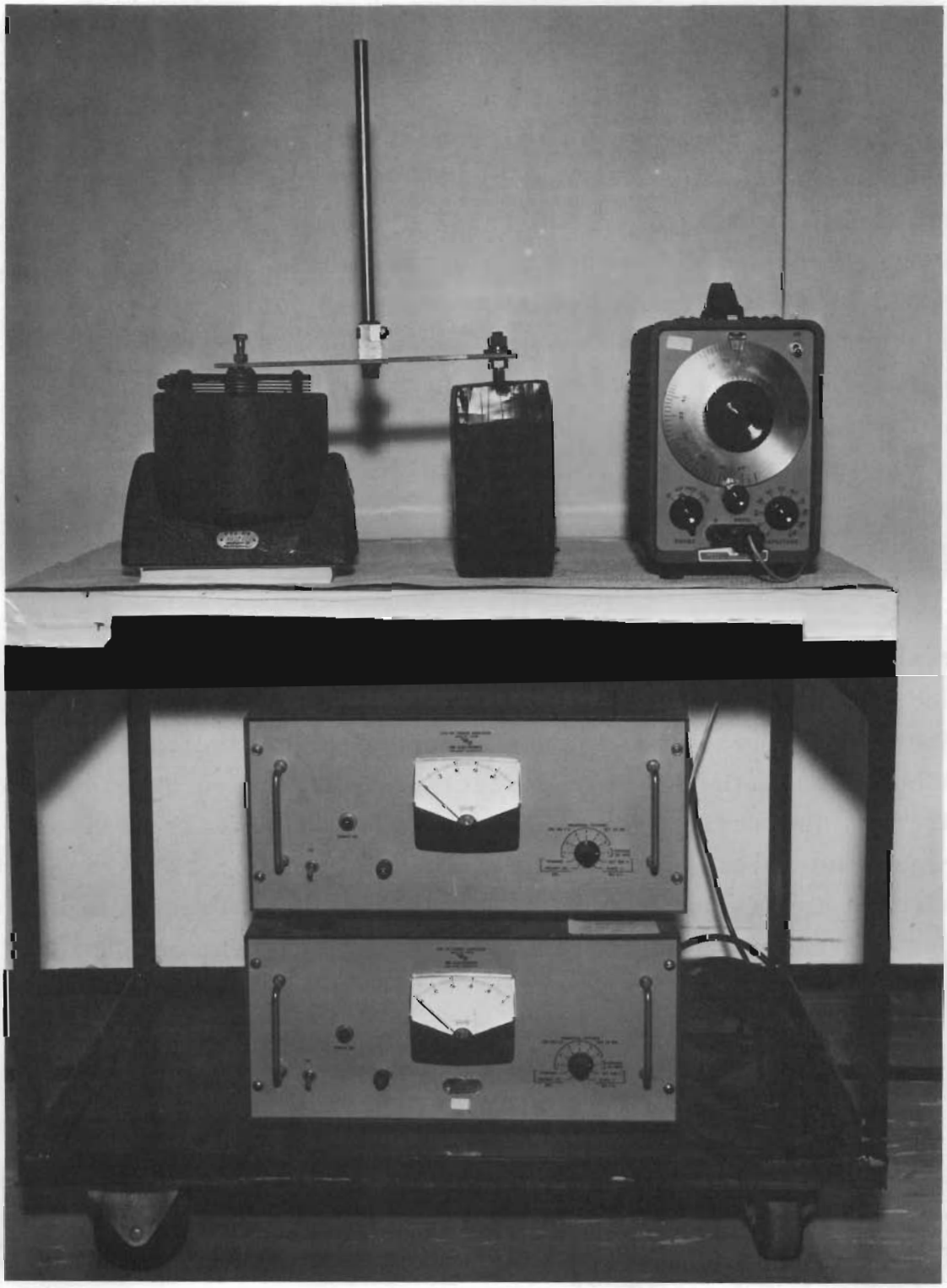

FIGURE 3.1
A 50 lb Force Vibrator

TABLE 3.1

COMPACTION EFFICIENCIES OF AGGLOMERATED PARTICLE MIXTURES

Mixture Number	wt% Coarse -6 + 10	wt% Medium, -35 + 65	wt% Fine -150	Compaction Efficiency,%
1	60	15	25	89.0
2	60	20	20	88.2
3	60	25	15	86.9
4	62	12	26	88.2
5	62	20	18	87.9
6	62	24	14	86.4
7	65	15	20	88.6
8	65	20	15	87.5
9	65	22	13	87.3
10	68	12	20	89.3
11	68	16	16	88.9
12	68	20	12	88.5
13	60	10	30	88.7
14	55	15	30	87.5
15	55	20	25	87.8
16	70	5	25	88.8
17	75	5	20	87.4
18	75	10	15	86.8

Each mixture was compounded in a 400 g batch, mixed well, and spread on a belt feeder. The frequency of the vibrator was varied between 1000 and 2000 cycles/sec. The vibration time was 7 min. The density of the compact was then determined. Three trials were made for each mix, and the reproducibility was about 0.5%. Figure 3.2 is a plot of ternary composition versus compaction efficiency; two clear maxima, denoted by circles, can be seen.

Mixture No. 1 was vibrationally compacted on a 5000 lb force electrodynamic vibrator, and a compaction efficiency of 90.7% was achieved.

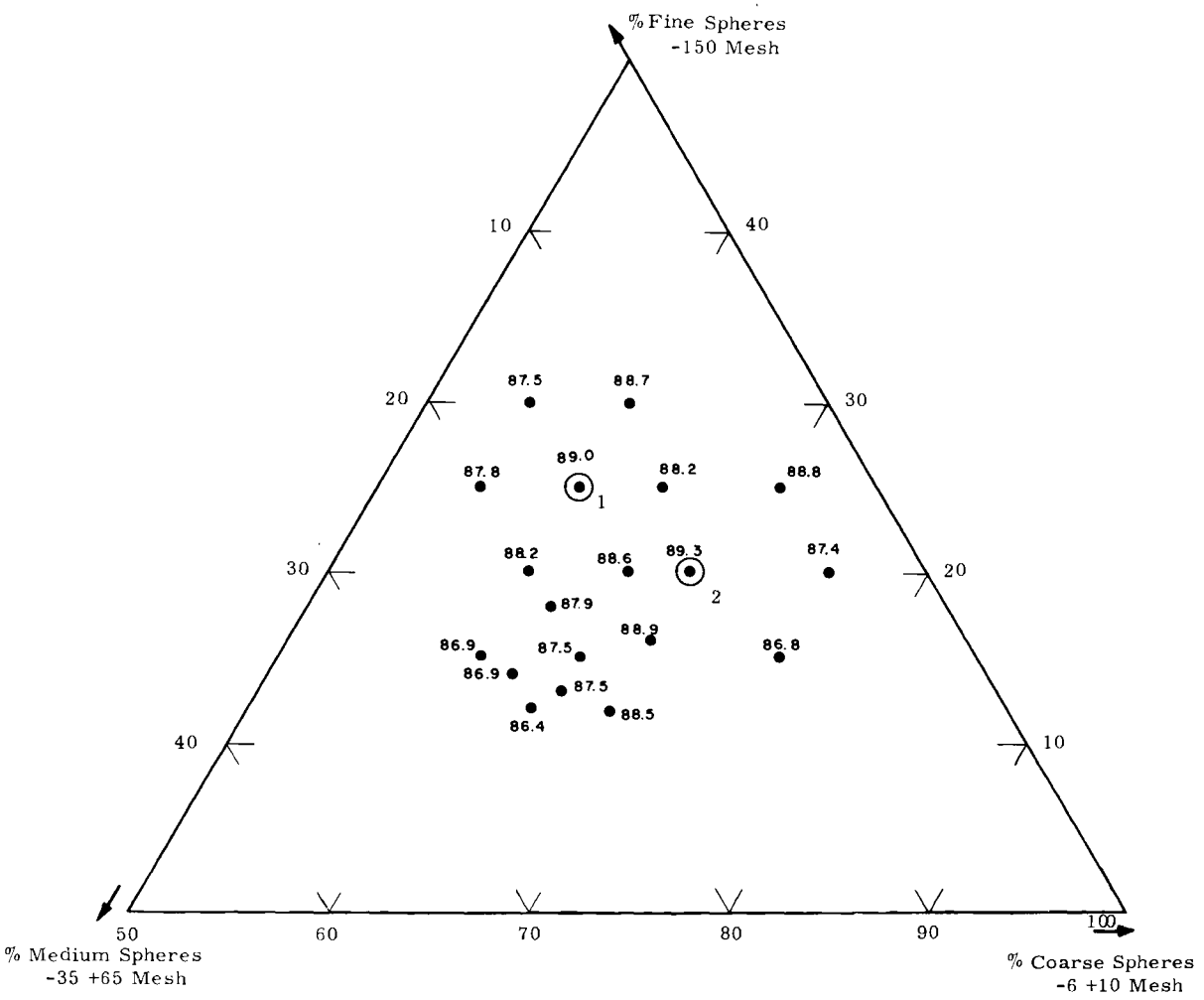

FIGURE 3.2

Packing Efficiencies Achieved as a Function of Composition of a Three-Component Mix

Plutonium Ceramics Irradiations - J. A. Christensen and C. A. Hinman

Irradiation to high exposure of plutonium ceramic wafer specimens continued uneventfully. Status of in-reactor capsules is summarized in Table 3.2. Fuel materials listed in Table 3.3 were previously discharged and subjected to postirradiation examination consisting, basically, of metallography and x-ray diffraction analyses.

TABLE 3.2

PLUTONIUM CERAMICS CURRENTLY BEING IRRADIATED

Material	GEH-14-	Reactor Insertion Date	Reactor Insertion Cycle	Fission/cm^3 as of 10-1-65	Goal Exposure Fissions/cm^3	Intended Discharge Date	Intended Discharge Cycle
PuN, Impacted	405	11-63	MTR 198	97.5×10^{20}	172.5×10^{20}	5-67	MTR 259
PuN, Impacted	407	11-63	MTR 198	43.5×10^{20}	77.5×10^{20}	5-67	MTR 259
PuC, Arc-cast	409	7-63	ETR 56	76.5×10^{20}	150×10^{20}	1-68	ETR 96
PuO_2, 95% TD, Sintered	411	9-63	MTR 196	102×10^{20}	166×10^{20}	1-67	MTR 256
βPu_2O_3, 95% TD, Sintered	413	9-63	MTR 196	73.0×10^{20}	116×10^{20}	1-67	MTR 256
PuN–50 vol% W, Impacted	538	2-64	MTR 203	60.5×10^{20}	124×10^{20}	8-67	MTR 266
PuN–50 vol% W, Impacted	540	2-64	MTR 203	35.0×10^{20}	62.5×10^{20}	8-67	MTR 266
PuN–24 vol% Pu, Arc-cast	549	2-64	MTR 203	35.0×10^{20}	67.0×10^{20}	8-67	MTR 266
PuN–15 vol% Pu, Arc-cast	551	2-64	MTR 203	15.5×10^{20}	32.0×10^{20}	8-67	MTR 266

TABLE 3.3

PLUTONIUM CERAMICS PREVIOUSLY IRRADIATED

Material	GEH-14-	Reactor Insertion Date	Reactor Insertion Cycle	Reactor Discharge Date	Reactor Discharge Cycle	Exposure Fissions/cm^3	Exposure % Pu Fissioned	Exposure Mwd/T Fuel
PuN, Impacted	406	9-63	MTR 196	2-64	MTR 202	20×10^{20}	6.2	57700
PuC, Arc-cast	408	6-63	ETR 55	9-63	ETR 57	8.3×10^{20}	2.6	23900
PuO_2, 95% TD, Sintered	412	9-63	MTR 196	2-64	MTR 202	22×10^{20}	9.1	84900
PuN–50 vol% W, Impacted	539	2-64	MTR 203	8-65	MTR 210	15×10^{20}	9.2	26000
PuN–15 vol% Pu, Arc-cast	550	2-64	MTR 203	7-65	MTR 209	8.0×10^{20}	6.2	56900

Irradiation Performance of Fast Reactor Fuel Candidates - UN–20 wt% PuN - J. A. Christensen and C. A. Hinman

Exploratory irradiations investigating burnup effects on highly rated UN–20 wt% PuN fast fuels were completed with the discharge of the third experimental capsule of the series. Irradiation conditions for each of the test capsules are summarized in Table 3.4.

TABLE 3.4

EXPLORATORY TESTS OF UN-PuN FAST REACTOR FUEL CANDIDATES

Test	Fuel	Linear Heat Rating, W/cm	Exposure f/cm^3	Exposure % Original Pu Fissioned	Exposure MWd/T Fuel
GEH-14-616	UN–20 wt% PuN, 70% TD, 1.09 cm diam	2130	2.4×10^{20}	4.9	9450
GEH-14-617	UN–20 wt% PuN, 70% TD, 1.09 cm diam	2130	6.0×10^{20}	12.5	22000
GEH-14-618	UN–20 wt% PuN, 70% TD, 1.09 cm diam	2130	13.0×10^{20}	37.0	47670

The highest burnup fuel (GEH-14-618) displayed features qualitatively similar to those observed in the lower burnup specimens. A transverse cross section (Figure 3.3) exhibited the following four multiphase zones:

Zone 1 is a central metallic region extending to 1/4 of the fuel radius. This region consists of a metal matrix and two dendritic phases which appear to have precipitated from a molten solution on cooling through a second order transition. The metallic character of this region was established by its microstructure and by its machining characteristics when drilled samples were taken.

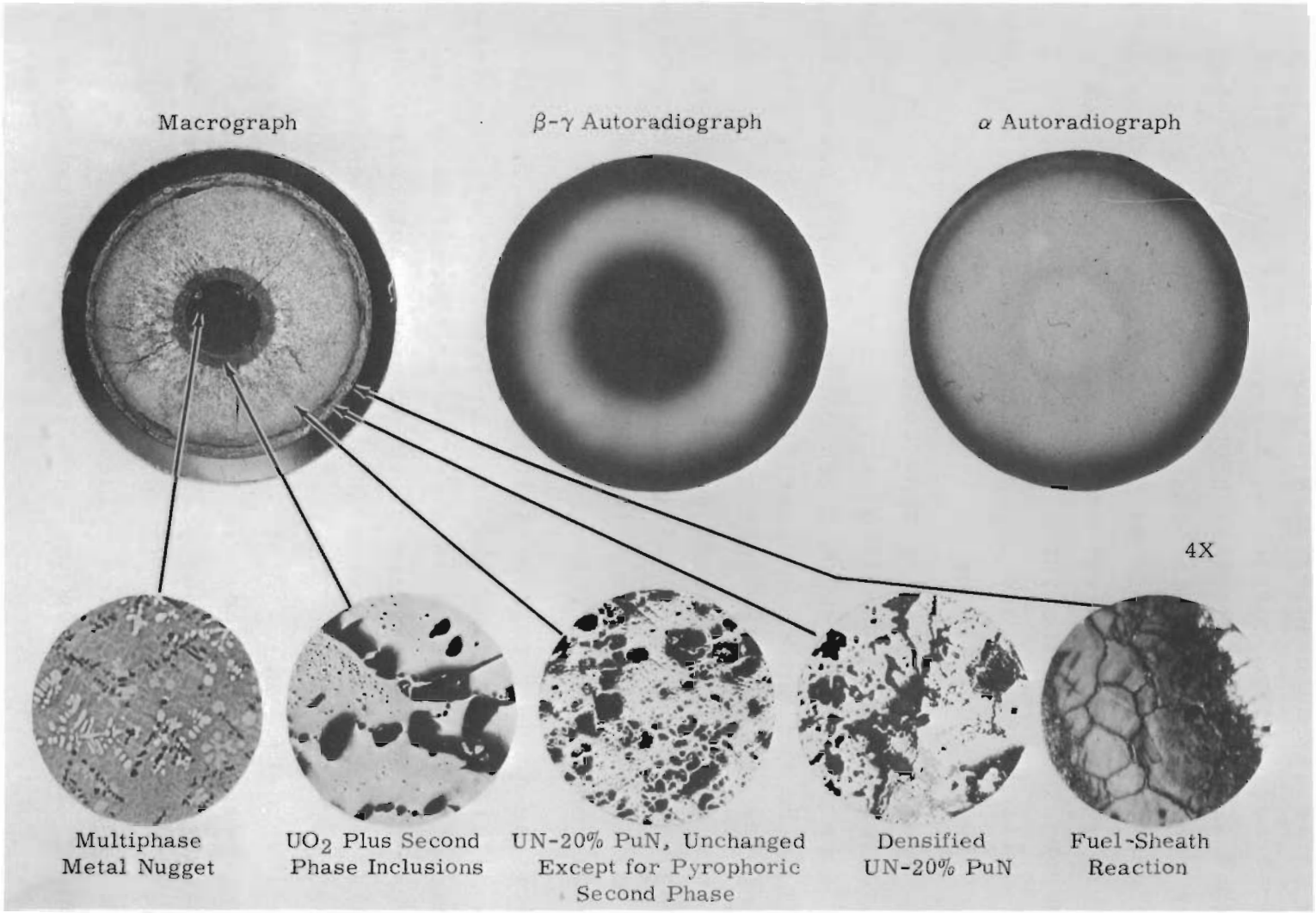

FIGURE 3.3

UN–20 wt% PuN Irradiated to 13 x 10^{20} Fissions/cm^3 at 2130 W/cm (Linear)(GEH 14-618)

Alpha autoradiographs (Figure 3.3) showed no detectable Pu in this region while β-γ autoradiographs(Figure 3.3) indicate this to be the most radioactive portion of the fuel. Drilled samples from this zone were 20 to 100 times higher in β-γ activity than samples from other fuel regions. These observations suggest that this region consists principally of fission fragment metals which may have migrated up the gradient by thermal decomposition of volatile compounds (i.e., the ruthenium oxides). Radiochemical analyses of drilled samples are expected to reveal which isotopes have migrated to the fuel center.

Zone 2 is a distinct annular zone comprising the region between approximately 1/4 and 3/8 of the fuel radius. This region consists of a ceramic matrix with a few equiaxed metal precipitates. This appears to be the material identified as UO_2 by x-ray diffraction analyses in a similar fuel pin discharged after reaching 2.4×10^{20} fissions/cm^3. Autoradiographs and drilled samples show this region to be slightly enriched both in fission fragments and plutonium. Possibly the Pu originally present in the porous fuel center was concentrated into this region.

Zone 3 is an annular region extending over one half of the fuel radius. This consists of the originally porous mixed nitride, unaltered except for formation of a few metal precipitates concentrated near the inner boundary of the region. Autoradiographs show a regular increase in fission fragment concentration toward the outer edge of this region. This was anticipated because of flux depression in the fuel. Plutonium concentration in this region is uniform, as expected. This was the only portion of the fuel appreciably oxidized during prolonged exposure to room temperature air. When drilled samples were taken in this region considerable "sparking" occurred. This was most intense nearest the fuel center, indicating an increase in pyrophoricity, perhaps because of the metal inclusions.

Zone 4 is the outermost (1/8 of radius) fuel annulus. This is also UN–20 wt% PuN but less porous than the parent material. Because of the steep flux gradient across the fuel radius, this region has sustained about five times the average fission density. Such exposures should cause gross swelling which sometimes manifests itself as apparent densification because the swelling porosity, which is too small to be resolved at low magnifications, causes expansion of the fuel into the pores remaining after sintering. As expected, this zone has a higher fission fragment concentration than the mixed nitride nearer the center. No Pu concentration gradients were detected in this region.

Fuel-sheath reaction is evident in the form of apparent deterioration of grain boundary regions in the stainless steel near the inner surface of the cladding. The extent of the reaction was approximately the same as observed in lower burnup specimens, i.e., the sheath is affected to about 10% of its thickness.

Work in progress includes:

- Electron microprobe analyses on the fuel sheath reaction zones from specimens GEH-14-616 and -618.
- A hardness survey of the transverse fuel section to aid in identifying the various phases present.
- X-ray diffraction and fluorescence surveys of the fuel, also to contribute to phase identification.
- Hardness measurements across the fuel-sheath reaction zone.
- Detailed metallography of the fuel-sheath reaction zone.
- Radiochemical analyses on drillings from various radial positions of specimens GEH-14-616 and -618 to quantitatively measure plutonium and fission fragment distribution.

Cladding-Core Interaction Studies - R. J. Lobsinger and F. E. Panisko

To evaluate the effects on Zircaloy-2 corrosion, five UO_2 capsules with several possibly harmful fuel contaminants were irradiated for one MTR cycle (15.3 days). Exposures ranged from 2.78×10^{20} to 3.04×10^{20} nvt (thermal). Radiometallurgical examination will determine the effects of the I_2, Zn, and ZnO contaminants on internal Zircaloy-2 corrosion.

Fast Fuel Preirradiation Test Computer Study - G. R. Horn

Irradiation test evaluation of fast reactor fuels in thermal flux reactors are not generally satisfactory because of the severely nonprototypic conditions produced in the fuel.

Calculations were made of several effects obtained by irradiating fast fuels in thermal fluxes. A typical fast reactor fuel considered in the calculations comprises UO_2–20 wt% PuO_2 clad in 1/4 in. OD by 0.015 in. wall stainless steel. The fuel pins would be several feet long and they will be gathered into square, hexagonal, or circular clusters. They would be irradiated to exposures on the order of 100,000 MWd/MT at heat generation rates between 15 and 12 kW/ft.

Although detailed calculations are no substitute for irradiation tests, such calculations show that the data required for fast reactor fuels cannot satisfactorily be generated by irradiating fast fuel elements in thermal reactors. The major problems arise because prototypic power generation profiles (relative both to fuel radius and time) cannot be produced in the fuel. The calculated total power generation as a function of exposure for a typical fast fuel pin irradiated in a thermal flux is shown in Figure 3.4. For

comparison in this and the following figures, it is assumed that if the pin was irradiated in a fast flux, the breeding ratio would be >1.0 so that the heat generation rate would be approximately constant with respect to exposure.

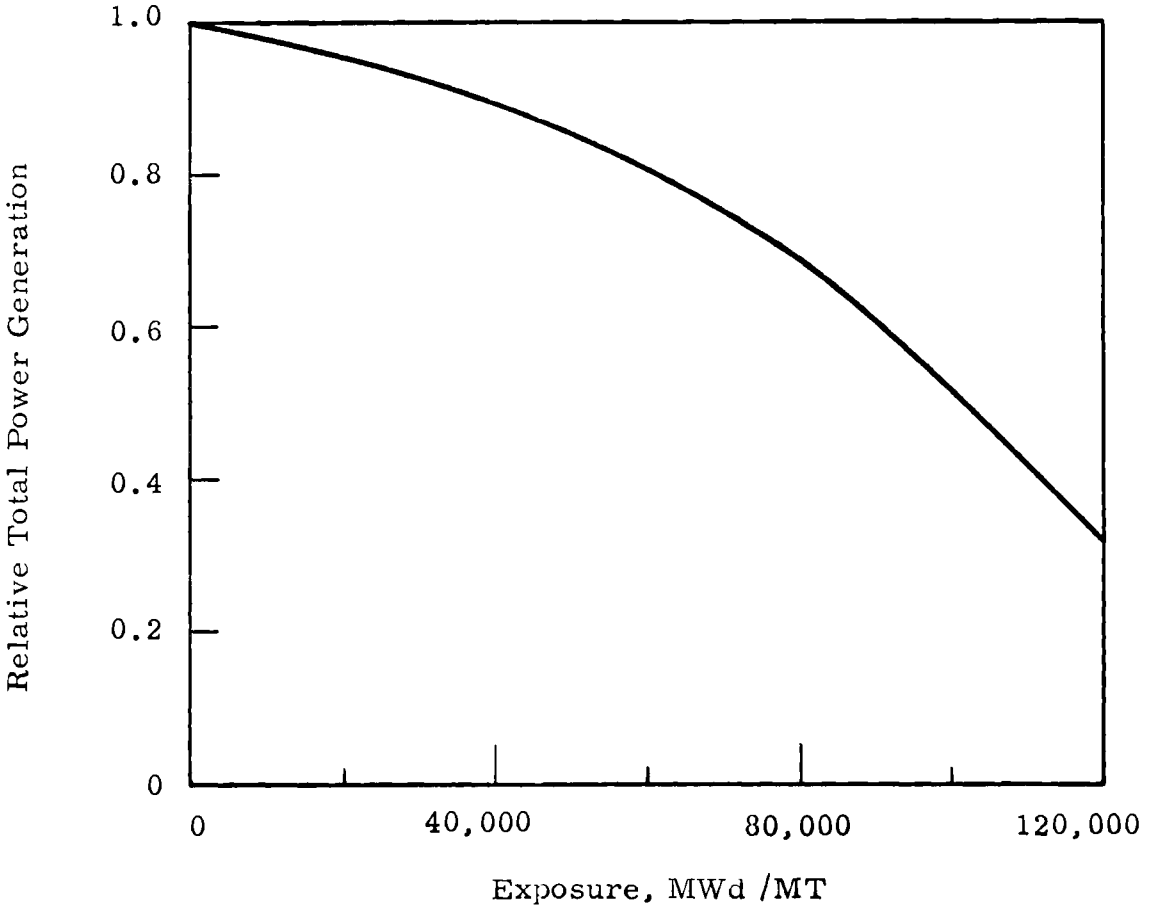

Fuel	UO_2-20 wt% PuO_2
Fuel Diameter	0.250 in.
Fuel Density	87% TD
Clad	304-L SS
Clad Thickness	0.012 in.

FIGURE 3.4

Heat Generation Rate as a Function of Exposure for a Fast Fuel Irradiated in a Thermal Flux

Because of self-shielding of the plutonium in the thermal flux, the power generation density at the outer surface of the fuel initially will be much greater than at the center. As irradiation continues, the fissile atoms near the outer edge of the fuel will be burned up much more rapidly than those at the center. As shown in Figure 3.5, the power density profile will change significantly with exposure. This will result in burnup at the outer edge of the fuel as much as 50% greater than at the center after an average exposure of 100,000 MWd/MT. Under these conditions, it would be difficult to reliably determine fuel swelling as a function of exposure.

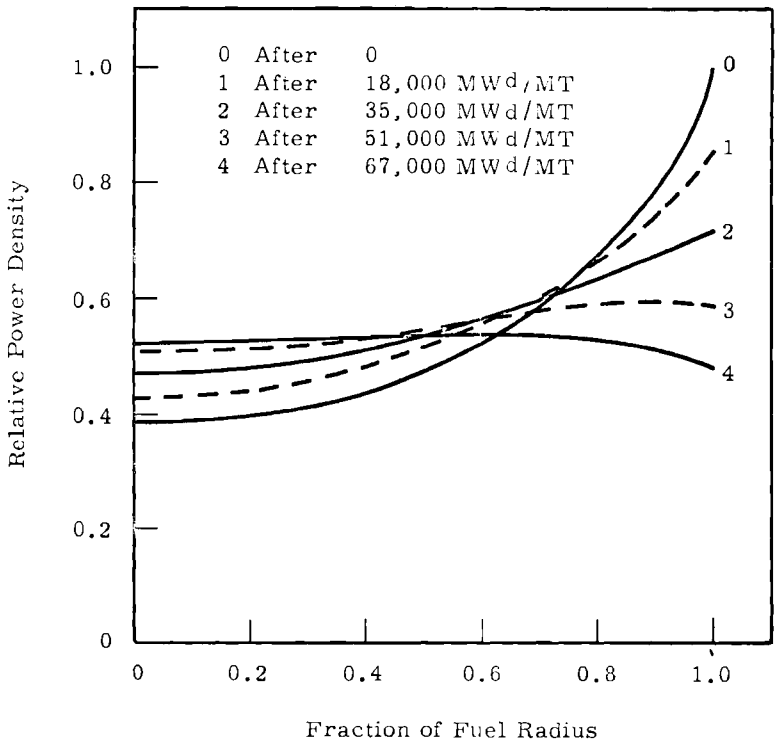

Fuel	UO_2-20 wt% PuO_2
Fuel Diameter	0.250 in.
Fuel Density	87% TD
Clad	304-L SS
Clad Thickness	0.012 in.

FIGURE 3.5a

Power Density Profile in a Fast Reactor Fuel Irradiated in a Thermal Flux

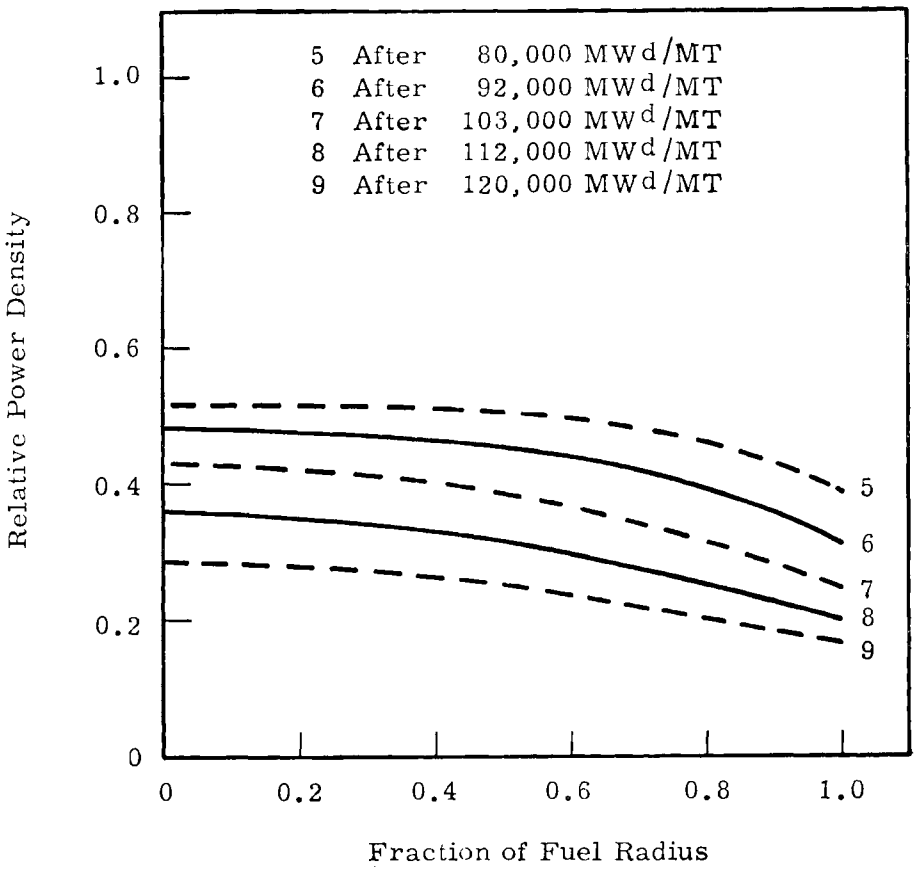

Fuel	UO_2-20 wt% PuO_2
Fuel Diameter	0.250 in.
Fuel Density	87% TD
Clad	304-L SS
Clad Thickness	0.012 in.

FIGURE 3.5b

Power Density Profile in a Fast Reactor Fuel Irradiated in a Thermal Flux

The nonprototypic power density profiles also give rise to nonprototypic temperature profiles. Central temperatures initially will be much lower in a thermal flux than in a fast flux and thermal gradients will not be as severe. These calculations show that the central fuel temperature will rise during the early part of the irradiation because of the reduction in self-shielding near the surface of the fuel. As irradiation continues,

the burnup of fissile atoms will override the reduction in self-shielding so that central temperatures will eventually decrease. These effects are illustrated by the curve in Figure 3.6. In deriving these curves it was assumed that the unperturbed neutron flux remained constant so that total power generation varied as shown in Figure 3.4. The changing and nonprototypic temperature gradients would also adversely affect any attempts to obtain reliable fuel swelling data. As the central temperatures changed, plasticity of the fuel and the extent to which fuel swelling could be accommodated by pores would change. Also, fuel structure changes and migration of fission products and/or plutonium would not be prototypic of fast reactor fuels because of the sensitivity of these phenomena to temperatures and temperature gradients.

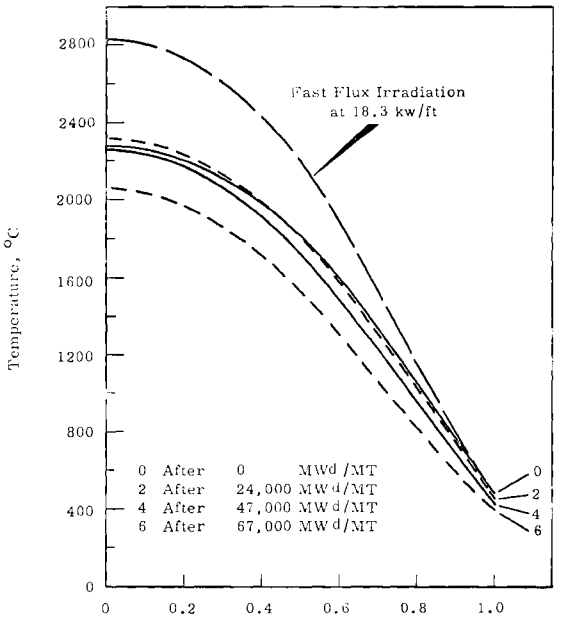

Fuel	UO_2-20 wt% PuO_2
Fuel Diameter	0.250 in.
Fuel Density	87% TD
Clad	304-L SS (0.012 in. Thick)

Initial Heat Generation Rate - 18.3 kw/ft

FIGURE 3.6

Temperature Profiles for a Fast Reactor Fuel Irradiated in a Thermal Neutron Flux

Much data were obtained from thermal reactor fuels irradiated in thermal fluxes to show how fission gas release depends on fuel temperature. In highly rated fuels, the fraction of fission gases released is essentially equal to the fraction of the fuel volume above about 1900 °C. Thus, referring again to Figure 3.6, fission gas release characteristics for fast reactor fuels could not be determined by irradiating these fuels in a thermal flux.

As the fissile atoms are burned in a thermal neutron flux, the presence of the fuel pin perturbs the thermal flux less and less, i.e., the "perturbed" neutron flux increases. Thus, as exposure increases, the ratio of the average neutron flux in the cladding to the average neutron flux in the fuel decreases as shown in Figure 3.7. This means that the cladding is being

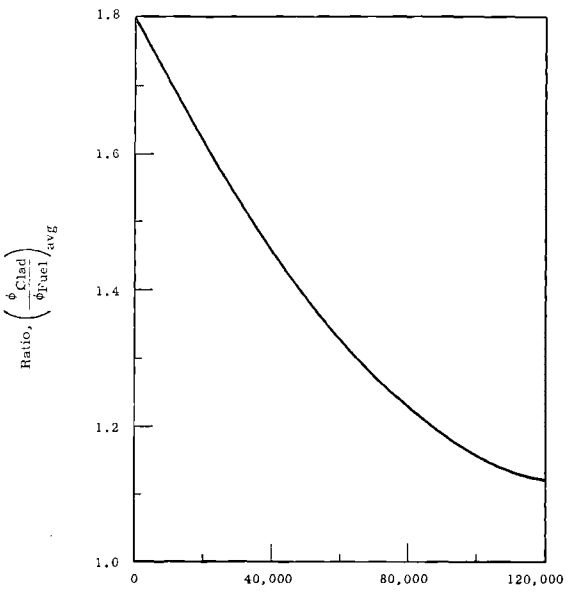

Fuel	UO_2-20 wt% PuO_2
Fuel Diameter	0.250
Fuel Density	87% TD
Clad	304-L SS
Clad Thickness	0.012 in.

FIGURE 3.7

Ratio of Average Flux in the Fuel to Average Flux in the Cladding as a Function of Exposure

"damaged" at a much different rate than the fuel and the ratio of their "damage rates" change drastically with time in-reactor. Therefore, both mechanical and chemical interactions between the fuel and cladding will be far from prototypic for fast reactor pins irradiated in thermal neutron fluxes.

High Exposure Plutonium Measurements Program - R. E. Bardsley

The use of high exposure plutonium in the production of ceramic fuel elements is of major interest in the nuclear fuel fabrication field. Plutonium with a high Pu^{240} content has been used in the production of fuel rods at PNL.(1) In this instance, the plutonium was recovered from metallic plutonium-aluminum alloy fuels, and is not representative of the plutonium which would be recovered from the burnup of ceramic fuels (mainly because of low Pu^{238} content). For this reason, a program was initiated in cooperation with other groups at PNL to obtain information that will apply to the handling and fabrication of elements containing high exposure plutonium, whose source was ceramic fuel material. Samples of fuel from various sources will be considered, and primary importance is being attached to the Shippingport, Yankee, and Dresden Reactors.

Shippingport assemblies from PWR are now at Hanford for separation. Each assembly contains seven vertically stacked fuel bundles and each bundle holds 120 fuel rods, 21.0 by 1.04 cm (10 in. by 0.41 in.). For this measurement program, several assemblies were selected on the basis of irradiation history. The exposures of two of these bundles are given in Table 3.5. Multiplication factors for individual rods, due to location relative to the blanket at PWR, substantially increase the exposure level.

---

(1) L. G. Merker, L. G. Faust, and W. J. Bailey. Battelle-Northwest Fuel Fabrication Experience with High Exposure Plutonium, BNWL-20. January 1965

These assemblies are now being dismantled and the bundles identified. The fuel bundles will be taken to Radiometallurgy for the study of specific fuel rods selected from bundle positions representing various exposures due to (1) longitudinal flux variance and (2) location relative to the blanket.

Fuel rods both from Phase I (13,000 MWd/MT) and Phase II (~23,000 MWd/MT) of the Yankee reactor are expected to arrive from Westinghouse during the next quarter.

TABLE 3.5

EXPOSURES OF TWO SHIPPINGPORT FUEL ASSEMBLIES FOR MEASUREMENTS PROGRAM

	Bundle Number	Assembly Number 014	Assembly Number 045
		MWd/TU	MWd/TU
Assembly Bottom	1	9900	13000
	2	16700	21600
	3	19000*	23800
	4	19000	23100
	5	17600	21100
	6	13400	16200
Assembly Top	7	7400	8800

* Due to location of the assembly relative to the PWR blanket, individual rod factors increase these values up to 1.5 times the figure given in the table above.

Plutonium Fuel Fabrication Economic Studies -

C. H. Bloomster

Studies are being made on the effect of fuel design parameters on the fabrication cost of plutonium fuel elements. Three reports[1] were issued last quarter and one report was in preparation describing the variable cost of fabricating UO_2-PuO_2 fuel rods of different fuel designs. The variable costs of fabricating plutonium fuel elements for four specific reactors are as follows:

- PRTR: $113 per kg of fuel (as oxide) or $205 per fuel rod
- EBWR: $198 per kg (as oxide) or $164 per fuel rod
- Saxton: $255 per kg (as oxide) or $136 per fuel rod
- PRCF: $88 per kg (as oxide) or $99 per fuel rod

A summary report is being prepared analyzing and classifying the variable costs with the fuel design parameters. The principal design parameters which influence fabrication costs are the weight of fuel in the individual fuel rod and the level of plutonium

---

(1) C. H. Bloomster. Fabrication Costs for Plutonium Fuel Elements.

PART A. "Variable Costs of Fabricating UO_2-PuO_2 Fuel Elements for the Plutonium Recycle Critical Facility" BNWL-131A. September 1965

PART B. "Variable Costs of Fabricating UO_2-PuO_2 Fuel Rods for the Experimental Boiling Water Reactor" BNWL-131B. September 1965

PART C. "Variable Costs of Fabricating UO_2-PuO_2 Fuel Rods for the Saxton Reactor" BNWL-131C. September 1965.

PART D. "Variable Costs of Fabricating UO_2-PuO_2 Fuel Elements for the Plutonium Recycle Test Reactor BNWL-131D. October 1965.

enrichment. Nearly all the variable costs are related directly or indirectly to these two design parameters. The variable fabrication cost expressed in dollars per kg of finished fuel varies inversely, but not linearly, with the weight of fuel in the finished fuel element (Table 3.6); conversely, the variable fabrication cost expressed in dollars per finished fuel rod varies directly, also not linearly, with the fuel weight in the finished fuel rod. The fabrication costs for the PRCF fuel do not fit these relationships because the PRCF fuels were fabricated for zero power critical experiments at substantially reduced fabrication costs.

TABLE 3.6

GEOMETRY AND COMPOSITION OF FINISHED FUEL ELEMENTS

(Cladding-Zircaloy-2)

Fuel Type	Fuel Diameter, cm	Fuel Length, m	Fuel Quantity per Rod, kg	Fuel Geometry	PuO_2 Enrichment wt%
PRTR	1.3	1.5	1.8	19-rod cluster	2
EBWR	0.95	1.2	0.83	single rods	1.5
Saxton	0.87	1.0	0.53	single rods	6.6
PRCF	1.3	0.9	1.1	single rods	2

Development of Advanced Fuel Concepts: PuN-UN Cost Study - J. B. Burnham

According to an analysis of potential production methods for mixed nitride fuel elements, carbon reduction of the oxides followed by nitridation in a fluidized bed reactor might be competitive with mixed carbide fuels. Calculations were made on the basis of a plant producing 16,000 kg/yr of mixed nitride fuel pins. It was estimated that mixed nitrides formed by the carbothermal reduction-nitridation technique and clad by gas pressure bonding could be produced for approximately $120/kg metal.

The use of metal as a starting material almost doubled the calculated cost of the fuel.

PART IV - PRTR FUEL ELEMENT PERFORMANCE AND FABRICATION

Irradiation Testing of High Power Density Elements in PRTR -

M. D. Freshley and F. E. Panisko

Fuel testing is continuing in support of the High Power Density Program (HPD) in PRTR. The HPD program in PRTR includes the evaluation of physics parameters of a plutonium enriched fuel loading as a function of burnup under controlled conditions, and the operation of UO_2-PuO_2 elements with molten fuel. The physics and fuel testing objectives of the program are closely related. The major fuel testing objective is to determine if there is unique behavior that would limit operation of plutonium-bearing fuels to powers less than those attainable with uranium-only oxide fuels.

During the Batch Core Experiment, UO_2–2 wt% PuO_2 HPD elements are being irradiated in the PRTR core under the expected maximum operating conditions, i.e., 623 W/cm (19 kW/ft) with fuel temperatures as high as 2600 °C. The maximum burnup on one of the eleven HPD type elements currently in the reactor is 1.3×10^{20} fissions/cm^3 (4950 MWd/MT fuel).

Nondefected and defected prototype HPD elements are being irradiation tested in the Fuel Element Rupture Test Facility (FERTF) in PRTR at power generations sufficient to cause fuel melting. Insignificant fuel washout occurred during the 6-day irradiation of vibrationally compacted UO_2–2 wt% PuO_2 HPD element (FE 6004) intentionally defected with a 1.59-mm diam hole through the cladding at the midplane of one rod (Figure 4.1). The element was irradiated in the FERTF at the maximum rod power generation (660 W/cm) expected to cause incipient melting at the plane of the defect. Prior irradiation of the element was sufficient to cause considerable

D1810 Macrophotograph
5X

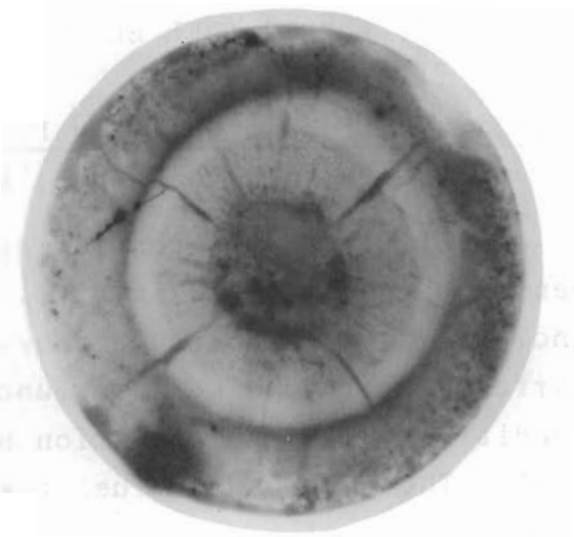

680 β Autoradiograph

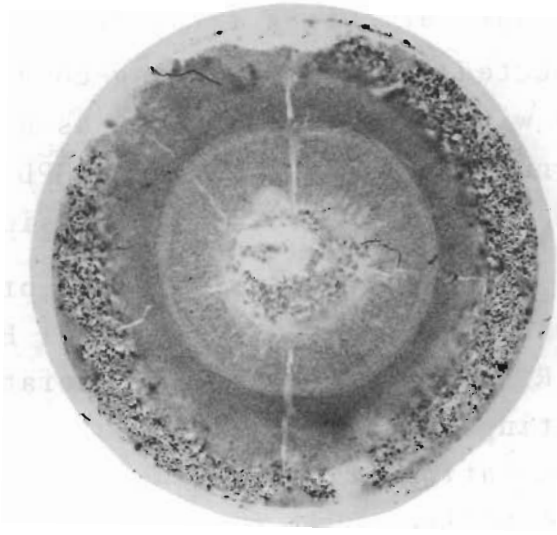

679 α Autoradiograph

FIGURE 4.1

Transverse Section Through an Intentionally Defected UO_2–2 wt% PuO_2 Rod from HPD FE 6004
(Estimated maximum power generation at the plane of defect was 660 W/cm.)

in-reactor sintering which undoubtedly improved the washout characteristics of the fuel. No significant dimensional changes in the rod were measured near the defect. Examination of the fuel structure formed during irradiation indicated a greater degree of melting than anticipated from the maximum rod power generation rates calculated. (The melting diameter is thought to have been 55% of the transverse section diameter shown in Figure 4.1.) An adjacent nondefected rod from the element will be examined to determine if the thermal conditions were affected by the defect and associated phenomena.

The alpha and beta autoradiographs in Figure 4.1 indicate that the symmetry of the fuel structure and fission product distribution patterns have been affected by the defect. Although some nonuniformity of alpha particle distribution is indicated on the alpha autoradiograph, comparison of the alpha and beta autoradiographs shows the patterns do not coincide. An unexplained source of fission product activity is present at the fuel periphery (dark spot on the β autoradiograph).

An examination is being made on two rods from a vibrationally-compacted UO_2–4 wt% PuO_2 HPD element (FE 6504) irradiated to 0.23×10^{20} fissions/cm^3 (920 MWd/MT fuel) at a maximum tube power of 1744 kW (Figure 4.2). This tube power produces approximately the maximum operating conditions anticipated during the planned Molten Core Experiment in the PRTR, i.e., a maximum rod power of 820 to 850 W/cm (25 to 26 kW/ft). The element successfully withstood a 20% overpower transient lasting about 11 sec during steady-state operation at 1744 kW. One rod was sampled for fission gas in the fuel region, and the other was sampled in the plenum region. Good communication exists between the plenum and fuel because each yielded about the same amount of total gas (Table 4.1). There were no measurable changes in rod dimensions.

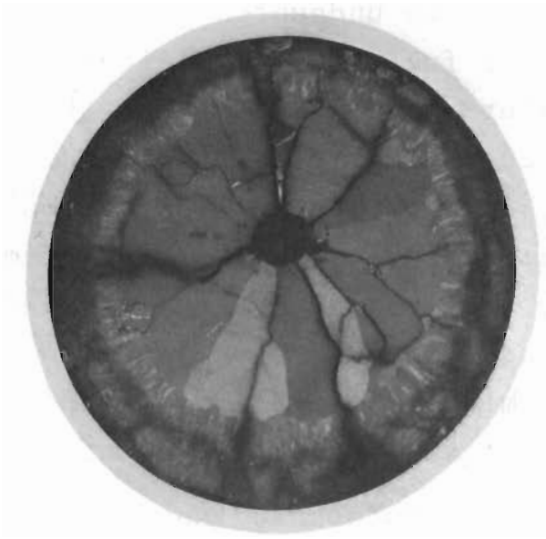

D-1775
Macrophotograph 5X

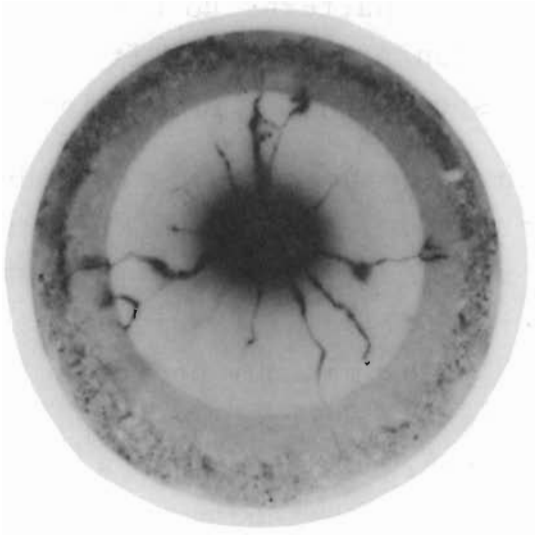

663
β Autoradiograph

FIGURE 4.2

Transverse Section at the Midplane of UO_2–4 wt% PuO_2 Rod (FR-3) from HPD FE 6504

TABLE 4.1

FISSION GAS RELEASE FROM HPD ELEMENTS IRRADIATED IN PRTR

HPD Element Number, wt% PuO_2	Rod Number	Position	Average Element Burnup, fissions/cm^3	Maximum Tube Power, kW	Maximum Rod Power, W/cm	Total Gas Collected, ml	Percent Xe + Kr Release	Comments
6000 (2)	50-30	Center	0.34×10^{20}	1350	270	34.7	10.4	
	50-35	6 RR			350	53.9	7.3	
	50-36	12 RR			640	117.4	32.8	
6502 (2)	5H-200	12 RR	0.12×10^{20}	1450	660	107.7	49.1	
	5H-197	12 RR				107.7	46.7	
6004 (2)	5K-0	12 RR	0.91×10^{20}	1465	665	215	*	
		12 RR						Defected
6504 (4)	FR-3	12 RR	0.23×10^{20}	1745	~820	218	*	Drilled in fuel
	FR-6	12 RR				208	*	Drilled in plenum
	Fr-4	12 RR						Defected
6505 (2)	FR-14	12 RR	0.03×10^{20}	1790	~820	145	*	Drilled in plenum

* Analysis not complete.

Examination of the fuel structures formed during irradiation indicates as much as 30% of the radius was molten during operation (Figures 4.3 and 4.4). This is somewhat less than the expected 50% for a rod power of 850 W/cm. Possible reasons for this apparent discrepancy are:

- An erroneous estimate of the maximum power generation rate. These data are suspect because an unusual nonsymmetrical axial flux scan was obtained from this element.
- A poor estimate of the self-shielding effects with 4 wt% PuO_2 enrichment. The central voids are noticeably displaced and nonsymmetrical due to flux skewing.
- A poor calculational model for the thermal conditions at the higher power generations.

Good agreement exists between observed and calculated thermal conditions versus rod power generation for UO_2–2 wt% PuO_2 fuel up to melting, assuming in-reactor sintering of the 86% bulk density fuel increases the effective conductivity to the value for 100% TD fuel at temperatures above 1600 °C. (These data also indicate that melting of 86% TD vibrationally compacted UO_2–2 wt% PuO_2 fuel begins at a rod power of 655 to 690 W/cm under PRTR conditions.) This calculational model may not be valid for power generation rates sufficient to cause considerable fuel melting.

Transverse sections along the length of the fuel rods show larger central voids above the midplane than below the midplane from areas of comparable power generation. The size of the void at the midplane where melting occurred is also smaller than the void farther up the rod where melting did not occur. Generally, the size of the central void above the midplane of the rods is about 13 to 15% of the sintered area. This would be expected if the bulk fuel with an initial density of 85 to 87% TD sintered to near 100% TD.

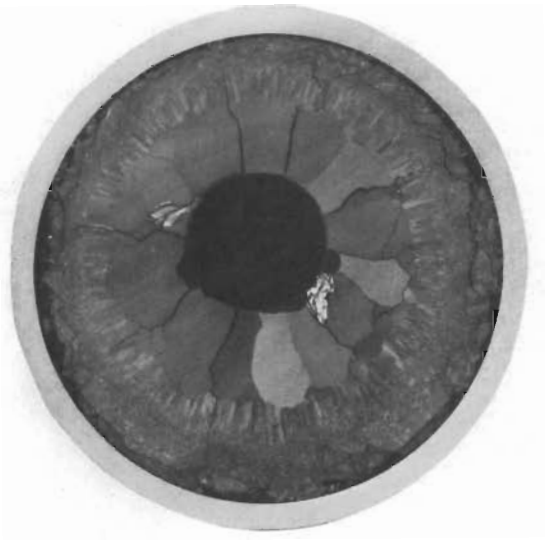

D-1776
Macrophotograph 5X

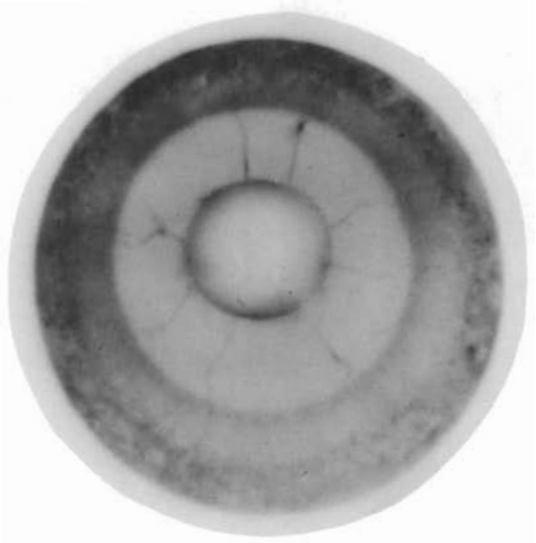

670
β Autoradiograph

FIGURE 4.3

Transverse Section 19 cm Above the Midplane of a UO_2–4 wt% PuO_2 Rod (FR-3) from HPD FE 6504

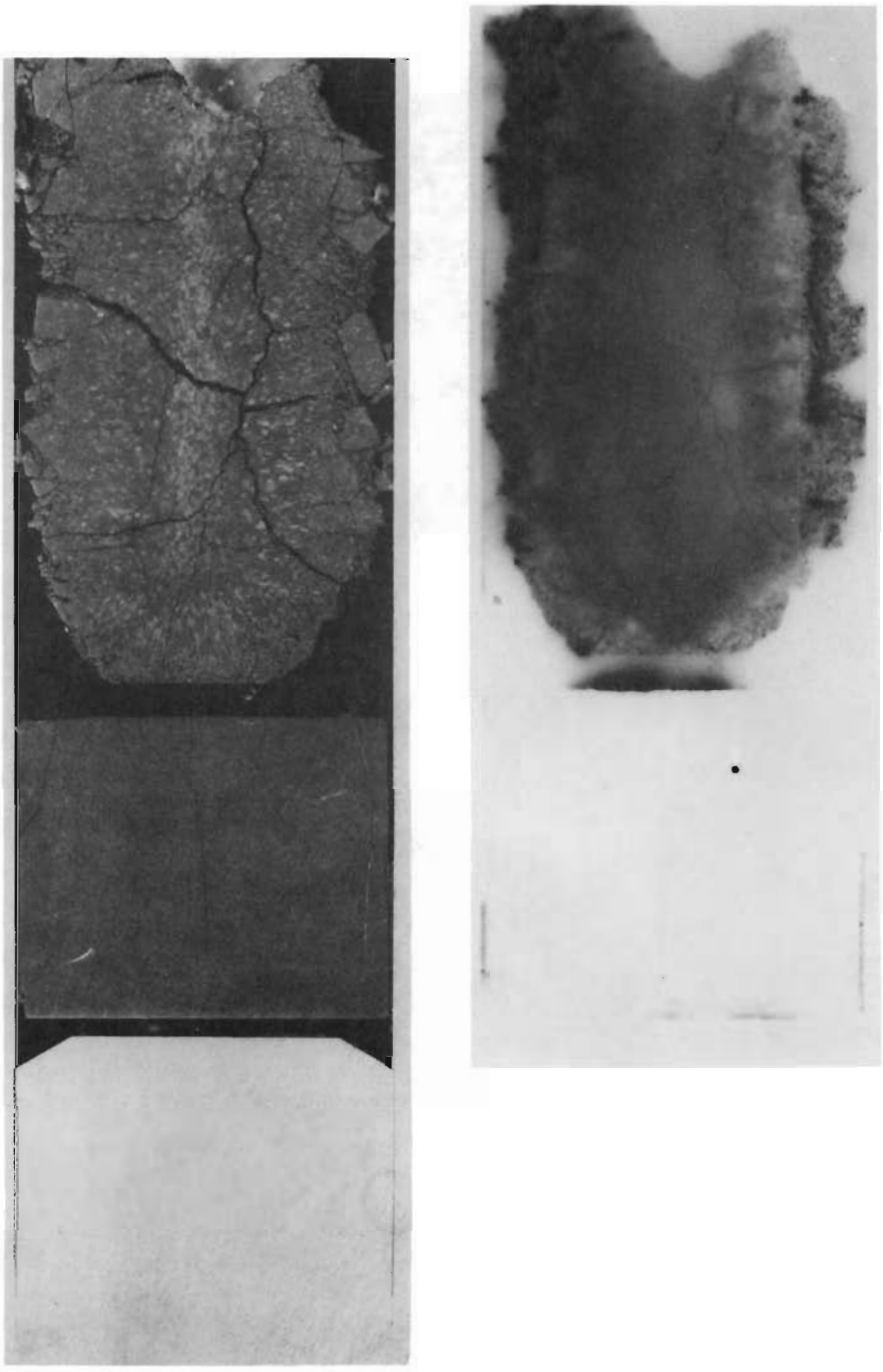

FIGURE 4.4

Longitudinal Section Through the Bottom of a UO_2–4 wt% PuO_2 Rod (FR-3) from HPD FE 6504
(The section shows the bottom 3.3 cm of the fuel column which includes the depleted UO_2 pellet adjacent to the end cap and the UO_2–1 wt% PuO_2 buffer region.)
No. 16674; 667

The size of the central void below the midplane of the rods, however, is usually only 2 to 5% of the sintered area. Presently, this apparent anomaly in mass balance is unexplained, particularly because no measurable changes in the balance point of the rods indicate no axial fuel movement occurred under these operating conditions.

Examination of the bottom end regions (Figure 4.4) of the irradiated rods showed that the depleted UO_2 pellet was essentially unaffected (only minor cracking). The 1 wt% PuO_2 fuel region had undergone sintering with maximum fuel temperatures of approximately 1700 °C indicated. Limited fuel melting occurred in the 4 wt% PuO_2 region, forming a very uniform central void (Figure 4.5). Typical fuel structural and fission product distribution patterns were formed. There is evidence of flow of liquid fuel into radial cracks.

There was no reaction between the plenum spring and the depleted UO_2 pellet in the top end region, although the pellet was more severely cracked than at the bottom, indicating higher fuel temperatures. Unexpected melting occurred in the 1 wt% PuO_2 region, whereas maximum fuel temperatures of about 1700 °C are indicated in the 4 wt% PuO_2 fuel region. In previous irradiations, higher fuel temperatures occurred in the bottom end regions.

Table 4.1 summarizes fission gas release data from HPD elements irradiated in PRTR. As high as 49% Xe + Kr has been released from a rod which operated at a maximum rod power of 660 W/cm with fuel molten to 13% of the radius. The fission gas data fit the release model of 100% release from that portion of fuel operating above 1800 °C and 10% release from that portion operating below 1800 °C.

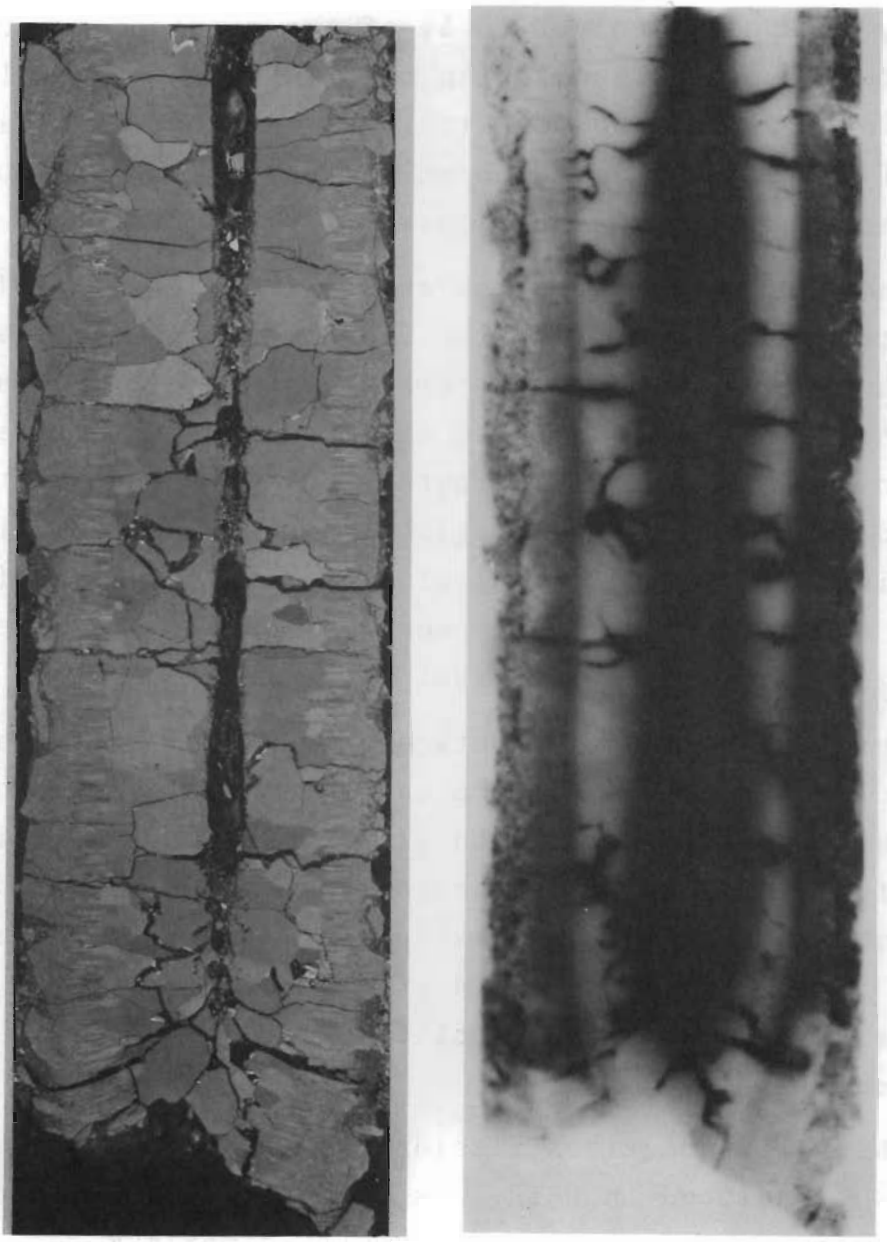

FIGURE 4.5

Longitudinal Section Through the Bottom of a UO_2–4 wt% PuO_2 Rod (FR-3) from HPD FE 6504
(The section shows the bottom portion of the UO_2–4 wt% PuO_2 fuel column which extends from 3.6 to 7.7 cm.)
No. 16675; 668

To study the nature of the reactor control instability phenomenon, a UO_2–2 wt% PuO_2 HPD element (FE 6505) was irradiated in the FERTF for a short time (0.029×10^{20} fissions/cm^3 or 115 MWd/MT fuel) at a maximum tube power near 1800 kW. The results of this test indicated that the instability may have been initiated by nucleate boiling and aggravated by mechanical problems in the control system. Changes have been made which have essentially eliminated the instability. Two rods were removed from this element for examination.

One rod in the previously irradiated UO_2–4 wt% PuO_2 element (FE 6504) has been defected with a 1.59 mm diam hole at the midplane. It is planned to irradiate this element for an extended time at a maximum rod power of about 850 W/cm.

PRTR-HPD Fuel Fabrication - R. L. Gulley and R. D. Reid

The previous schedule[1] for PRTR-HPD fuel fabrication anticipated a total of 60 Mark I-R series fuel elements to be fabricated from June through November 1965. Additions to this schedule have increased the total number of elements to 64. The present schedule for delivery of these elements is in Table 4.2. Figure 4.6 shows 13 of the 25 completed elements.

Zircaloy tubing with an ID of 1.278 to 1.288 cm (0.503 to 0.507 in.) and an OD of 1.420 to 1.450 cm (0.559 to 0.571 in.) is specified for PRTR-HPD fuel rod cladding. One Mark I-R_1 fuel element was fabricated with 1.290 to 1.295 cm (0.508 to 0.510 in.) ID and 1.432 to 1.458 cm (0.564 to 0.574 in.) OD Zircaloy tubing. It is expected that two other elements will be fabricated with the larger diameter tubing. One of these elements will be the Mark I-R_4-Th (ThO_2-5 wt% PuO_2) element and the other will be a Mark I-R_1 element.

---

1. Ceramics Research and Development Quarterly Report, April-June 1965, BNWL-150.

TABLE 4.2

PRTR-HPD FUEL ELEMENT FABRICATION SCHEDULE

Element Type	Fuel Material	Graded Ends	Number of Removable Rods	Number of Separable Rods	Elements Delivered	Elements Ready for Delivery	Elements to be Fabricated by 11-1-65	Elements to be Fabricated by 12-31-65
Mark I-R_1	UO_2–2 wt% PuO_2	No	None	None	12	6		24
Mark I-R_2	UO_2–2 wt% PuO_2	No	3	None			4	8
Mark I-R_3	UO_2–4 wt% PuO_2	Yes	3	None	1	1		
Mark I-R_4	UO_2–2 wt% PuO_2	Yes	3	None	1			
Mark I-R_5	UO_2–2 wt% PuO_2	Yes	None	None	2	1		
Mark I-R_6	UO_2–2 wt% PuO_2	No	None*	3	1			
Mark I-R_2 (Pressure) Test	UO_2–2 wt% PuO_2	No	3	None			1	
Mark I-R_4Th	ThO_2–5 wt% PuO_2	Yes	3	None			1	1
TOTAL					17	8	6	33

* Roll pins will be used to hold the rods to the end bracket.

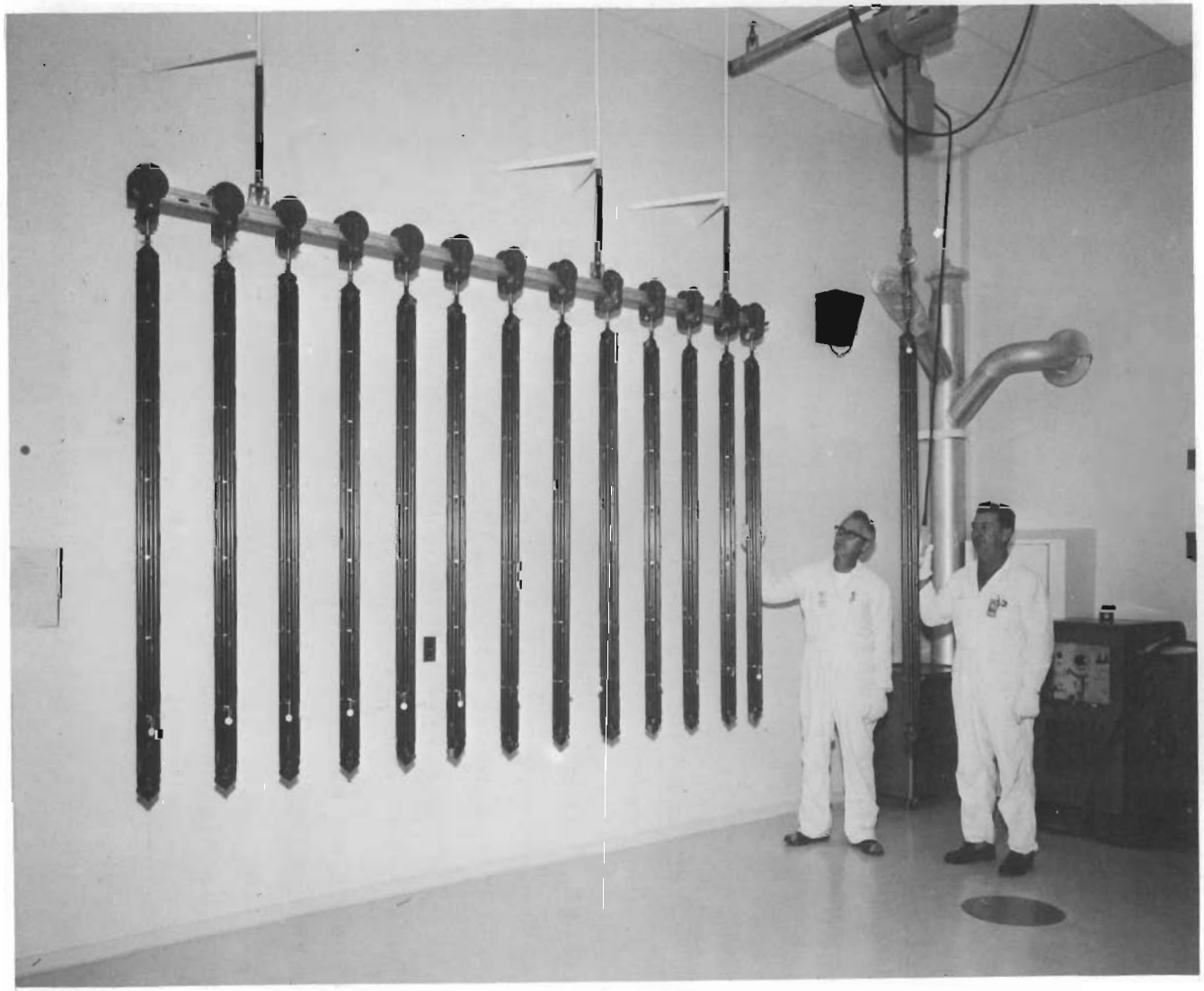

FIGURE 4.6
PRTR-HPD Fuel Element Assemblies

Upon initial loading of the PRTR-HPD experiment, two elements with larger diameter tubing will be positioned in the 12-element buffer zone rather than in the 43-element batch core.

A total of 80 kg of UO_2–1 wt% PuO_2 and 40 kg of UO_2–4 wt% PuO_2 were crushed to -65 mesh (Tyler) particle size and blended and recycled through the pneumatic impaction process to obtain 120,000 g of UO_2–2 wt% PuO_2 fuel material. Sixty-six rods will be fabricated with this fuel material.

Preliminary design of the ThO_2–5 wt% PuO_2 PRTR element suggests that the fuel column should contain, from bottom to top respectively, a 1 cm thick ThO_2 pellet, 2 cm of fused ThO_2, and a 1 cm thick ThO_2 pellet. A bulk fuel density of 80 to 85% TD is expected, and the higher density will be attempted.

Magnetic Force End Closure Weld: PRTR Fuel Elements -

R. F. Boolen

Work was begun on the development of a magnetic force welded end closure for PRTR fuel elements. Preliminary studies indicated that magnetic force welding offers possible cost and strength advantages over conventional TIG welding of end closures in zircaloy fuel elements.

Based on an earlier design not fully evaluated, end closures with a 4° tapered end cap were forced into the tube end (press fit lap joint); the resulting pressure and electrical resistance heating produced coalescence.

Figures 4.7 and 4.8 are photomicrographs of a cross section of a typical weld. This weld, with a wide closure area (about twice the wall thickness) between cap and tube, is typically upset and flash free. It is noteworthy that the process produces no grain growth; in fact, grain size is reduced in such alloys as zircaloy and similar metals. In this case, the large grains of the cast cap work piece and

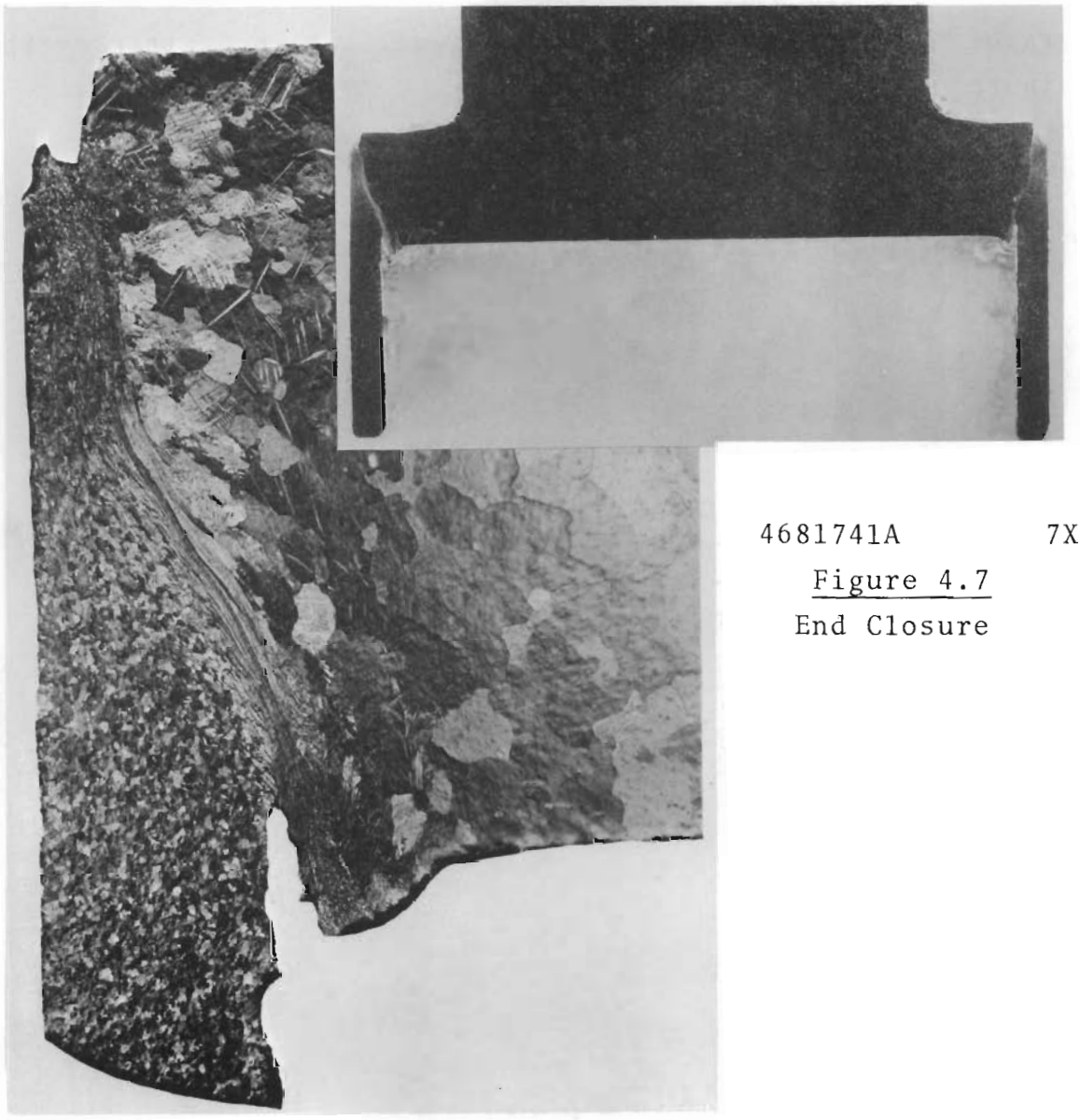

4681741A 7X

Figure 4.7
End Closure

5651741B 50X

FIGURE 4.8

Magnetic Force Welded
Zircaloy End Closure

and the press fit lap joint weld configuration reduce the effect of grain size reduction, as shown in the photomicrographs of straight butt joints of small grained zircaloy in Figure 4.9.

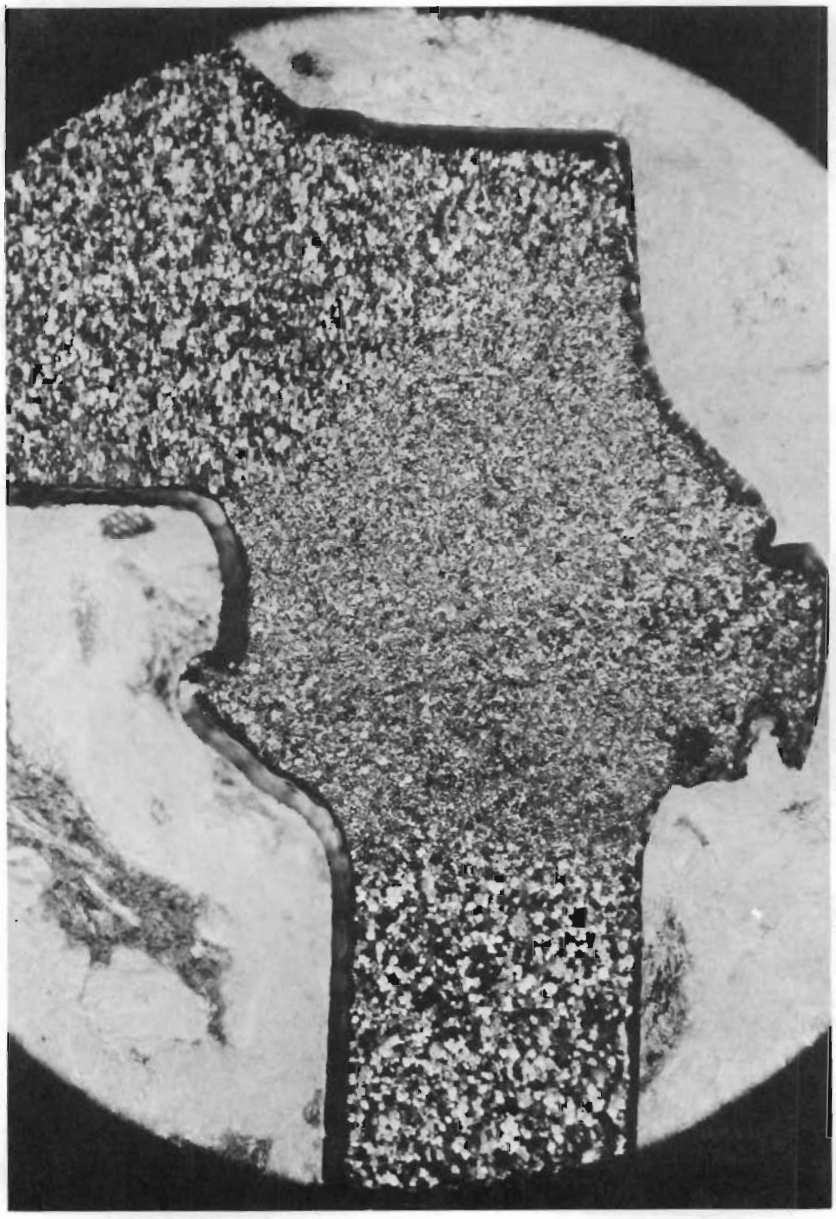

FIGURE 4.9

Straight Butt Joint
Magnetic Force Welded Zircaloy Showing Grain Size Reduction
50X

No. S-G 1538B

Short capsules 9/16 in. diameter were produced for weld evaluation by destructive testing. Tensile tests of several end closures resulted in ultimate failure of the tubes, indicating a weld of satisfactory strength. A special modified room temperature burst test was designed and performed. For this test, the zircaloy tube was encased in an outer steel tube to prevent longitudinal splitting of the capsule, thereby putting higher tensile and shear forces on the weld. Several of these end closures were made at parameters which gave unsatisfactory strength (as determined by tensile test); however, all samples failed in the tube in the modified burst test. Test results of the modified burst test are compared with tensile test results in Table 4.3. Although the modified burst test, like the tensile test, does not provide ultimate strength values for the weld material, it evidently provides a higher strain than tensile testing.

Work pieces were fabricated for the development of an ultrasonic test for the end closure. Other work pieces were fabricated to perform a comparative study on a straight butt joint type of end closure in the zircaloy.

TABLE 4.3

TENSILE AND MODIFIED BURST TEST RESULTS FOR MAGNETIC FORCE WELDED END CLOSURES

Sample	Ultimate ksi*	Failure Incidence
Tensile (from previous work)		
T-1	56.7	Tube
T-2	56.2	Tube
T-3	57.0	Tube
T-4	59.1	Tube
T-5	59.4	Tube
T-6	58.7	Tube
T-7	58.8	Tube
T-8	57.8	Tube
T-9	58.0	Tube
T-10	58.0	Tube
Internal Pressure Modified		
B-1	27.8	Tube, longitudinal
B-2	64.5	Tube, circumferential
B-3	63.5	Tube, circumferential
B-4	64.0	Tube, circumferential
B-5	30.0	Tube, longitudinal
B-6	63.2	Tube, circumferential

* Strain on weld, not ultimate weld strength

PRTR Fuel Element Performance - F. E. Panisko

The present PRTR fuel loading includes one UO_2–4 wt% PuO_2 and ten UO_2–2 wt% PuO_2 elements. The maximum fuel burnup is 2.60×10^{20} fissions/cm^3.

TABLE 4.4

PRESENT PRTR FUEL ELEMENT LOADING AND CORRESPONDING MAXIMUM BURNUP

Number of Elements	Type of Fuel*	wt% PuO_2	Maximum Burnup		
			Fuel Element	fissions/$cm^3 \times 10^{20}$	MWd/MT$_{fuel}$
1	Vibrationally Compacted	4.0	6504	0.28	1140
7	Vibrationally Compacted	2.0	6001	1.20	4910
2	Swaged	2.0	6002	1.01	4150
1	Vibrationally Compacted Recycle Fuel	2.0	6500	0.38	1570
1	Vibrationally Compacted	1.5	6501	0.71	2740
11	Vibrationally compacted	1.0	5227	1.48	5760
20	Swaged	1.0	5224	1.90	6880
1	Swaged	0.75	5221	1.90	6900
6	Incrementally Loaded, Vibrationally Compacted	0.48	5118	2.60	10,110
20	Swaged	0.48	5142	2.38	8630
3	Swaged, Natural UO_2	0.00	1037	2.22	8780

* All the fuel in PRTR containing more than 0.48 wt% PuO_2 was pneumatically impacted before vibrational or swage compaction.

Postirradiation examination of the defective rod from FE 5237 which failed in January, 1965, revealed massive hydriding of the Zircaloy-2 cladding in the defect area and in another discolored spot on the cladding. The hydriding was so severe that pieces of cladding fell from the hydrided areas during remote handling.

A fingerprint was placed at the midpoint of a removable rod in FE 6504. The UO_2–2 wt% PuO_2 element operated for 22 days at an average rod power of 640 W/cm. No cladding discoloration occurred during this irradiation period. The rod was removed from the cluster for destructive postirradiation examination.

There was an indication of a leaking element in the reactor during September, but as yet a defective element has not been located. Radioactivity in the primary coolant system has not hampered reactor operation.

During this quarter 21 PRTR fuel elements were visually examined, and seven elements with possible Zircaloy-2 hydride areas were identified. All examined elements were acceptable for recharging.

PRTR Thermocouple Fuel Element - D. R. Doman

Radiometallurgical examination was completed on the High Power Density thermocoupled fuel element (FE 6502). As previously reported,[1] this UO_2–2 wt% PuO_2 fuel element used reduced enrichment zones of 1 wt% PuO_2 and depleted UO_2 to reduce flux and temperature peaking effects near the end caps. W 26 Re sheathed thermocouples of W 5 Re/W 26 Re thermocouple wires with ThO_2 insulation were inserted 0.7 cm into the UO_2–1 wt% PuO_2 zones on the top and bottom of two fuel rods. This location was selected to limit the temperatures to the values measurable by this type of thermocouple. Maximum temperatures of 1900 to 2050 °C were indicated by the top and bottom thermocouples, but one bottom thermocouple open-circuited after 3 days of operation and the other bottom thermocouple indicated intermittent shorting. Radiometallurgical examination showed temperatures at the bottoms of both rods were sufficient to cause fuel-thermocouple sheath reaction. Also, both bottom thermocouple sheaths had broken at about 0.6 cm from the junction (Figures 4.10 and 4.11). Little reaction and no breakage were found on either top thermocouple (Figure 4.12).

---

1. Ceramics Research and Development Quarterly Report, April-June 1965, BNWL-150.

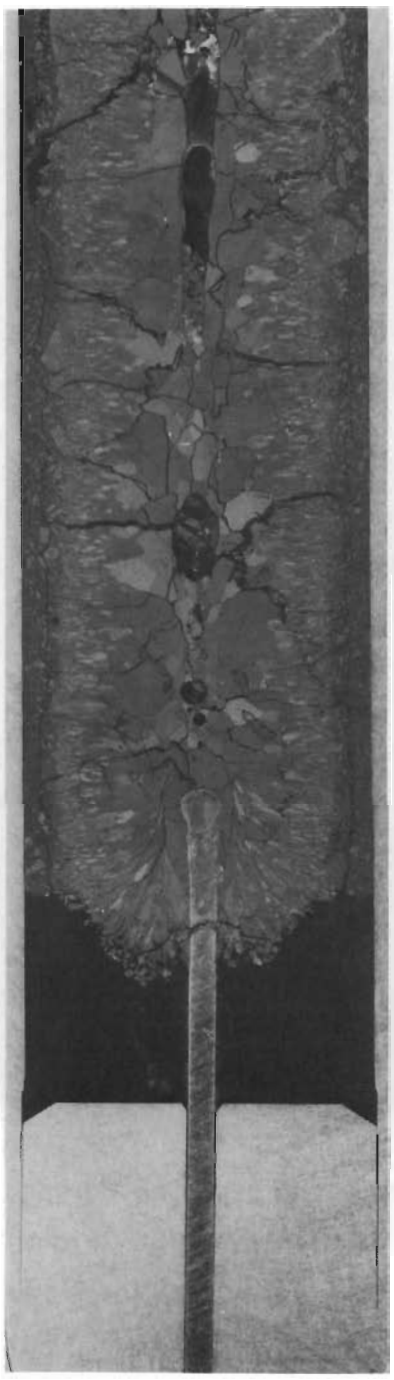

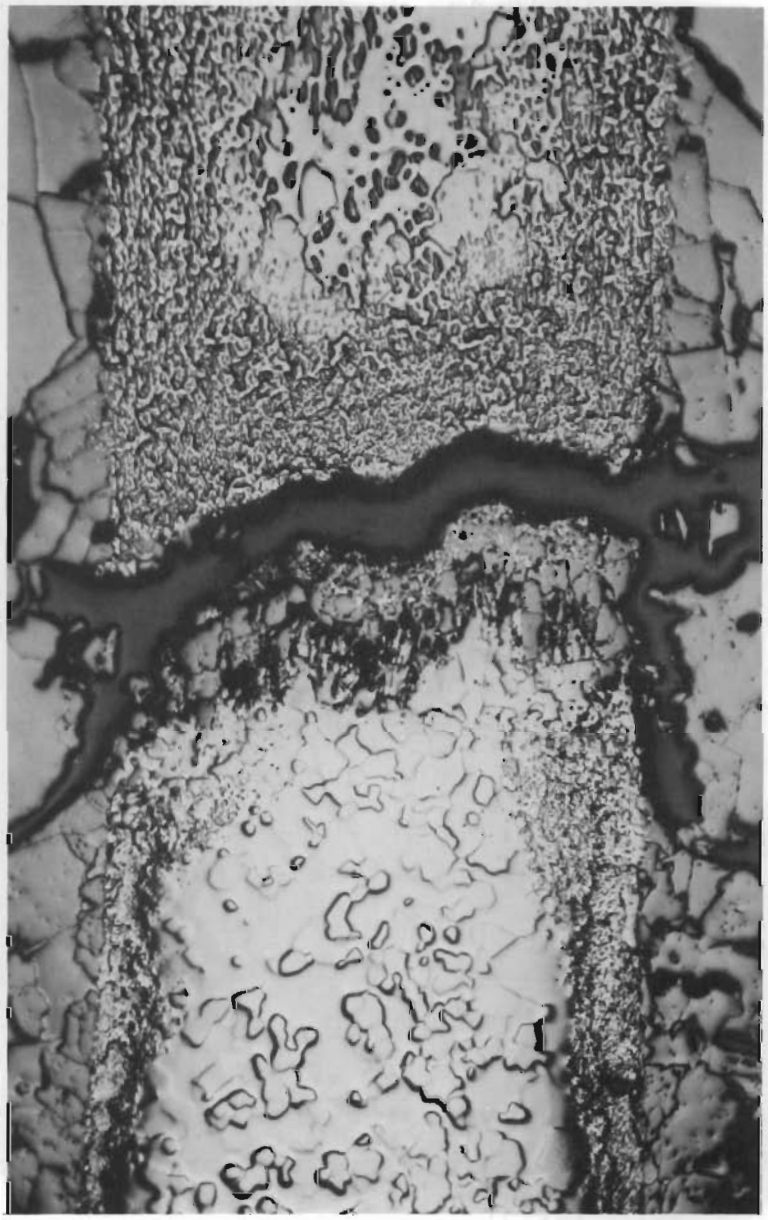

45X

3 1/2X

FIGURE 4.10

Fuel Structure and Thermocouple at Bottom of Rod CTC-2
from FE 6502 (Left);
Reaction Zone on Thermocouple Sheath
in Vicinity of Break (Right)
No. 16617; D 1133

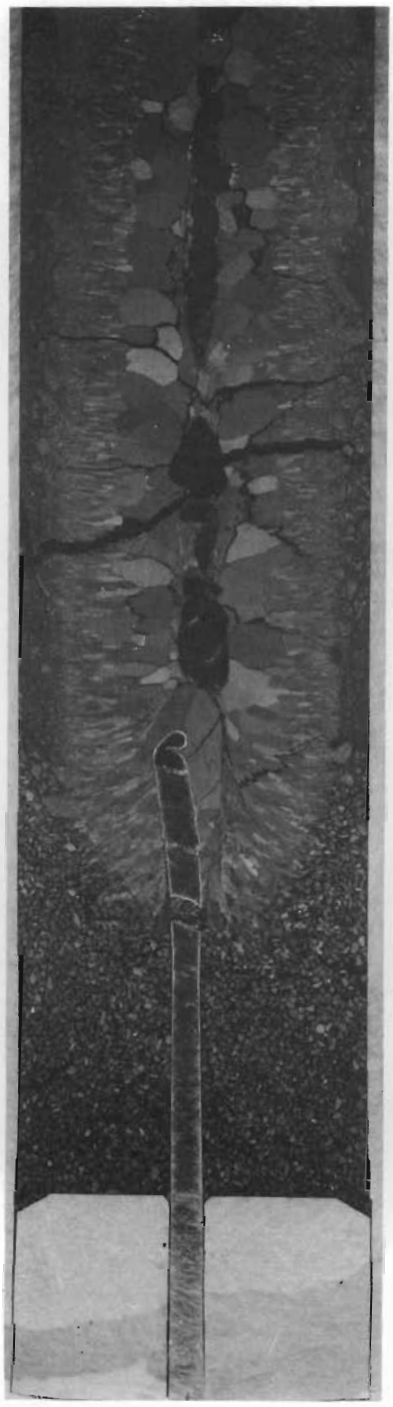

3 1/2X

75X

FIGURE 4.11

Fuel Structure and Thermocouple at Bottom of Rod CTC-1 from FE 6502 (Left); Reaction Zone on Thermocouple Sheath in Vicinity of Break (Right)

No. 16618; D 1152

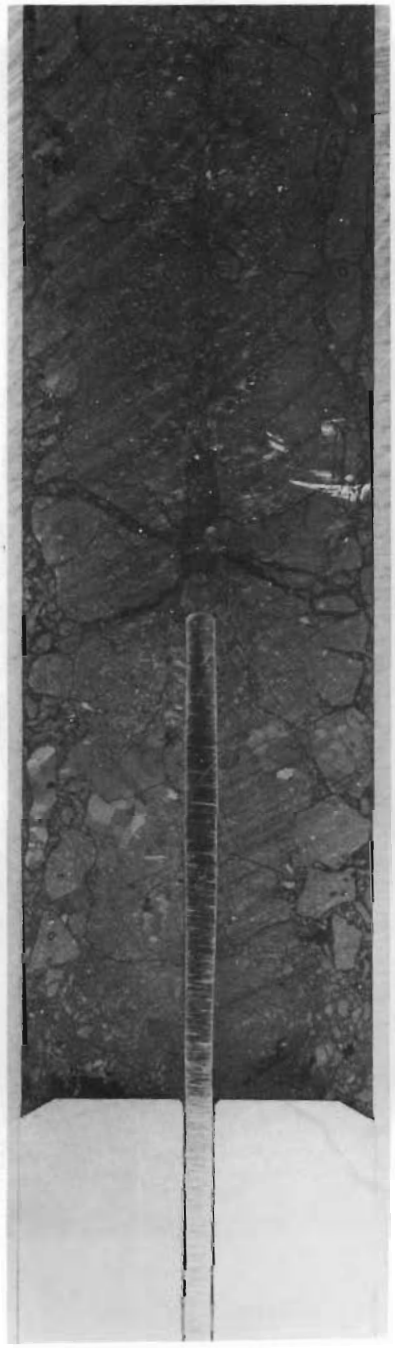

45X

3 1/2X

FIGURE 4.12

Fuel Structure and Thermocouple at Top of Rod
CTC-1 from FE 6502 (Left);
Slight Reaction Zone on Tip
of Thermocouple Sheath (Right)
No. 16619; D 1309

PRTR Fuel Element Internal Gas Pressure Measurement - D. R. Doman

Design calculations on the Mark I-R 19-rod cluster PRTR fuel element showed that in attaining a goal exposure of 15,000 MWd/MT_{fuel} with some fuel operating molten, a gas plenum was required to accommodate gases released from the fuel without overstressing the cladding.(1) This work also showed that more data are required to increase the accuracy of such calculations, especially on fuel elements operating for extended periods with molten cores. To help obtain this data, three rods on operating Mark I-R fuel elements in two reactor locations are being instrumented to measure gas plenum temperatures and pressures. Temperatures will be measured with 0.159 cm (1/16 in.) diam stainless steel sheathed chromel-alumel thermocouples. Pressures will be measured with the null pressure balance Booth-Cromer type transducer which was successfully developed and used at General Electric-Vallecitos.(2) This transducer uses controlled-pressure gas against one side of a diaphragm to balance fuel rod gas pressure on the other side, with balance indicated by the opening of an electrical contact. One fuel element with such instrumentation will be charged into the PRTR core during November, with the other element to be charged when operation of the Batch Core Experiment begins.

Diffusion Test Element Irradiations - M. K. Millhollen and L. A. Pember

Two diffusion test elements (GEH-4-115 and GEH-4-117) were successfully irradiated in the MTR B-3 loop to obtain

---

1. R. E. Sharp. Unpublished Data, Battelle-Northwest. (Personal Communication)
2. M. B. Reynolds. "Measurement of Free Fission-Gas Pressure in Operating UO_2-Filled Fuel Rods," Nucl. Sci. and Eng., vol. 20, pp. 386-391. Also published in GEAP-4135, General Electric, Vallecitos.

information on PuO_2 migration during irradiation. The first test element (GEH-4-115) was a four-rod cluster in which UO_2–2 wt% PuO_2 sintered pellets were interspersed between natural-UO_2 sintered pellets.[1] The second test element (GEH-4-117) was identical to the first element except 2.8 wt% U^{235} enriched UO_2 pellets were used in place of natural-UO_2 pellets.[2] The UO_2–2 wt% PuO_2 pellets used in both tests were fabricated in the same batch. The cladding in both cases was 1.44 cm (0.565 in.) OD by 1.282 cm (0.505 in.) ID Zircaloy-2.

The first test element (GEH-4-115) was irradiated in the MTR for 15 effective full power days. Maximum exposure was 0.38×10^{20} fissions/cm^3 (2080 MWd/MT_{fuel}) on the UO_2–2 wt% PuO_2 pellets in the maximum flux zone. Calculations based on assumptions made before irradiation indicated 211 W/cm^2 (668,000 Btu/(hr)(ft^2) maximum surface heat flux on the UO_2–2 wt% PuO_2 pellets, giving a 2748 °C maximum central core temperature.

Postirradiation examination of the cluster revealed that the fuel rod cladding was bulged over each UO_2–2 wt% PuO_2 pellet in or near the high flux location (Figure 4.13). The bulges in the cladding suggest that the UO_2–2 wt% PuO_2 pellets had operated in-reactor with appreciable fuel melting. Recalculations based on the actual maximum flux encountered during irradiation indicate a surface heat flux near 315 W/cm^2 (1.0×10^6 Btu/(hr)(ft^2) with gross central melting.

One rod in the cluster was removed from the assembly for examination. Several diameter measurements were made showing the cladding had bulged a maximum of 0.36 mm (0.014 in.) on the diameter. A transverse cross section was made near the center of one of the UO_2–2 wt% PuO_2 pellets in the maximum

---

1. Ceramics Research and Development Quarterly Report, January-March 1965, BNWL-91.
2. Ceramics Research and Development Quarterly Report, April-June 1965, BNWL-150.

PRTR Fuel Element Internal Gas Pressure Measurement - D. R. Doman

Design calculations on the Mark I-R 19-rod cluster PRTR fuel element showed that in attaining a goal exposure of 15,000 MWd/MT_{fuel} with some fuel operating molten, a gas plenum was required to accommodate gases released from the fuel without overstressing the cladding.(1) This work also showed that more data are required to increase the accuracy of such calculations, especially on fuel elements operating for extended periods with molten cores. To help obtain this data, three rods on operating Mark I-R fuel elements in two reactor locations are being instrumented to measure gas plenum temperatures and pressures. Temperatures will be measured with 0.159 cm (1/16 in.) diam stainless steel sheathed chromel-alumel thermocouples. Pressures will be measured with the null pressure balance Booth-Cromer type transducer which was successfully developed and used at General Electric-Vallecitos.(2) This transducer uses controlled-pressure gas against one side of a diaphragm to balance fuel rod gas pressure on the other side, with balance indicated by the opening of an electrical contact. One fuel element with such instrumentation will be charged into the PRTR core during November, with the other element to be charged when operation of the Batch Core Experiment begins.

Diffusion Test Element Irradiations - M. K. Millhollen and L. A. Pember

Two diffusion test elements (GEH-4-115 and GEH-4-117) were successfully irradiated in the MTR B-3 loop to obtain

---

1. R. E. Sharp. Unpublished Data, Battelle-Northwest. (Personal Communication)
2. M. B. Reynolds. "Measurement of Free Fission-Gas Pressure in Operating UO_2-Filled Fuel Rods," Nucl. Sci. and Eng., vol. 20, pp. 386-391. Also published in GEAP-4135, General Electric, Vallecitos.

information on PuO_2 migration during irradiation. The first test element (GEH-4-115) was a four-rod cluster in which UO_2–2 wt% PuO_2 sintered pellets were interspersed between natural-UO_2 sintered pellets.[1] The second test element (GEH-4-117) was identical to the first element except 2.8 wt% U^{235} enriched UO_2 pellets were used in place of natural-UO_2 pellets.[2] The UO_2–2 wt% PuO_2 pellets used in both tests were fabricated in the same batch. The cladding in both cases was 1.44 cm (0.565 in.) OD by 1.282 cm (0.505 in.) ID Zircaloy-2.

The first test element (GEH-4-115) was irradiated in the MTR for 15 effective full power days. Maximum exposure was 0.38×10^{20} fissions/cm^3 (2080 MWd/MT_{fuel}) on the UO_2–2 wt% PuO_2 pellets in the maximum flux zone. Calculations based on assumptions made before irradiation indicated 211 W/cm^2 (668,000 Btu/(hr)(ft^2)) maximum surface heat flux on the UO_2–2 wt% PuO_2 pellets, giving a 2748 °C maximum central core temperature.

Postirradiation examination of the cluster revealed that the fuel rod cladding was bulged over each UO_2–2 wt% PuO_2 pellet in or near the high flux location (Figure 4.13). The bulges in the cladding suggest that the UO_2–2 wt% PuO_2 pellets had operated in-reactor with appreciable fuel melting. Recalculations based on the actual maximum flux encountered during irradiation indicate a surface heat flux near 315 W/cm^2 (1.0×10^6 Btu/(hr)(ft^2)) with gross central melting.

One rod in the cluster was removed from the assembly for examination. Several diameter measurements were made showing the cladding had bulged a maximum of 0.36 mm (0.014 in.) on the diameter. A transverse cross section was made near the center of one of the UO_2–2 wt% PuO_2 pellets in the maximum

---

1. Ceramics Research and Development Quarterly Report, January-March 1965, BNWL-91.
2. Ceramics Research and Development Quarterly Report, April-June 1965, BNWL-150.

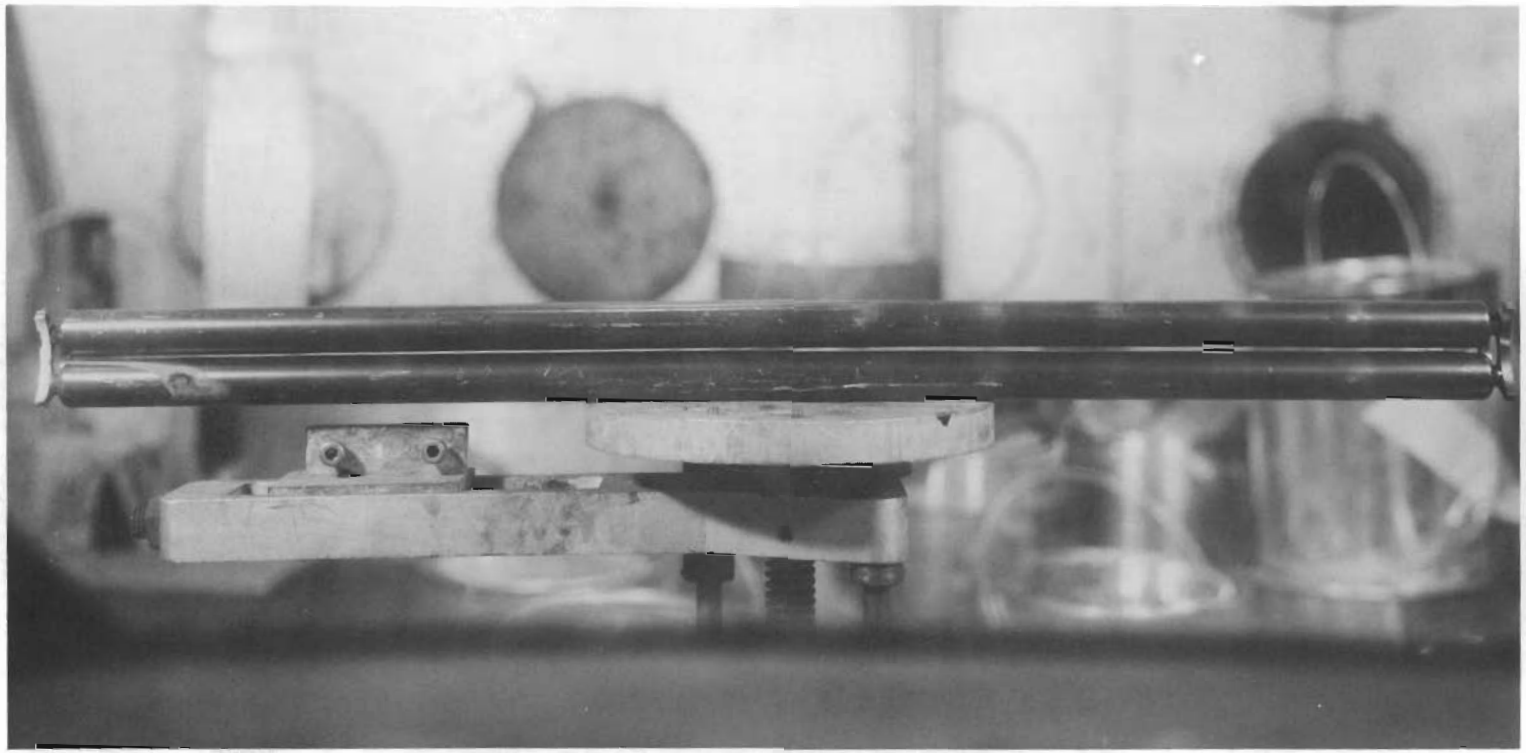

FIGURE 4.13
Diffusion Test Element (GEH-4-115) After Irradiation

flux region. A 2 in. long longitudinal section of the rod was also made immediately above the transverse cross section. Each of the two specimens was examined visually and macrographs, beta-gamma autoradiographs, and alpha autoradiographs were made (Figure 4.14 and 4.15). The relatively new alpha autoradiographic technique was adapted from the method used at Vallecitos Atomic Laboratory.(1)

The macrographs revealed extensive central melting in the UO_2–2 wt% PuO_2 pellets. The beta-gamma autoradiographs showed fairly normal fission product distribution patterns for molten core pellet fuel. The alpha autoradiographs revealed that homogenization occurred in the molten zones with very little plutonium migration into the natural UO_2. A careful study of the pictures in Figure 4.15 shows that the only PuO_2 movement was along the long columnar grains surrounding the molten regions. Where the temperature was sufficient, this columnar grain region extended into the normal UO_2 pellets. An area of apparent plutonium depletion in the UO_2–2 wt% PuO_2 pellets will be investigated further.

The second diffusion test element (GEH-4-117) was irradiated for 34.3 effective full power days, also in the B-3 loop of the MTR. The element was returned to PNL and was visually examined. The cluster is warped, but no cladding bulges are apparent. One rod was removed from the cluster for an examination similar to that for the first element.

Molten UO_2-Water Reaction Studies - R. L. Gibby

In anticipation of an overall analysis of safeguards for the Molten Core Experiment in PRTR, a study is being made of molten uranium-water reactions to determine the following:

---

1. J. H. Davies and R. W. Darmitzel. "Alpha Autoradiographs Technicque for Irradiated Fuel," Nucleonics, vol. 23, no. 7, pp. 86-87. 1965.

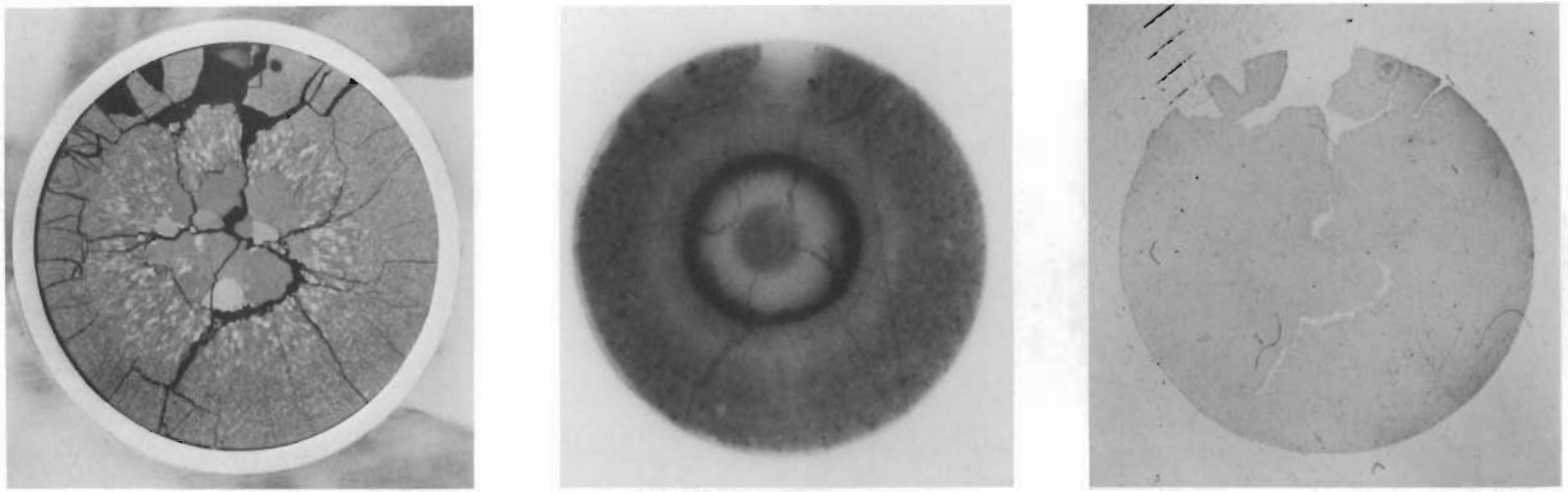

Macrograph Beta-Gamma Autoradiograph Alpha Autoradiograph

FIGURE 4.14

Transverse Cross Section of GEH-4-115 Fuel Rod
5X

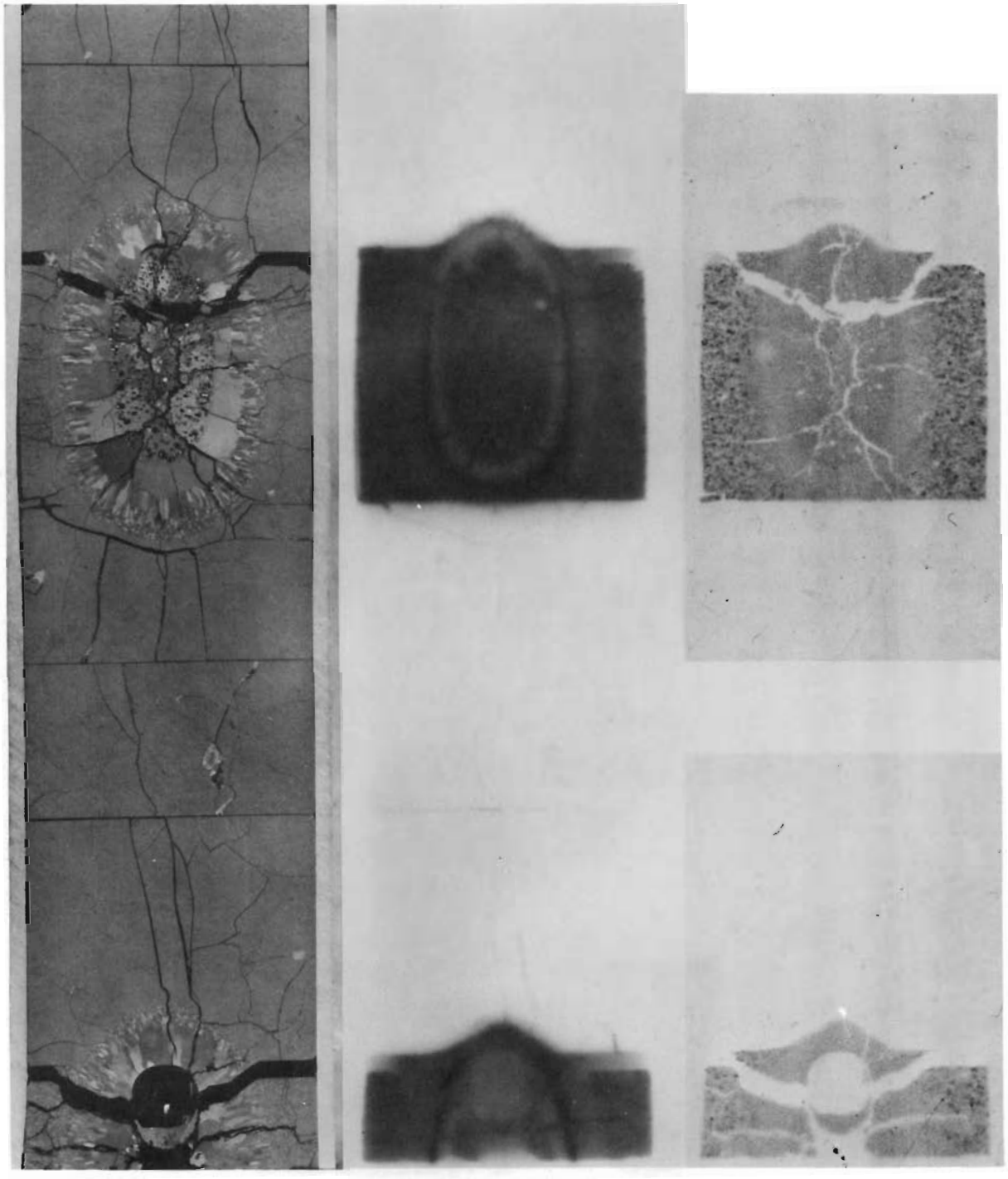

(1) (2) (3)

FIGURE 4.15

Longitudinal Cross Section of GEH-4-115 Fuel Rod
(1) Macrograph (2) Beta-Gamma Autoradiograph
(3) Alpha Autoradiograph

- The amount of hydrogen released when molten UO_2 is injected into pressurized, heated water
- The amount of fragmentation of the urania upon injection
- The rates of water temperature rise and pressure increase after injection.

The experimental apparatus (Figure 4.16) consists of a pressure furnace capable of operation to 160 atm and a small resistance heater water container. A thin aluminum membrane (0.005 cm) is used to cover the water container to prevent evaporation losses at temperatures to 260 °C (Figure 4.17). Molten urania is formed by self-resistance melting of 1.3 cm diam by 1.3 cm long sintered pellets. Molten drops of urania readily penetrate the aluminum membrane, coming in contact with the water. In two experiments, Zircaloy-2 membranes were substituted for aluminum. The molten urania melted through a 0.012 cm Zircaloy membrane but only caused slight warping when impinged on a 0.075 cm membrane.

The furnace is pressurized to 67 atm with cylinder argon to reduce urania volitalization and also to prevent water losses from the container to the furnace proper. During successive runs, the water temperature was controlled at different temperatures in the range 30 to 260 °C. An iron-constantan thermocouple, inside the water vessel, measured the temperature rises associated with UO_2 injection. After amplification, the thermocouple signal was fed to a recording oscillograph to obtain a trace of temperature versus time. A pressure transducer circuit was used to measure and record pressure transients.

Oxidation of UO_2 was determined from changes in O:U ratios. Oxygen to uranium ratios from reacted and unreacted portions of the same pellet were compared to calculate the volume of hydrogen produced. Coulometric titrations were used to determine O:U. Table 4.4 presents the experimental data.

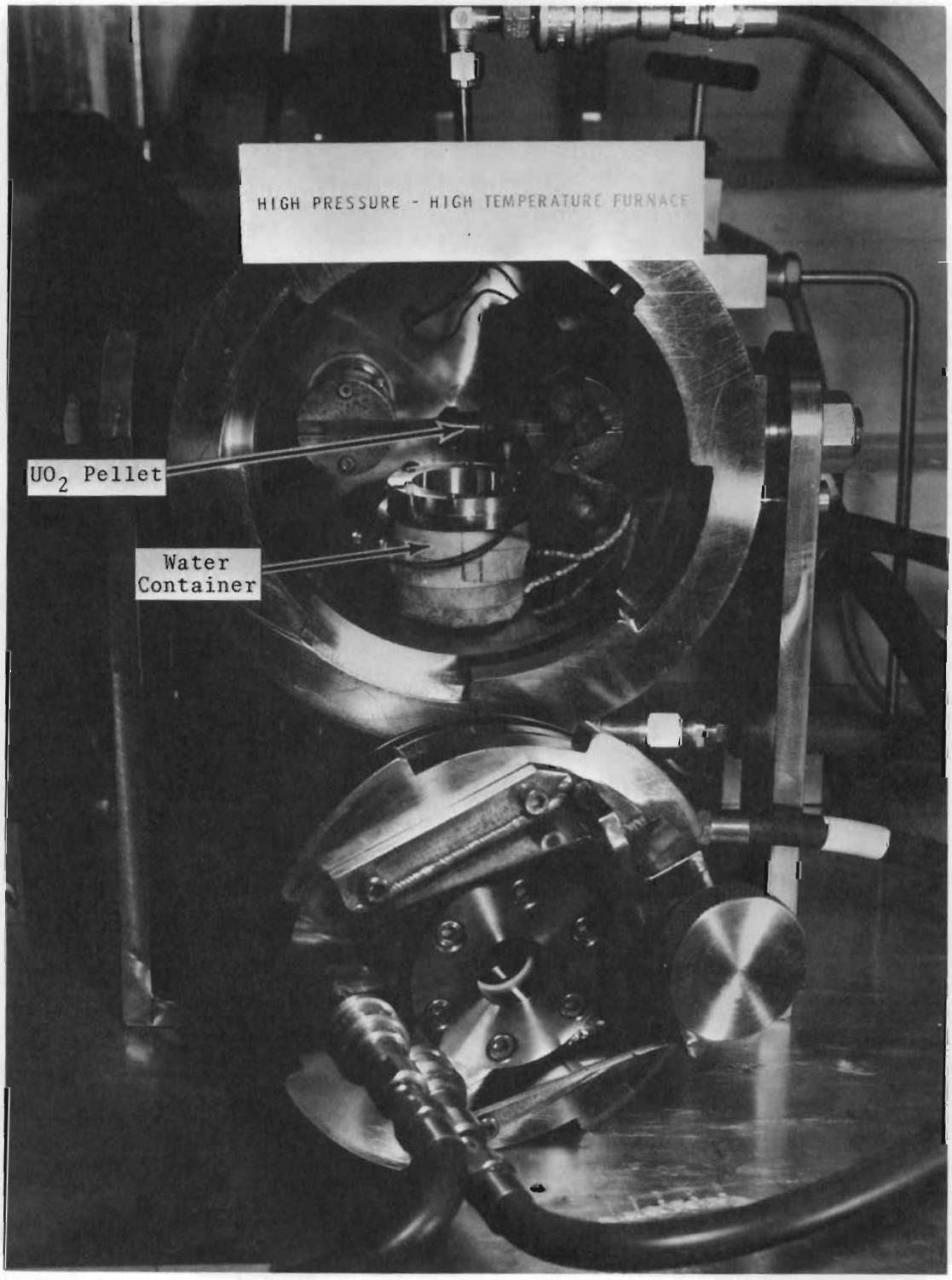

FIGURE 4.16

Pressure Furnace with Water Container in situ

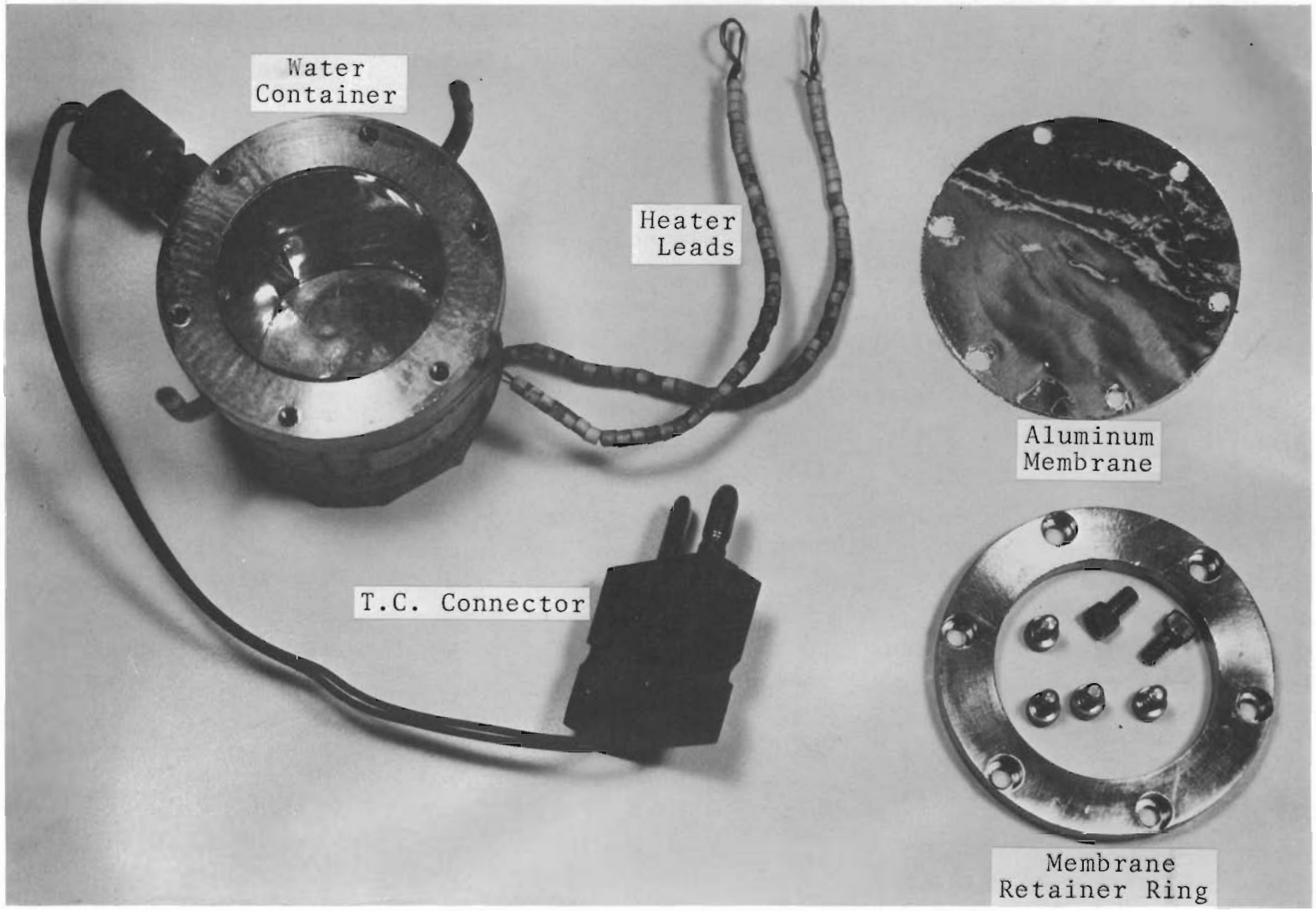

FIGURE 4.17

Water Container Components

TABLE 4.5

MOLTEN URANIA-WATER REACTION STUDIES

Sample Number	Weight of Melt, g	Water Temperature, °C Before	Water Temperature, °C After	Pressure, psi Before	Pressure, psi After	O:U Before	O:U After	Calculated H_2 Release ml(STP)/g UO_2	Rate of Water Temperature Rise (°C/sec)	Average Particle Diameter, cm	Remarks
GP-1	0.76	27	32	1000	1000	2.002	2.058	4.5	--	--	
GP-2	1.13	106	121	1000	1000	2.004	2.082	6.5	--	--	
GP-3	0.57	101	106	1000	1000	2.002	2.077	6.2	--	--	
GP-4	2.95	33	67	1000	1000	--	--	---	19	--	
GP-5	7.71	110	171	900	--	2.012	2.128	9.6	15	0.072	
GP-6	8.49	210	280	1000	--	2.012	2.155	11.9	7	0.065	
GP-7	11.38	255	304	1000	>1500	2.029	2.146	9.7	4	0.070	
GP-8	--	38	114	--	--	--	--	---	19	--	0.013 cm Zr-2 membrane
GP-9	--	--	--	--	--	--	--	---	--	--	0.076 cm Zr-2 membrane
GP-10	9.37	28	101	1000	1270	2.005	2.080	6.2	15	--	
GP-11	9.25	100	180	1000	1150	2.002	2.087	7.0	18	--	
GP-12	9.13	260	300	1000	1420	2.006	2.142	11.5	13	--	

Attempts to determine pressure increases during urania injection into water were mostly unsuccessful. Expansion of the argon in the furnace during urania melting caused pressure rises which tended to mask-out pressure contributions from steam formation. Also, the comparatively large volume of the furnace and the compressibility of the gas atmosphere tended to attenuate any pressure rises which did occur, thus decreasing the possibility of distinguishing small increases. Significant pressure increases were observed only when urania was injected into water heated to 250 °C or above. In this case, considerable steam formation occurred upon injection, as the vapor pressure of the water, heated by the molten urania, was equal to or greater than the ambient furnace pressure. The rate of water temperature increase was similar for all initial water temperatures. Lower values were observed with water at 250 °C or above, but this was probably caused by excessive water losses from the water container, leaving the thermocouple above the water level.

Water-quenched urania samples were not fragmented when removed from the water container. In every case, a puddle of urania formed at the bottom of the water container, an indication that solidification did not occur upon immediate contact with the water but after reaching the floor of the vessel. Although fragmentation did not occur during the water quench, the melted urania was extremely friable and could be readily reduced to a fine aggregrate by only moderate agitation, a strong indication that the samples were densely populated with microfissures. Moderate agitation of three samples in plastic vials resulted in fine aggregate with similar particle size distributions and about the same average particle size. In many cases large unbroken pieces of quenched UO_2 contained large central cavities, a feature probably related to rapid cooling.

Calculated hydrogen generation volumes do not appear to vary greatly with initial water temperature or with urania melt size. Although the changes in O:U are greater for the initially hotter water, some urania oxidation probably occurred before injection because at the higher water temperatures some vapor leaked from the water container into the furnace chamber. The magnitude of the hydrogen volume release values compare favorably with melt-down experiments being performed in TREAT,[1] where urania pellets, immersed in room temperature water, are rapidly melted by a nuclear pulse.

Reactor Basin Underwater Work - C. H. Allen

Three experimental fuel elements were irradiated in the PRTR. After some irradiation, one or two fuel rods were removed from the fuel element in the reactor storage basin, replaced with new fuel rods, and then the element was returned to the reactor for further irradiation.

The rods were removed and replaced under about 2 to 3 m of water, using the storage basin fuel element handling tray and special extended reach hand tools.

To accomplish rod replacement (Figure 4.18), the original bands securing the 19-rod fuel bundle are cut and the bundle is rebanded.

Replacement of rods in the fuel bundle in the reactor basin will be done more frequently in the future because it allows complete examination (metallurgy, ceramics, and physics) of an irradiated fuel rod without interrupting continued irradiation of the rest of the element.

---

1. R. C. Liimatainer and F. J. Testa. Studies in TREAT of Uranium Dioxide Fuel, ANL-RCV-3391, Argonne National Laboratory, pp. 63-72.

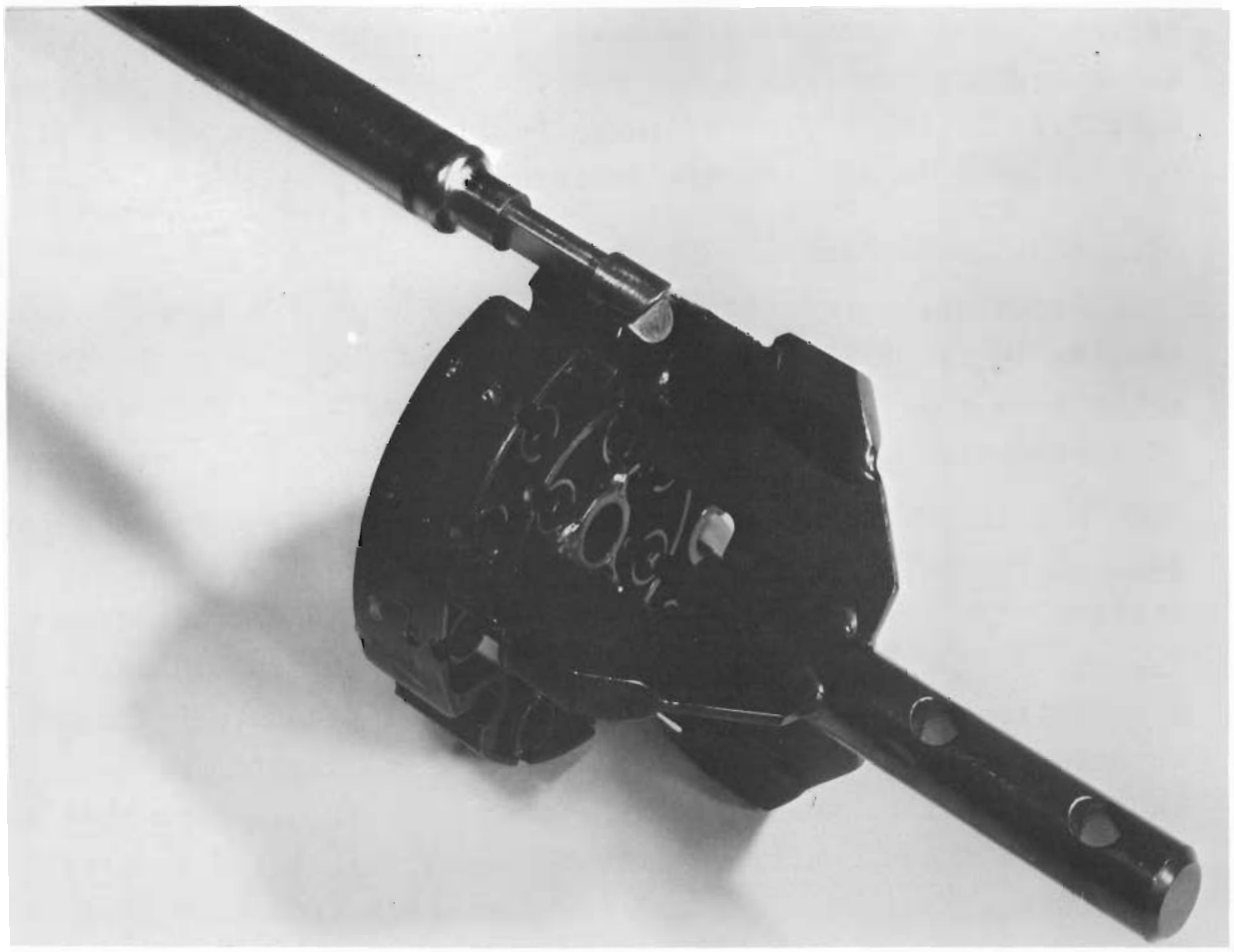

FIGURE 4.18
End Hanger Design for Replaceable Rods

Salt Cycle - C. H. Allen, R. F. Klein, R. C. Smith, and R. R. Sharp

Fourteen salt cycle recycle fuel rod segments were fabricated in a Radiometallurgy facility cell. These segments were in addition to the 19 previously fabricated from salt cycle fuel material. The 14 segments consisted of six segments of 2.02% PuO_2 material to be made into two 60-in. long PRTR fuel rods for eventual reaction irradiation, three segments of 2.00% PuO_2 and four segments of 1.45% PuO_2 which were made for fuel storage purposes. The fuel material in the latter seven

segments may be reclad at a later date. The fabrication of these segments concludes the recycle fuel fabrication program conducted in the Radiometallurgy Facility. Future work will be performed in the new 324 Building.

Salt Cycle Fuel Recycle - R. C. Smith

Irradiation testing of the salt cycle fuel element is continuing in the PRTR where the element had acquired a burnup of about 0.38×10^{20} fissions/cm^3 (~1540 MWd/MT_{fuel}) at the end of September.

Postirradiation examination was essentially completed for the single fuel rod segment irradiated at the Idaho Testing Station. No effects were detected which would detract from the use of this type of fuel for power production or long irradiations. Two items in the postirradiation study should be noted. The bottom Zircaloy end cap was slightly dished, indicating a zone sufficiently hot to melt or dissolve some of the metal[1] and confirming the desirability of the present fabrication policy of graded end enrichment for PRTR fuel rods containing a 2% or greater plutonium enrichment. Definitely higher fuel temperatures occurred in the bottom end regions than in the top area.

There is some indication the fuel may have contained PuO_2 inclusions. X-ray diffraction data show Salt Cycle fuel is normally a solid solution; however, a check of the run data for the particular fuel used in this segment revealed a discontinuous period during which the salt bath conditions would allow PuO_2 precipitation. The pure PuO_2 would then be trapped in the growing mixed oxide crystals as the electrodeposition proceeded. Fuel in subsequent rods (those still under irradiation) is from later electrodeposition runs and contains more homogeneous fuel material.

---

1. Ceramics Research and Development Quarterly Report, April-June 1965, BNWL-150, Figure 3.12, p. 3.22.

Recycle Fuel Fabrication - R. C. Smith and D. C. Lehfeldt

Construction of the Shielded Metallurgical Facility (Figure 4.19), 324 Building, is nearing completion. In part, this facility will be used for the remote fabrication of irradiated fuels for recycling in a reactor.

Three preliminary process flow charts (Figures 4.20 through 4.22) illustrate the fabrication of recycled PRTR fuel elements. With minor changes, these same processes and alternates are applicable to fabricating recycled oxide fuel elements of widely varying designs. These preliminary process flow charts will (1) serve as bases for present and future process and equipment development prior to and continuing through the operation of the Shielded Metallurgical Facility and (2) assist in cost studies on remote fuel fabrication.

The "Salt Cycle" and "PEPPER Cycle" (Plutonium Enriched Particle Process for Extended Reactivity) recycle fuel element fabrication processes (Figures 4.20 and 4.21, respectively) involve removing the fuel from the cladding, reprocessing the spent fuel to partially remove the neutron poisons, adding enriched fuel to increase the reactivity, and fabricating the fuel elements for reirradiation. The "Salt Cycle" fuel is electrodeposited irradiated fuel. A previous report[1] described the remote fabrication and irradiation of a 19-rod cluster PRTR fuel element using "Salt Cycle" recycle fuel prepared in a hot cell by Chemical Development personnel.

Reprocessing-refabricating experiments will be initiated on the "PEPPER Cycle." Not shown on the flow chart are several alternate processes under consideration for partial removal of neutron poisons from the spent fuel, i.e., selective sublimation and/or oxidation-reduction cycles.

---

1. Ceramics Research and Development Quarterly Report, January-March 1965, BNWL-91.

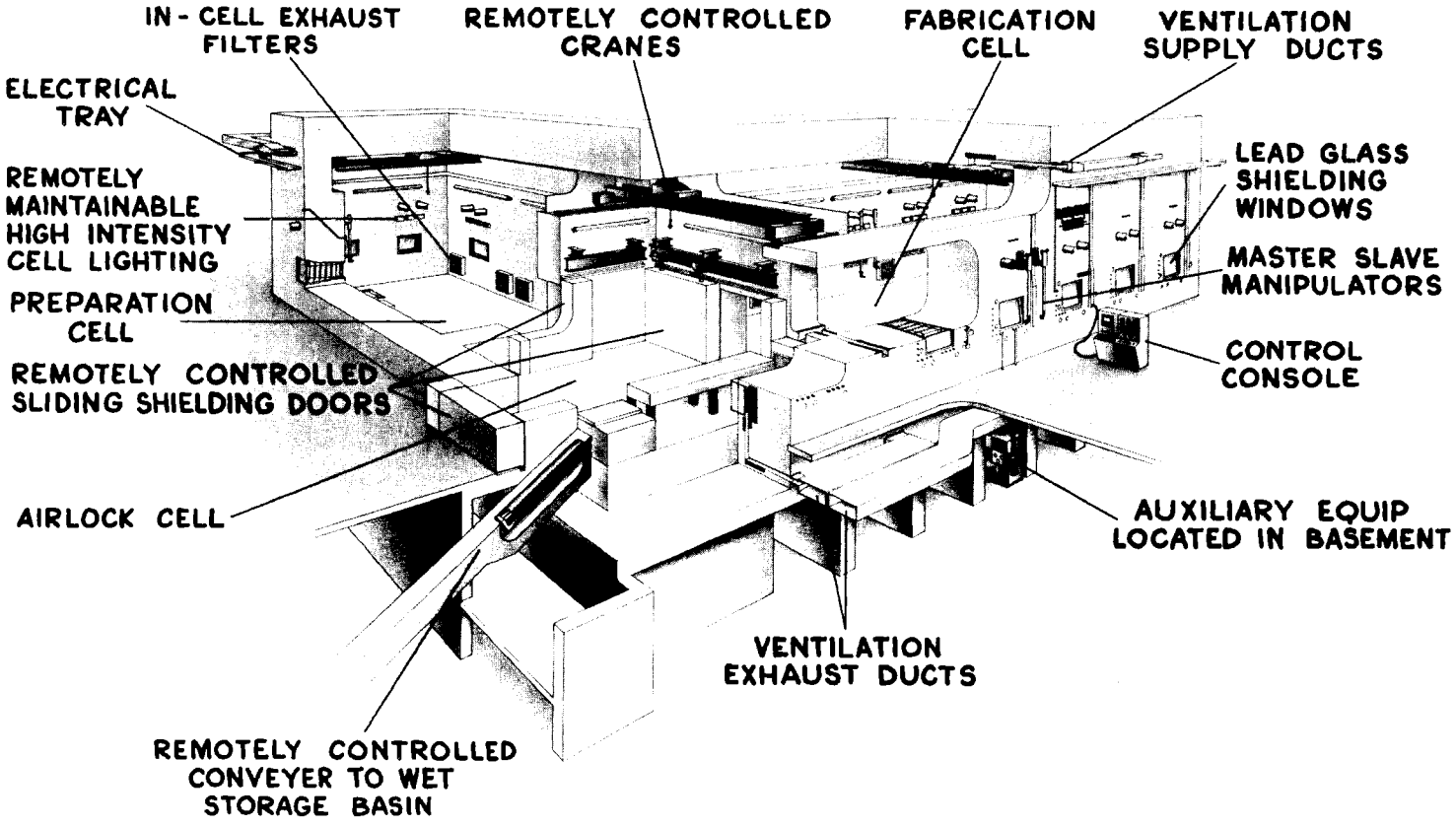

FIGURE 4.19

Shielded Metallurgical Facility - 324 Building

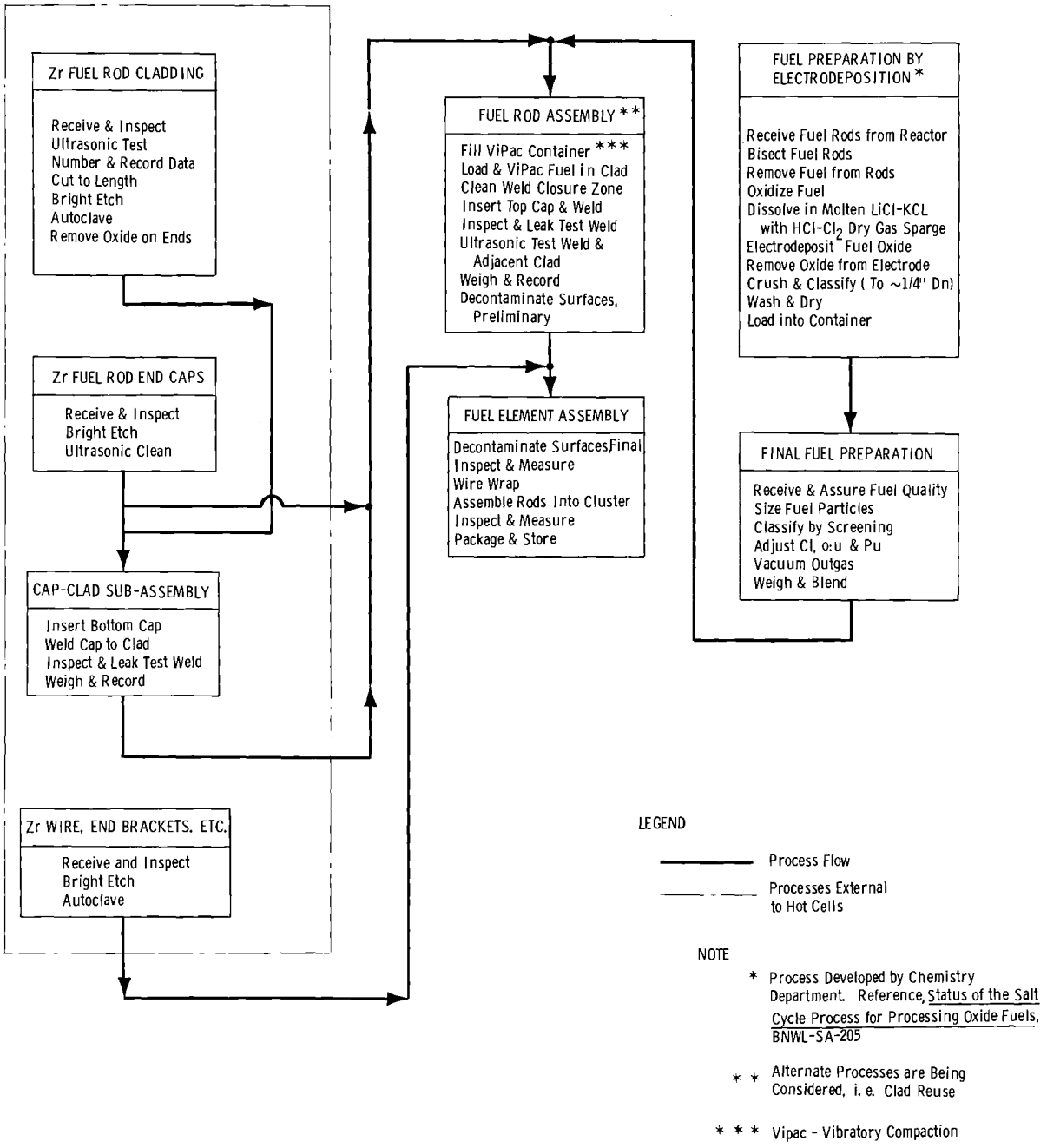

FIGURE 4.20

Preliminary Process Flow Chart
for Salt Cycle Fuel Fabrication

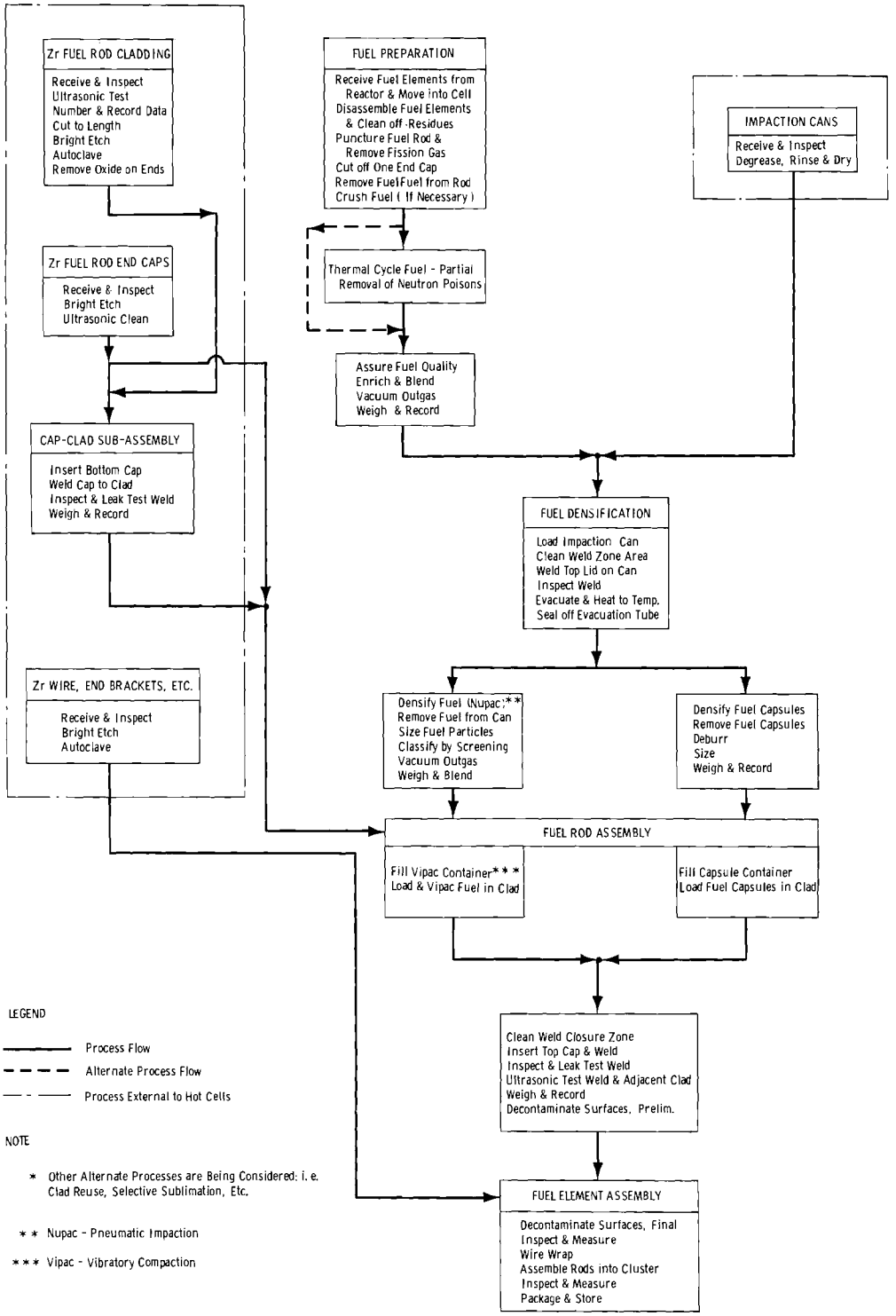

FIGURE 4.21

Preliminary Process Flow Chart
for PEPPER Cycle Fuel Fabrication

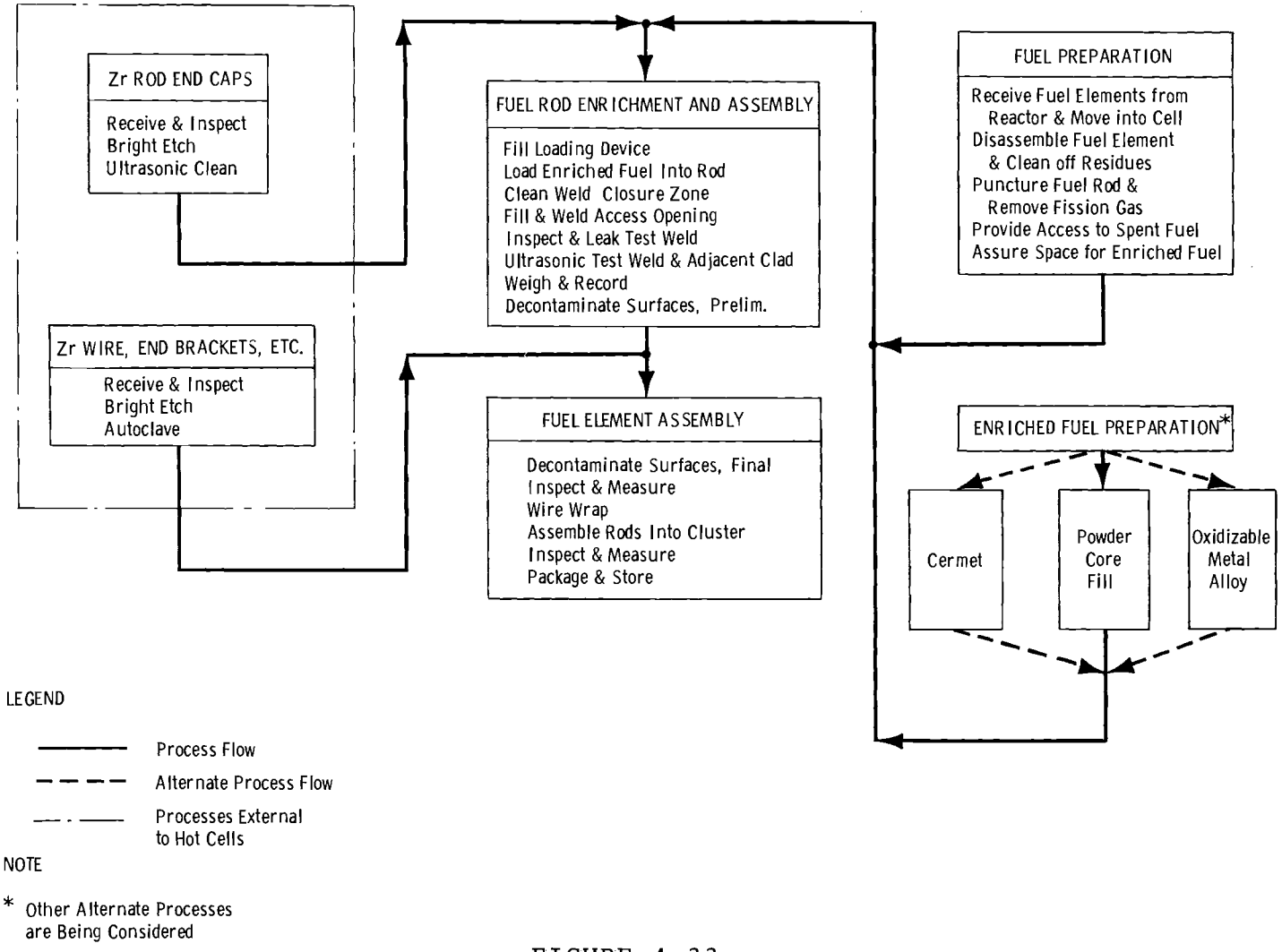

FIGURE 4.22

Preliminary Process Flow Chart for Rejuvenation Cycle Fuel Fabrication

Clad reuse, a strong potential fuels recycle cost reduction concept, is applicable to most fuel element recycle processes. Reusing the irradiated cladding, from which the spent fuel is removed requires development to prove feasibility. Part of the development effort will be in conjunction with the rejuvenation or reenrichment process.

The "Rejuvenation Cycle" (Figure 4.22) differs from the previous processes in that no pyrochemical or thermal cycling processes are used to remove sorbed neutron poisons. To increase the nuclear reactivity, the free or dissociated fission gases are removed before the addition of fissionable isotopes. Central, peripheral, or blended fuel enrichment methods, using a variety of fuel material types and forms, are being considered.

The preliminary fuel recycle processes do not include all possible processes to recover spent fuel and the subsequent encapsulation for reirradiation. With the progress of development efforts, inevitable changes to these processes will eventually result in one or more economically feasible recycle processes.

PART V - JOINT FUEL DEVELOPMENT PROGRAMS

Collapse Testing: EBWR Tubing - J. P. Keenan and G. Testa

Six EBWR pressure capsules were fabricated from standard EBWR tubing (1.08 cm OD by 0.069 cm wall). Two of the capsules contained standard EBWR gas plenum springs. Three empty capsules were autoclaved for 72 hr at 290 °C, with each capsule subjected to a different pressure: 3000, 4000, and 4500 psi. The first two capsules were not deformed by autoclaving. However, the third capsule (4500 psi) collapsed during autoclaving Autoclaved for 72 hr at 290 °C and 4500 psi, a spring-loaded capsule collapsed around the spring. These tests were conducted at temperatures and pressures far greater than EBWR operating conditions (maximum 254 °C and 600 psi).

Irradiation Testing of EBWR Prototype Fuel Rods - W. J. Bailey and G. Testa

Capsule and prototype rod tests continue to indicate the UO_2-PuO_2 rods will perform satisfactorily under proposed 42 MW EBWR conditions (60 W/cm^2 maximum heat flux), and to the exposure of most interest (~2.5 by 10^{20} fissions/cm^3).

Vibrationally compacted UO_2 (depleted) - 1.5 wt% PuO_2 rods were prepared at PNL for the cooperative Argonne National Laboratory-PNL Plutonium Recycle Demonstration Experiment in the EBWR. Each PNL-ANL designed rod (148 cm long) contains 122 cm of impacted fuel (86 to 89% TD) in Zircaloy cladding (0.945 cm ID, 0.064 cm wall), with a plenum (14.6 cm long) incorporating a stainless steel (302 alloy) spring separated from the fuel by a ZrO_2 insulator pellet (0.64 cm thick).

Short rod specimens (77 to 84% TD), some with prototype fission gas plena, are being irradiated to achieve burnups to 6.8 by 10^{20} fissions/cm^3 to evaluate fission gas release,

sintering, plutonium and/or fission product migration, and spring-pellet-fuel compatibility. Of the 32 capsules (29 discharged), the maximum burnup, as of September 1965, was 5.2 x 10^{20} fissions/cm^3 (20,900 MWd/MT of fuel). Excellent performance is indicated, and no failures have occurred (Table 5.1). Reactions, noted with early low-burnup samples at high heat flux values, are now observed with lower heat flux, high-burnup samples.

TABLE 5.1

EBWR PROTOTYPE FUEL ROD IRRADIATION TEST RESULTS

Rod Heat Flux, W/cm^2	Burnup (fissions/cm^3) x 10^{-20}	Molten Fuel	Center Void	Fuel-Zircaloy Reaction	Fuel-Insulator Reaction
340-374	0.61-1.6	X	X	X	X
298-304	0.46-0.55	X	X	-	X
218-298	0.40-1.9	-	X	-	X
135-188	0.24-2.2	-	X	-	-
171-189	3.7 -4.4	-	X	X	X
53-132	0.40-2.1	-	-	-	-

The fission gas release data (Figure 5.1) indicate 100% release in the fuel regions that were at temperatures >1800 °C.

Production-run EBWR fuel rods are being irradiated in the PRTR. A 21-rod bundle, currently under irradiation with a maximum heat flux of 61 W/cm^2, reached a burnup of 0.7 x 10^{20} fissions/cm^3 in September 1965. One rod was removed after a burnup of 0.52 x 10^{20} fissions/cm^3 and replaced by a new one, as planned. Bundle goal burnup is at least 2.7 x 10^{20} fissions/cm^3. Examination of the rod indicates that it is in good condition with no corrosion evident in the bottom end cap region (only unautoclaved part of rod).

Three-rod cluster tests (36 rods total) continue to indicate satisfactory in-reactor performance. Cluster goal burnups

are 0.4, 1.4, and 6.8 x 10^{20} fissions/cm^3, and 12 rods which have achieved the lowest goal burnup were discharged.

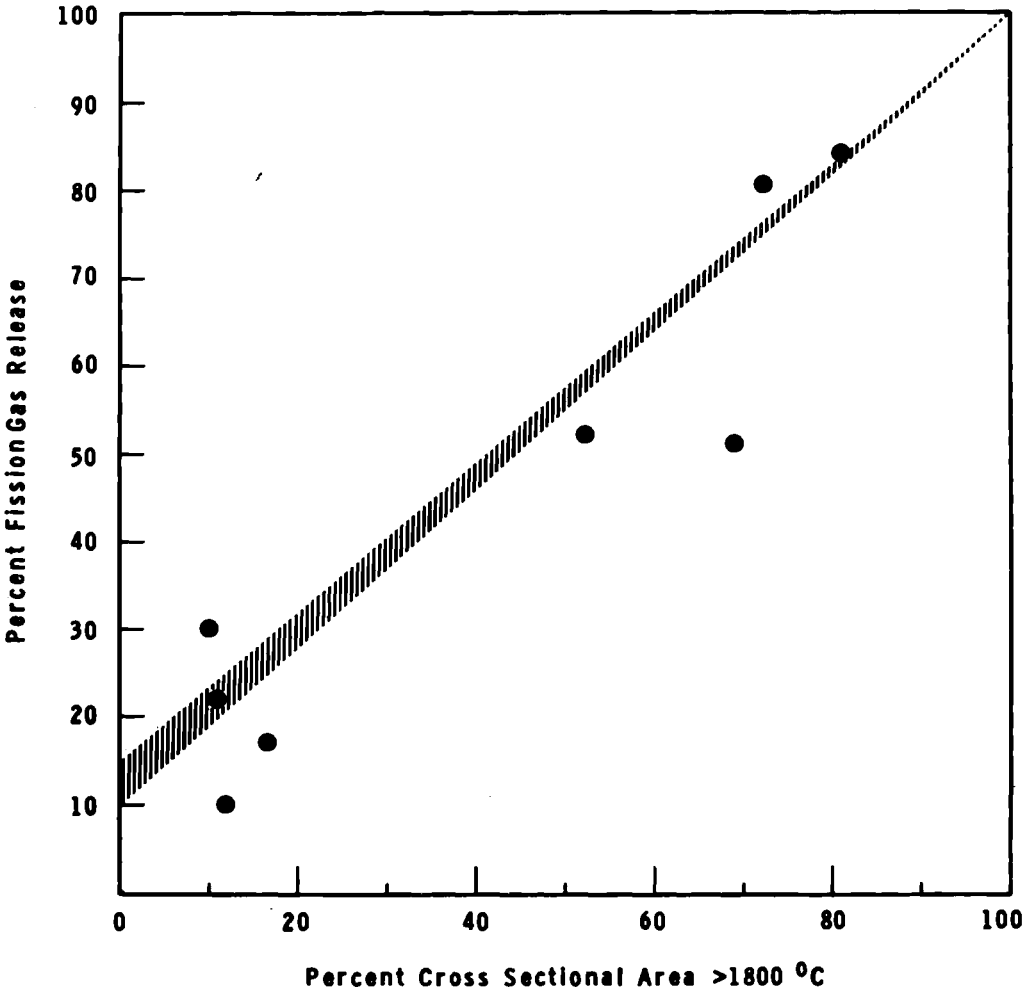

FIGURE 5.1

Fission Gas Release from Irradiated Impacted UO_2-PuO_2

HTLTR Fuel Element Design - L. C. Lemon, R. J. Lobsinger, and R. E. Sharp

Fuel element design was begun for the High Temperature Lattice Test Reactor (HTLTR). Operating at temperatures to 1000 °C in a nitrogen atmosphere, the HTLTR is a low power (2 kW) horizontal-tube, graphite-moderated reactor. The reactor is heated by graphite resistance heaters in the moderator.

The reactor requires the following fuel:

- Driver Fuel Elements: Over 1000 fuel rods containing about 1000 kg of enriched UO_2
- Flux Adjusting Elements: 100 fuel rods containing 1.27 cm natural UO_2 pellets
- Poison Shims: 30 rods containing Gd_2O_3 dispersed in a matrix of graphite or Al_2O_3
- Experimental Fuel Rods: Several different types containing various fuel combinations of $U^{233}O_2$, PuO_2, ThO_2, and UO_2.

The present major effort is to choose a suitable cladding material. According to previous environmental testing,* thoria-dispersed nickel and graphite are the primary candidates. Developmental quantities of thoria-dispersed nickel tubing were obtained for evaluation and testing.

---

* D. P. O'Keefe, Metallurgy Development Section.

PART VI - CUSTOMER WORK

PRCF Separable Rods - R. J. Shogren and R. E. Lyon

Twenty-eight PRCF separable mixed oxide fuel rods with 0.005 in. end caps were successfully vibrationally compacted. Eighteen of the rods were 18 in. long and 10 were 10 in. long. The diameter of all rods was 0.505 in. Rod densities varied from 85 to 87% TD.

Fifteen grams of -20 mesh fuel were placed in the end cap region (Figure 6.1) to prevent rupture by the larger particles during compaction. Figure 6.2 shows the stainless steel clamp with the nylon inserts which protected the end cap weld region from the vibration stress.

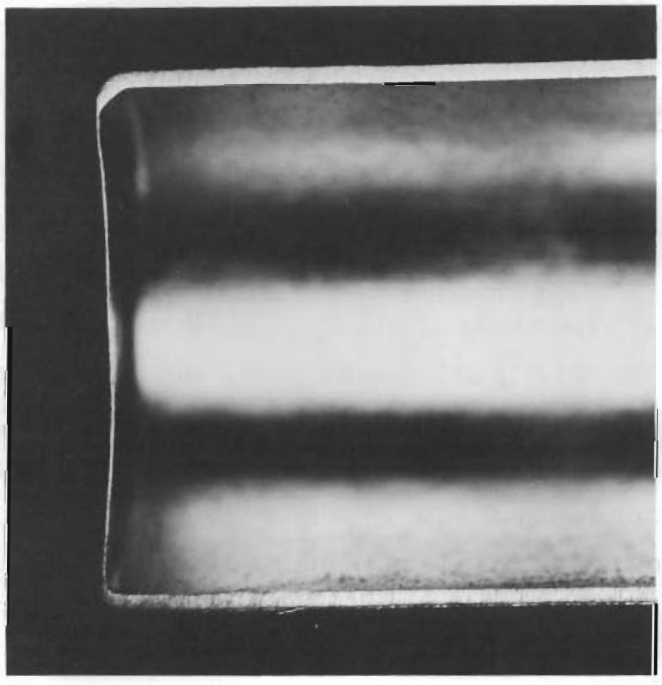

5X

FIGURE 6.1

Cross Section of PRCF Separable Rod
Showing 0.005 in. End Cap

No. 5652112D

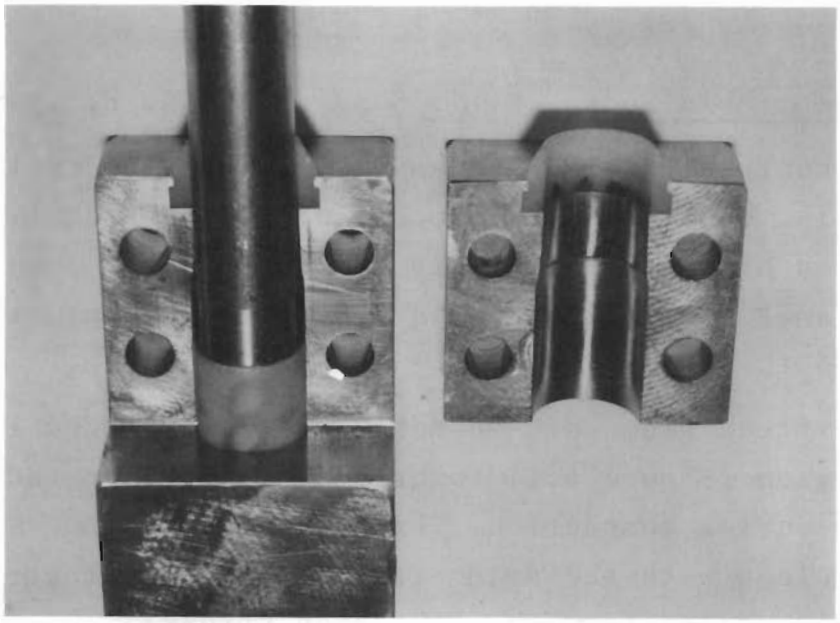

FIGURE 6.2
Stainless Steel Clamp with Nylon Inserts

Phoenix Fuels - J. P. Keenan

A 5.5 kg batch of plutonium (Pu^{240}, ~8%) was converted into Phoenix wafers measuring 4.98 cm OD and 0.51 mm thick. The wafers were made from an alloy of 20% plutonium in aluminum. In the final accounting, 7328 acceptable discs were fabricated from 4550 g of plutonium, about 200 g of plutonium were used in samples, and the remaining plutonium is in the form of scrap for reclamation. The chemical analyses for plutonium concentration are not complete. When these data have been obtained, it may be necessary to reject a small percentage of the wafers which fall outside the specification range of 19 to 21% plutonium. With this exception the project was completed on October 2, 1965.

The work was moved in batches from step to step. Training, quality requirements, and manpower availability made this method more feasible than a continuous process flow. Throughput

increased continuously throughout the fabrication period, reaching a peak of 1000 wafers per week during 2 of the last 3 weeks. Throughput during the last week dropped because of inefficiently small batches which had to be processed at the end of the run.

As with most processes, interacting process variables complicated production of the wafers. The early stages of work involved a large amount of process troubleshooting, equipment fabrication and process testing, with correspondingly low throughput rates. As techniques improved, so did quality and throughput. The size of the project does not justify the compilation of complete process standards, although much pertinent information has been recorded and filed. The most noteworthy process improvement developed during this run was the use of ethyl alcohol as a coolant and lubricant for the machining phase of wafer fabrication. (A nitrogen atmosphere in the glove box reduced the fire hazard.) This change increased throughput substantially.

Pu^{240} and Pu^{241} Irradiation Samples for Phillips Petroleum Company - C. H. Bloomster

Twenty-three test samples of pure (95%) Pu^{240} and Pu^{241} were fabricated for fission product transient measurements in the MTR by Phillips Petroleum Company. The tubular samples, 2.5 OD by 0.15 cm wall (1 in. OD by 0.060 in. wall), were made by a coextrusion process. The cladding was high purity Al–1 wt% Si alloy. The inner and outer cladding was 0.05 cm (0.020 in.) thick. The Pu^{240} and Pu^{241} were alloyed with aluminum in five different concentrations each.

The Pu^{240} and Pu^{241} were alloyed in graphite crucibles and cast into graphite molds. Rings were cut from the castings, pressed and machined to size and weight, chemically

cleaned, and assembled into billets. Adjacent to each ring, samples were taken for chemical analyses, in quadruplicate. Three rings were assembled in tandem, with aluminum rings as spacers, in each billet. The billets were hot outgassed and extruded at a 10 to 1 reduction in area, over a floating mandrel, using a streamlined die with a 60° entrance angle. The extruded tubes were radiographed for core location and machined to length. Before final assembly, each sample was ultrasonically bond tested, autoclaved, and visually inspected. To complete the assembly, end caps and thermocouple tubes were welded in place. Two final radiographs were taken at 90° angles for core location and wall thickness. Figure 6.3 shows a composite of the samples, machined casting, billet assembly, and finished test sample.

Radiation levels on the Pu^{241} alloys were between 1000 and 2000 mr/hr (contact), while the radiation levels on the Pu^{240} alloys were less than 100 mr/hr (contact).

Some difficulty with stringers was experienced in the very low Pu^{240}–Al alloys. Minute amounts of the alloys worked into the faying surfaces of the billet components where they acted like lubricants, extending as stringers for several centimeters. Too thin to be detected by radiography, the stringers were resolved by autoradiography. A modified welding procedure was developed to eliminate contamination in the weld zone.

Metal Sources Using P^{32} Isotope - D. C. Lehfeldt, R. C. Smith, D. E. DeWitt, and R. R. Sharp

Radiological Physics Operation at PNL requested that beta emitting isotope and metal sources be fabricated to perform interface dosimetry measurements. They selected P^{32} isotope in a matrix of aluminum and in a matrix of lead for the sources.

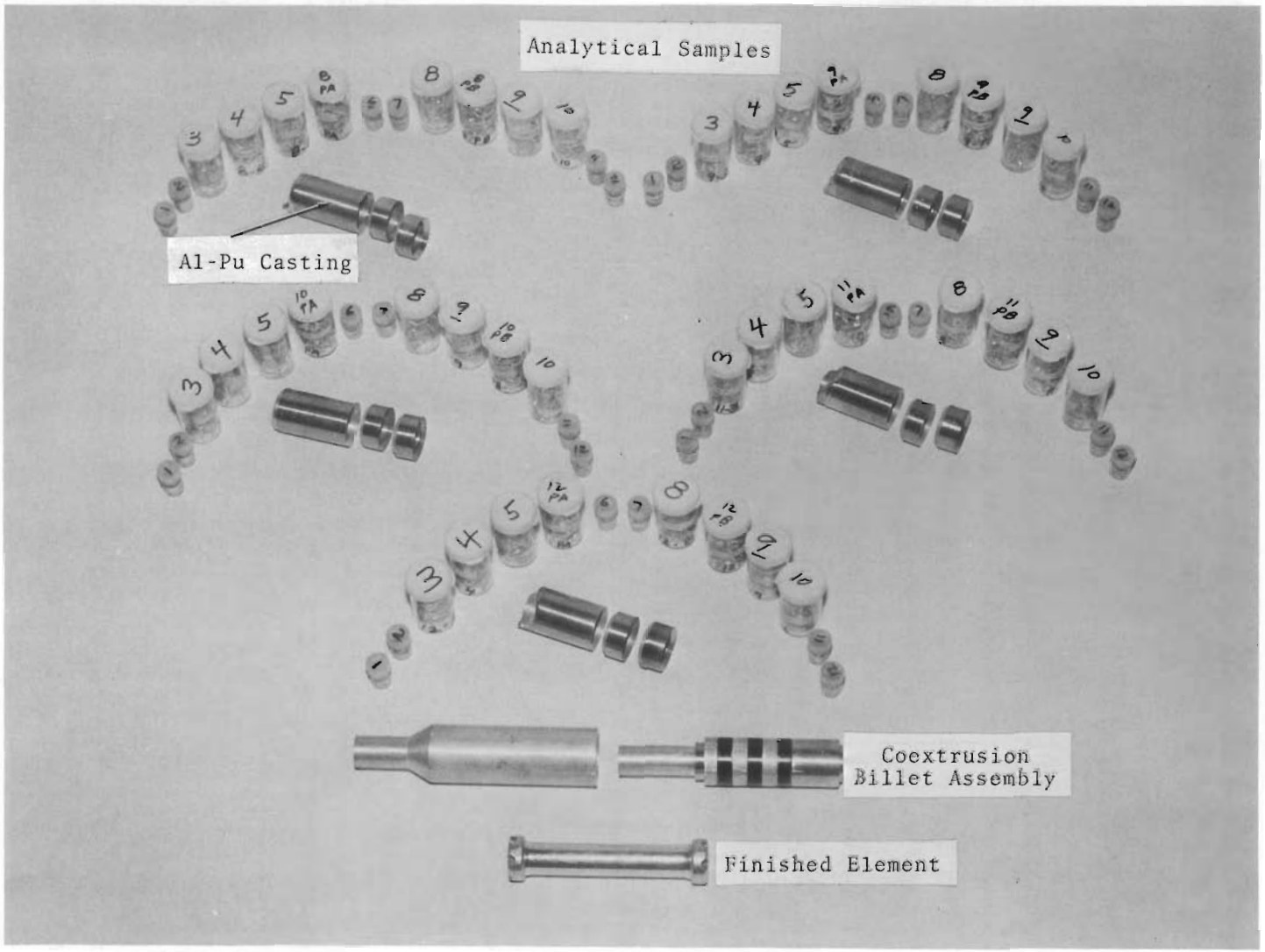

FIGURE 6.3

Al-Pu Irradiation Samples

The requirements of the isotope metal sources were as follows:

- Nominal dimensions
  - Al-P^{32} Source: 3 in. diam by 1/4 in. thick
  - Pb-P^{32} Source: 3 in. diam by 1/8 in. thick
- Commercially pure (99+%) aluminum and lead
- Uniformly dispersed P^{32} in source volume
- Uniform density and 90 to 100% of theoretical
- Top and bottom surfaces parallel to 0.005 in. TIR
- Sources mounted on special lucite holders.

All sources were made 1/32 in. thicker to allow for machining parallel faces. Machining parallel faces on the sources was considered unnecessary; therefore, machining was discontinued after the first set of sources were fabricated.

Three sets of Al-P^{32} sources were fabricated (Figures 6.4 and 6.5). All sources were fabricated by cold pressing the blended powders without a binder at about 85,000 psi. A punch and ring die system (Figure 6.6) was used in a shielded 300-ton hydraulic press (Figure 6.7) for cold pressing the powders.

The first two sets of Al-P^{32} and Pb-P^{32} sources fabricated, having a specific activity of about 3.4×10^6 disintegrations/min/g aluminum or lead, did not completely satisfy the requirements either of uniform isotope dispersion or 90 to 100% TD. Also, the Pb-P^{32} sources laminated. Between the first and second fabrication runs changes were made to the die assembly and in the slurry blending method.* As a result, the isotope dispersion was greatly improved, but other source characteristics were not completely satisfactory.

---

* Slurry blending and specific activity analysis were performed by Analytical Laboratories Operation, Battelle-Northwest.

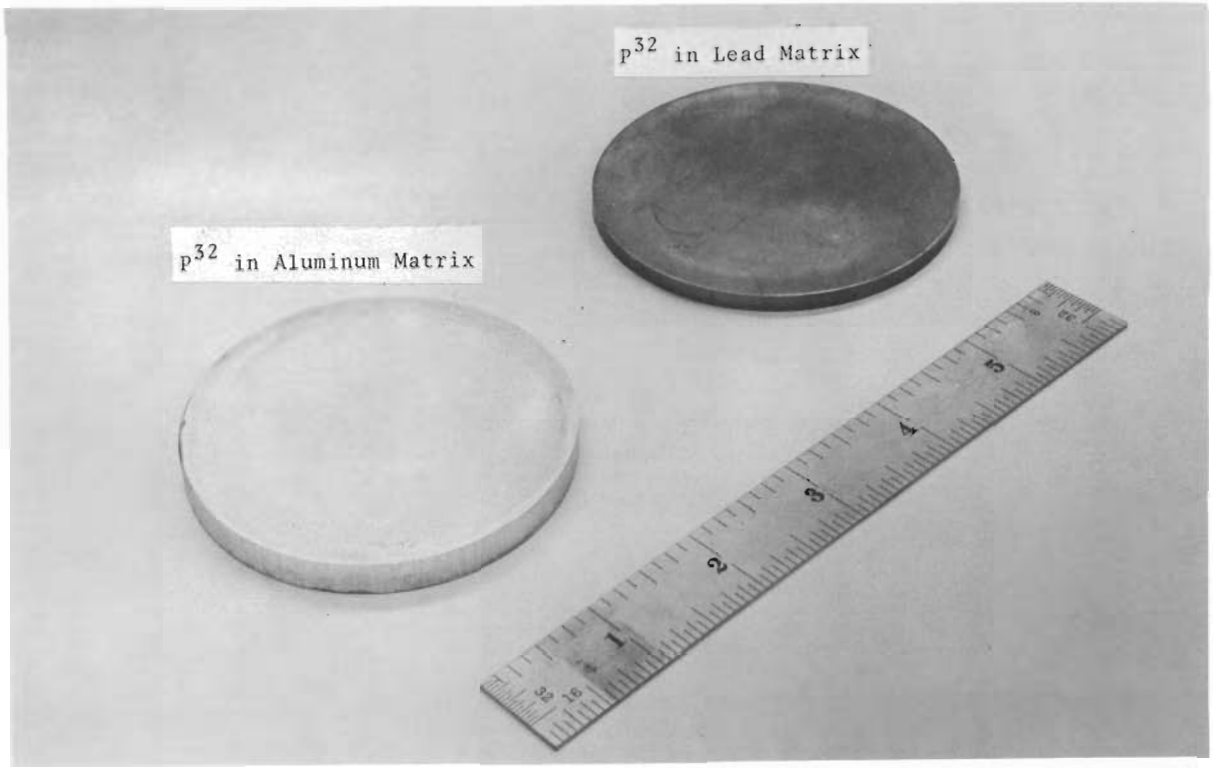

FIGURE 6.4
P^{32} Isotope Sources

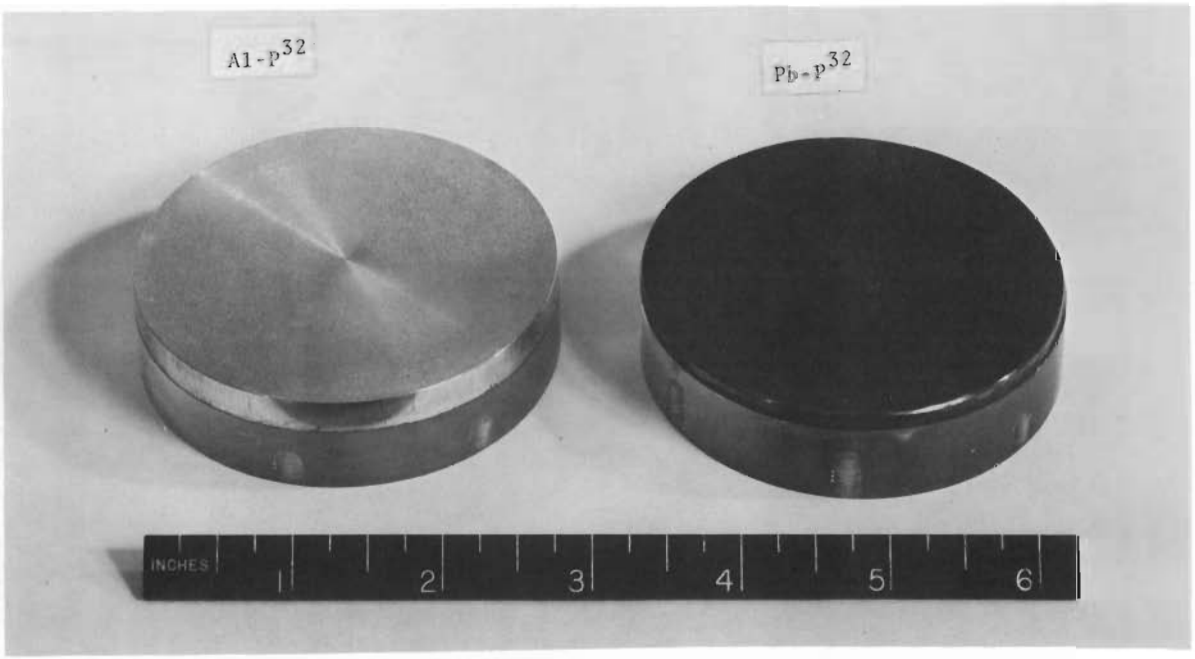

FIGURE 6.5

Finished Sources Mounted on Lucite Holders
No. 0650948-2; 0651209-2

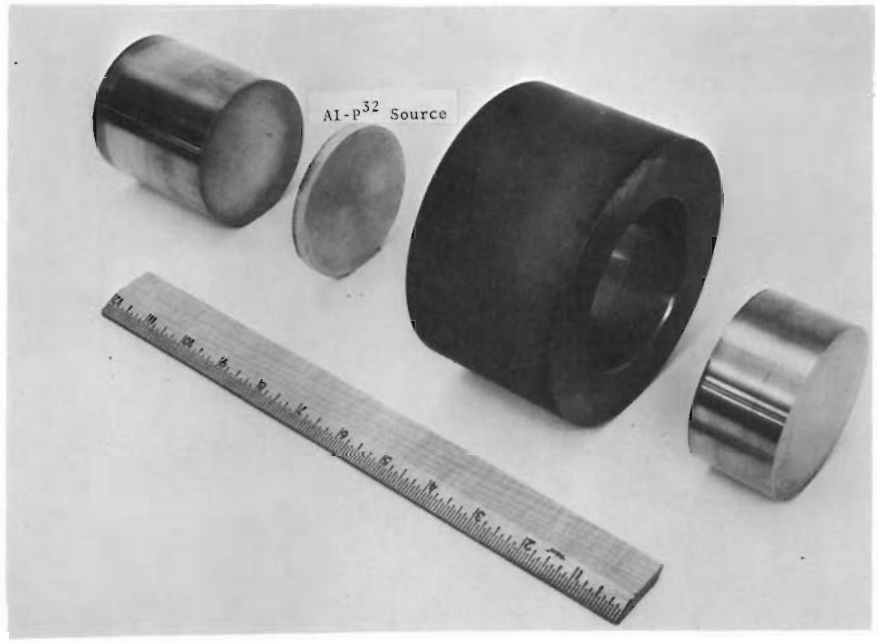

FIGURE 6.6
Punch and Ring Die

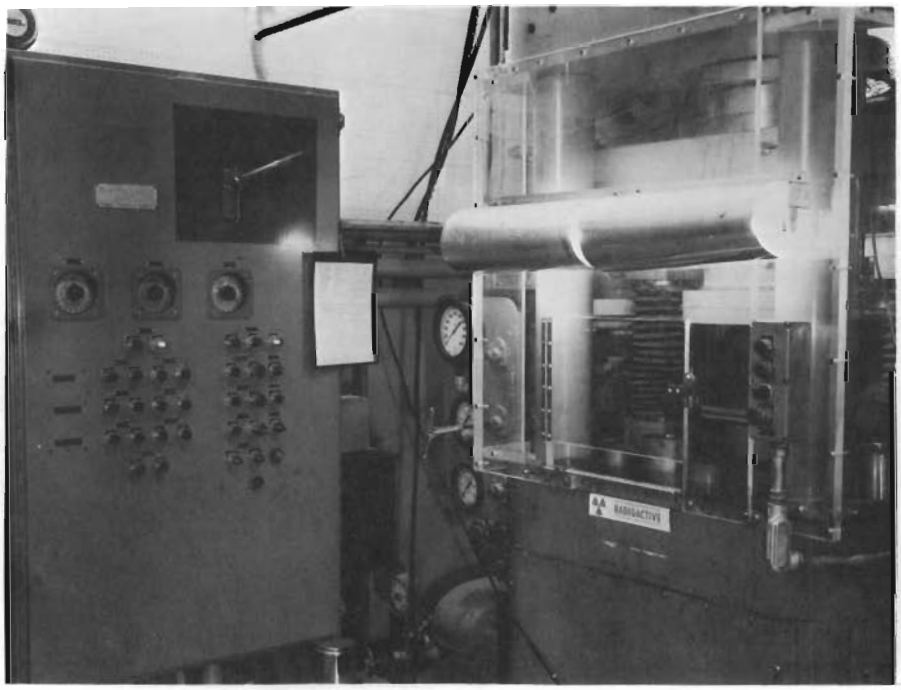

FIGURE 6.7
300-Ton Hydraulic Press
No. 40592-1; 0650948-8

Before the third fabrication run, the slurry blending of P^{32} with the aluminum and lead was changed from a water base to an alcohol base, and the powder drying was performed in a partial vacuum rather than in air. These modifications were made to minimize the water available for sorption by the phosphorus compound. The third set of Al-P^{32} and Pb-P^{32} sources fabricated, with this material, met all requirements. The sources had a specific activity of about 21.83×10^6 disintegrations/min/g aluminum or lead, a uniform dispersion of P^{32}, and a density of 93 to 100% TD.

XAP End Closure Parameters - R. F. Boolen

A Request for Proposal from Atomics International was processed and work was begun under the contract. This contract calls for a study to provide magnetic force welding parameters for XAP-001 (an Alcoa experimental aluminum powder alloy) cladding, which contains a 6 wt% dispersion of aluminum oxide. The material is being considered as a fuel cladding for the HWOCR.

Integrity requirements, from which parameters would be determined, specified that the end closures must be leak proof and withstand greater internal pressure than the tubular cladding at room temperature and 400 °C.

Based on earlier work with S.A.P., end closures in the 0.503 in. ID by 0.027 in. wall ribbed tubes were of straight butt joint design. The resulting weld cross-sectional area is larger than that of the cladding (minus ribs). Ribs were removed 1/2 in. from the ends of the tubes to provide a more than adequate electrical contact during welding.

In addition to the previously used mechanical cleaning (wire brushing), two types of chemical cleaning (Diversey and Oakite) were satisfactory for preweld deoxidizing.

Figures 6.8 and 6.9 illustrate the tube configuration and microappearance. About 75 end closure welds were made during the course of study. Tensile tests were used to distinguish satisfactory welds, i.e. tests where ultimate failure occurred totally in the tube material. Incomplete bonds caused partial failures in the weld interface. The following parameters produced satisfactory end closures: 75,000 A current (peak, approximately sine curve) for 5.85 msec at a forging force of about 2000 lb (peak, static). For the initial area of 0.045 $in.^2$, these values represent a current density of 1.7×10^6 $A/in.^2$ and a static pressure of approximately 45,000 psi. Cross section of a typical end closure is shown in Figures 6.10 and 6.11. External flash or upset was removed by lathe cutting; for all other samples, the upset was sheared off with a screwdriver tip.

To seal the ribbed tubes during welding, a special sealing tube was designed, fabricated, and tested as satisfactory. Since tensile testing resulted in failure of the tube, its longitudinal ultimate strength (unribbed) was an average 37,000 psi.

Twenty end closures were tested, ten by room temperature burst test and ten at 400 °C. Longitudinal splitting caused all ultimate tube failures. Ultimate average pressure was 3912 psig (maximum variation 250 psig) for room temperature tests and 1746 psig (maximum variation 270 psig) for the samples tested at 400 °C. Tubes tested at room temperature showed very marked bulges in the end regions; those tested at 400 °C had only slight bulges.

No leaks were found by leak testing of 30 representative samples (detection level = 2×10^{-10} atm cm^3/sec). Fabrication and testing necessary to the contract was initiated and completed. Parameters for consistent welding of end closures which surpass requirements were determined.

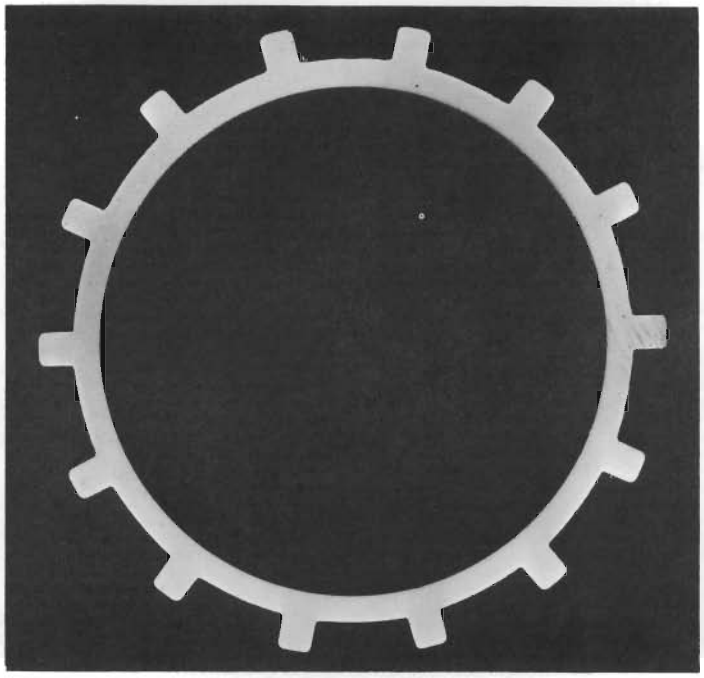

5X

FIGURE 6.8
XAP-001 Tube Cross Section

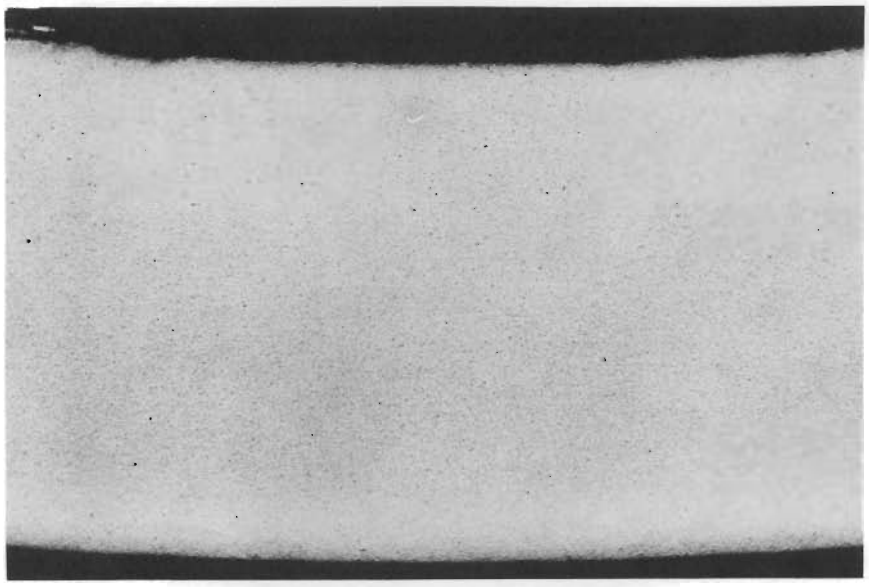

100X

FIGURE 6.9
XAP-001 Tube Wall Section
No. 4652027A; 4652025A

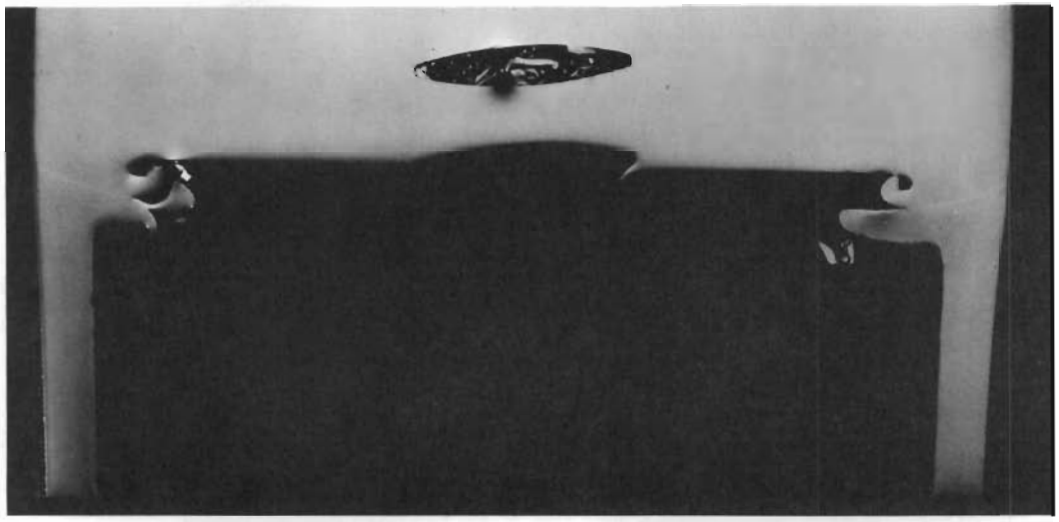

10X

FIGURE 6.10

Cross Section of XAP-001 Magnetic Force Welded End Closures

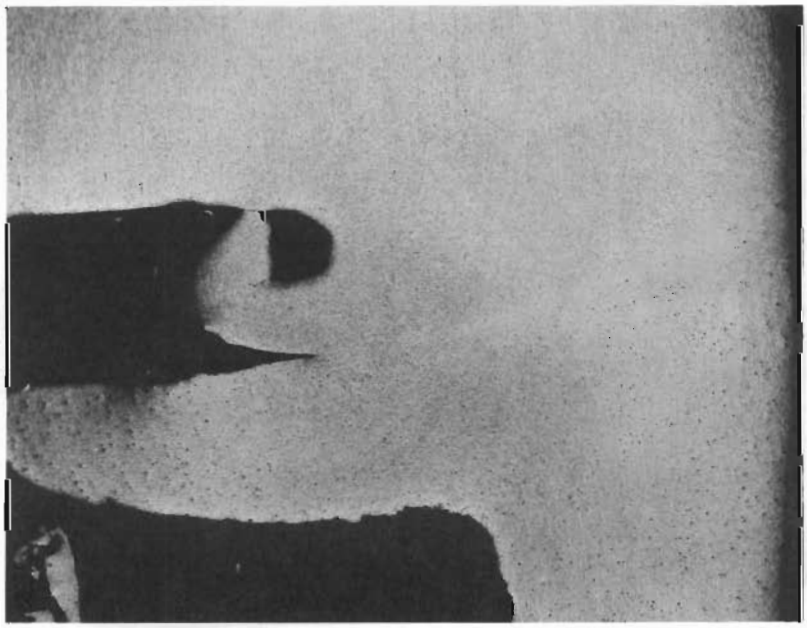

50X

FIGURE 6.11

Cross Section of Magnetic Force Welded XAP-001

No. 5652078E; 4652078A

ONSITE DISTRIBUTION

Copy Number

Pacific Northwest Laboratory

1	F. W. Albaugh
2	H. J. Anderson
3	R. J. Anicetti
4	E. R. Astley
5	J. A. Ayres
6	W. J. Bailey
7	R. J. Baker
8	J. M. Batch
9	J. L. Bates
10	T. K. Bierlein
11	C. H. Bloomster
12	D. W. Brite
13	C. L. Brown
14	C. A. Burgess
15	J. B. Burnham
16	S. H. Bush
17	J. J. Cadwell
18	T. D. Chikalla
19	G. S. Cochrane
20	R. E. Dahl
21	G. M. Dalen
22	J. L. Daniel
23	F. G. Dawson, Jr.
24 - 34	D. R. deHalas
35	R. F. Dickerson
36	R. L. Dillon
37 - 46	K. Drumheller
47	E. A. Eschbach
48	S. L. Fawcett
49	J. C. Fox
50	P. L. Farnsworth
51	M. D. Freshley
52	R. L. Gibby
53	S. Goldsmith
54	W. L. Hampson
55	L. A. Hartcorn
56	H. Harty
57	J. J. Hauth
58	R. J. Hennig
59	G. R. Horn
60	B. M. Johnson

ONSITE DISTRIBUTION (Contd)

Copy Number	
61	G. A. Last
62	W. R. Lewis
63	R. J. Lobsinger
64	C. E. McNeilly
65	L. G. Merker
66	M. K. Millhollen
67	J. E. Minor
68	T. C. Nelson
69	R. E. Nightingale
70	R. E. Olson
71	R. S. Paul
72	A. M. Platt
73	W. D. Richmond
74 - 83	W. E. Roake
84	R. K. Robinson
85	M. R. Schwab
86	D. P. Shively
87	R. E. Sharp
88	R. E. Skavdahl
89	R. C. Smith
90	E. A. Snajdr
91	D. H. Stewart
92	R. W. Stewart
93	K. R. Sump
94	W. H. Swift
95	H. A. Taylor
96	G. L. Tingey
97	E. E. Voiland
98	M. T. Walling
99	E. T. Weber
100	R. G. Wheeler
101	O. J. Wick
102	H. R. Wisely
103	F. W. Woodfield
104	D. C. Worlton
105	H. H. Yoshikawa
106 - 107	700 Technical Publications
108 - 112	Technical Information Files

ONSITE DISTRIBUTION (contd)

Copy Number

General Electric Company, Richland

113	R. L. Dickeman
114	T. W. Evans
115	M. Lewis
116	C. H. Shaw
117	E. A. Smith
118	GETA File Copy

Douglas United Nuclear, Inc.

119	T. W. Ambrose
120	L. E. Kusler
121	J. T. Stringer

Isochem, Inc.

122	H. H. Hopkins
123	R. Y. Lyon

Richland Operations Office

124	P. G. Holsted
125 - 126	R. K. Sharp
127	Technical Information Library

OFFSITE DISTRIBUTION (Special)

Number of Copies

1	ALKEM 7501 Leopoldshafen Karlsruhe, Germany Attn: W. Stoll
5	Argonne National Laboratory Attn: C. H. Bean J. H. Handwerk J. H. Kittel R. Macherey J. F. Schumar

OFFSITE DISTRIBUTION (Special)(Contd)

Number of Copies	
1	Associazione Euratom- CNEN Per I Reattori Veloci Via Mazzini 2 Bologna, Italy Attn: F. Pierantoni
6	Atomic Energy Commission, Washington Division of Reactor Development Attn: R. Grube J. M. Morrisey J. M. Simmons W. R. Voigt M. J. Whitman
1	Atomic Energy Research Establishment Chemistry and Metallurgy Branch Fuels Development Branch Chalk River, Ontario, Canada Attn: J. A. L. Robertson
4	Atomic Energy Research Establishment United Kingdom Atomic Energy Authority Harwell, Didcot, Berks, England Attn: P. Murray (3) L. E. Russell (1)
1	Atomics International Attn: B. R. Hayward
2	Atomic Power Development Associates 119 First Street Detroit 26, Michigan Attn: W. H. Jens A. A. Shoudy
4	Battelle Memorial Institute Attn: D. L. Keller S. W. Porembka (2) W. F. Heenan (1)
1	Brookhaven National Laboratory Attn: D. H. Gurinsky
1	Centre d'Etudes Nucleaires de Cadarache Poite Postale No. 1 Saint-Paul-Lez-Durance, France Attn: Dr. B. Defreyn

OFFSITE DISTRIBUTION (Special) (Contd)

1 Combustion Engineering, Inc.
Attn: J. C. Tobin

1 European Atomic Energy Community
51-53 Rue Belliard (Euratom)
Brussels 4, Belgium
Attn: Pierre Kruys

1 General Electric Company, APD
Special Purpose Nuclear Systems Operation
P. O. Box 846
Pleasanton, California
Attn: J. E. Van Hoomissen

3 General Electric Company, Cincinnati
Attn: E. A. Aitken
W. Briskin
J. McGurty

3 General Electric Company, Pleasanton
Attn: L. P. Bupp
E. A. Evans
A. I. Kaznoff

5 General Electric Company, San Jose
Attn: K. Cohen
A. N. Holden
T. J. Pashos
B. Weidenbaum
E. L. Zebroski

1 Kerr-McGee Indus. Inc.
Oklahoma City, Oklahoma
Attn: Harold Lambertus

1 Knolls Atomic Power Laboratory
Attn: W. K. Barney

5 Los Alamos Scientific Laboratory
Attn: R. Baker
M. Bowman
H. Hessing
D. MacMillan
R. Spence

2 NASA Lewis Research Center
Attn: A. F. Lietzke
N. T. Saunders

OFFSITE DISTRIBUTION (Special) (Contd)

Number of Copies

1 Transuranium Institute (Euratom)
Karlsstrasse 42-44
Karlsruhe, Germany
Attn: H. M. Mattys

4 Union Carbide Corporation (ORNL)
Attn: R. M. Carroll
J. L. Scott
W. C. Thurber
T. F. Connally

1 United Aircraft Corporation
Research Laboratory
East Hartford, Connecticut
Attn: G. H. McLafferty

1 University of Arizona
Nuclear Engineering Department
Tucson, Arizona
Attn: Monte V. Davis

1 University of Michigan
College of Engineering
Ann Arbor, Michigan
Attn: W. Kerr

3 U. S. Atomic Energy Commission
Brussels, Belgium
Attn: C. F. Schank

2 Westinghouse Bettis Atomic Power Laboratory
Attn: J. Belle
B. Lustman

4 Westinghouse Electric Corporation
Attn: Robert Allio
A. A. Bishop
A. Boltax
N. R. Nelson

1 Wright Air Development Center
AF Materials Laboratory
Wright-Patterson AFB, Dayton, Ohio
Attn: S. W. Bradstreet